Using Cold Spray to Package Electronic Implants

by

Molly A. Berringer

B.S.E. Biomedical Engineering with Highest Distinction

University of Iowa, 2016

Submitted to the Department of Mechanical Engineering

in partial fulfillment of the requirements for the degree

of

MASTER OF SCIENCE IN MECHANICAL ENGINEERING

at the

MASSACHUSETTS INSTITUTE OF TECHNOLOGY

February 2018

Author . . . . . Signature redacted

Department of Mechanical Engineering

January 12, 2018

Certified by . . . . . Signature redacted

Brian W. Anthony

Principal Research Engineer, Dept. of Mechanical Engineering

Thesis Supervisor

Certified by . . . . . Signature redacted

Caroline Bjune

The Charles Stark Draper Laboratory, Inc.

Technical Director

Thesis Supervisor

Accepted by . . . . . Signature redacted

Rohan Abeyaratne

Chairman, Department Committee on Graduate Thesis

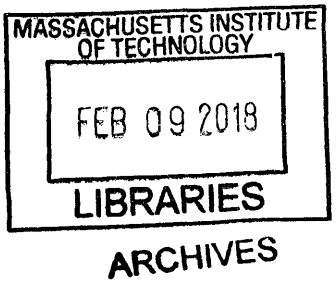

Using Cold Spray to Package Electronic Implants

by

Molly A. Berringer

Submitted to the Department of Mechanical Engineering

on January 12, 2018, in partial fulfillment of the

requirements for the degree of

Master of Science in Mechanical Engineering

Abstract

Due to improvements in electronics manufacturing, electronic implants keep decreasing in size and are moving towards integrated-circuit (IC) based designs. As implant electronics become significantly smaller with the use of ICs, traditional implant packaging become a limiting factor on implant miniaturization. Additionally, current packaging techniques can be expensive, and time and labor intensive. Building electronic packages can require many materials, multiple machines, and several manufacturing steps. This thesis explores cold spray as an alternative packaging method that would address the issues associated with traditional packaging. Cold spray could be used to create conformal packaging around electronic implants. Two biocompatible packaging materials, ultra high molecular weight polyethylene (UHMWPE) and titanium, were cold sprayed on two different electronic material substrates, silicon and polyimide. The results from these experiments are presented in this work.

Thesis Supervisor: Brian W. Anthony
Title: Principal Research Scientist, Dept. of Mechanical Engineering

Thesis Supervisor: Caroline Bjune
Company: The Charles Stark Draper Laboratory, Inc.
Title: Technical Director

Acknowledgements

There are so many people I would like to thank for helping me complete my master's thesis. First off, I would like to thank The Charles Stark Draper Laboratory, Inc. (Draper) for giving me the opportunity to work for them and conduct novel and exciting research. My fellowship with Draper was a wonderful experience. The fellowship allowed me to gain real work experience at a company with outstanding resources and people. Additionally, there are many people at Draper that have gone out of their way to help me. Joseph Louis helped me through many stages of the experimental design process and he made sure I was connected to the right people to get everything done. Moreover, Joseph cared about my career goals and was always there to give me career advice and I truly thank him for that. Phillip Bari has also been a great coworker at Draper. He took the time to train me to pot and polish my material cross-sections so that I could analyze them under the SEM. I would like to thank Phillip Bari because without this training I would not have been able to complete my thesis. I would also like to thank Elizabeth Brundage who taught me how to use and take images on the SEM. Another person I would like to thank is Daniel Frigon who diced all of my substrates to for the experiments. I would also like to thank Caroline Bjune who was my advisor at Draper. It was great to work with her while completing my thesis. She was always supportive and encouraging. I couldn't have asked for a better Draper advisor. There are also so many others at Draper that helped me along the way and I would like to thank all of those people that I have not mentioned above.

Additionally, there are many people at MIT I would like to thank. Brian Anthony has been a great MIT advisor and I can't thank him enough for being so helpful throughout my time at MIT. He was very supportive and made sure that I was having a great experience at MIT and Draper. I also had a great time getting to know, working with, and learning from all of the students in Brian's lab at MIT.

Throughout my research I have also spent several days with Sophia Lauwers, Bailie McNaly, Bob Allegretto, and Ozan Ozdemir from VRC Metal Systems L.L.C. and Northeastern University. They have all had many years of experience with the cold spray manufacturing process and I would not have been able to complete my thesis work without them. They are all truly hard working people and even went out of their way to help me many times.

Lastly, I would like to thank my family for their support while I worked on my thesis. They were always there for me to talk to during my worst times and my best. I would not be where I am today without my parents who taught me the importance of hard work. I am truly lucky to have parents like them. My siblings, Amanda, Amber, Brooke, and Blake are amazing people and they have always encouraged me to follow my dreams. I am so happy to have such a supportive family. Thank you.

Table of Contents

1 Introduction

1.1 Electronic Implant Packaging

Medical electronic implants are devices that improve or save people's lives. Pacemakers ensure a properly functioning heart, spinal neural stimulators reduce or remove chronic back pain, brain neural stimulators fix motor or psychiatric problems, and other electronic implants coordinate movements between prosthetic limbs and the body.

Electronic implants have changed and improved over the past century. In the 1950s and 1960s the first battery powered and the first implantable pacemakers were invented by Earl Bakken and Wilson Greatbatch, respectively. One of the issues with the first implantable pacemaker invented by Greatbatch was the hermetic (airtight) seal of the device. The devices were not always hermetic and bodily fluids often penetrated through the device, destroying the electronics [1]. A hermetic seal is essential to prevent the failure of implanted electronics. From the invention of the pacemaker to today, packaging techniques to create hermetic seals have improved. With modern technology, hermetic seals can be created consistently with many different implant packaging methods.

Electronic implant packages not only need to achieve a hermetic seal, but must also be long-term biocompatible and corrosion resistant in the human body. These requirements greatly limit the materials that can be used in implant packages. Current packages generally use metals, ceramics, and glass to create hermetic seals. Recent research has also looked at polymers to package electronic implants [2]. However, since all polymers absorb some amount of moisture, they are non-hermetic packages because they do not form fully hermetic seals [3]. However, for some polymers the percentage of absorption is so low that they may be acceptable for specific applications. Even with all the current options for packaging, there is still the challenge of sealing electronics compactly and inexpensively.

1.1.1 Simple Metal Can Packages

Some of the most common metals used in medical implants are grades of titanium, cobalt chromium, tantalum, nitinol, zirconium, stainless steel, gold, platinum, and nickel alloys [4]. Of these metals, titanium is one of the most commonly used to hermetically package medical electronics since it is biocompatible, corrosion resistant, lightweight, strong, and easy to weld [5], [6]. Usually, these metal electronic implant packages come in the form of cans where two sides are created and are then bonded together once the electronics are placed inside. Metal can packages are very common among current implantable devices on the market since they are simple and relatively inexpensive to manufacture compared to alternative package designs. The metal sides of the can are usually either machined from bulk material or are cast in molds. Laser welding is the most common bonding technique. However, electrical resistance welding, electrode welding, rolled seam welding, cold welding, crimp connection, and soldering may also be used. Many pacemakers and neural stimulators use these metal can packages. For example, a Medtronic pacemaker with a titanium can package can be seen in Figure 1. Notice the visible line between the two metallic sides where the can was bonded together around the electronics.

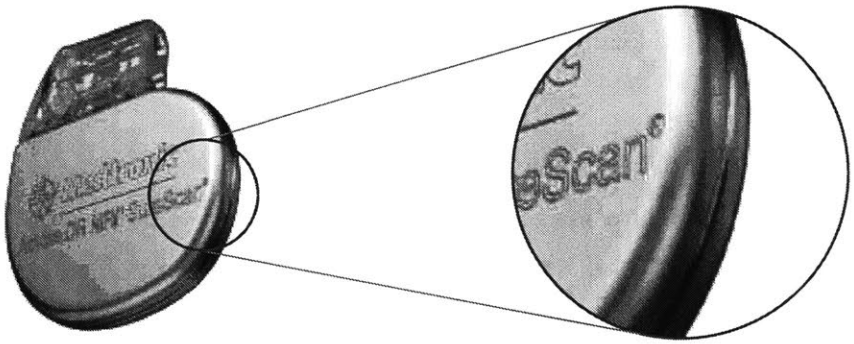

Figure 1. Medtronic pacemaker with a titanium can package [7]. The connection between the two sides of the can is more clearly shown in the magnified section.

1.1.2 Incorporating Feedthrough Pins in Package

Feedthrough pins are incorporated in hermetic packages to connect external electrical components to the electronics sealed within the package. The addition of feedthrough pins in a hermetic package can make the package design more complicated.

A schematic of a metal can with feedthrough pins acquired from a *Hermetic Packaging and Sealing* document from SCHOTT can be seen in Figure 2 [8]. In Figure 2(a) the feedthrough pins

are hermetically sealed to the base plate by melting glass around them. This glass also acts as an insulation barrier between the pins and the baseplate. Figure 2(b) shows that after the pins are attached to the baseplate, an electronic component is placed on the baseplate and connected to the feedthrough pins. Afterwards, a metal cap is placed around the electronics and is bonded to the base plate, as see in Figure 2(c) – 2(d).

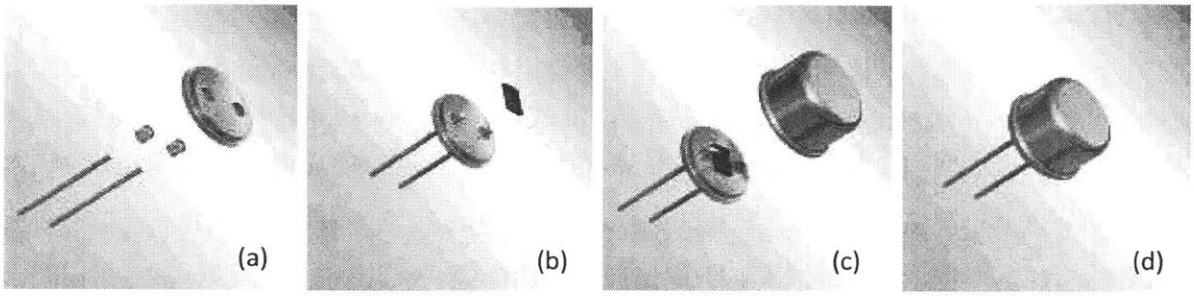

Figure 2. Schematic of hermetic packaging of electronics with feedthrough pins. (a) Feedthrough pins are put through the base plate and glass is melted around the wires to create a hermetic seal. (b) An electronic component is added to the baseplate and is wire bonded to the feedthrough pins. (c-d) A cap is added to the device and is bonded to the base plate. Images reprinted with permission of SCHOTT AG [8]. SCHOTT produced and owns all images.

Another way to create feedthrough pins is by using a nonconductive base plate to act as the insulation barrier between the feedthrough pins and the surrounding metal casing. Then to create a hermetic seal, metal is brazed around the feedthrough pins. An example of gold brazed around 64 platinum/iridium pins in a ceramic alumina base plate can be seen in Figure 3 [9]. With either of these manufacturing techniques, the cross-sectional area that the wires take up on the base plate increases (either due to the glass or brazed metal). Therefore, the number of feedthrough pins that can fit on a feedthrough plate is restricted, which can be a limiting factor for implant design.

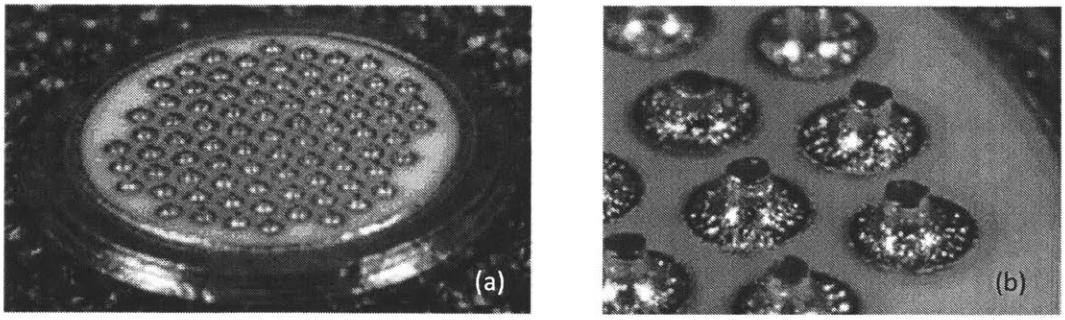

Figure 3. (a) Gold brazed around 64 platinum/iridium feedthrough pins in a ceramic alumina base plate. (b) Closer view of brazing around feedthrough pins [9].

1.1.3 Packages for RF Transmission

For some implant applications radio-frequency (RF) wave transmission is essential for the function of the implant. RF transmission between the implant and an external sources can be used for two main tasks: energy transfer and communication.

Energy transfer occurs when inductive coupling is achieved between a coil within the implant and a coil external to the patient. Power is sent to the coil that is external to the patient which then creates a magnetic field. This magnetic field then induces a voltage in the receiver coil in the implant [10]. The power received in the implant can then be used to charge a battery or to directly provide power to electronics in the implant. A schematic of mutual inductance for energy transfer can be seen in Figure 4 [10]. RF waves can also be used to transfer data between the implant and an external device. Data can be transmitted by modulating the signal applied to the external coil. A variety of modulation schemes including amplitude modulation, frequency modulation, and phase shift keying have been applied to medical implants.

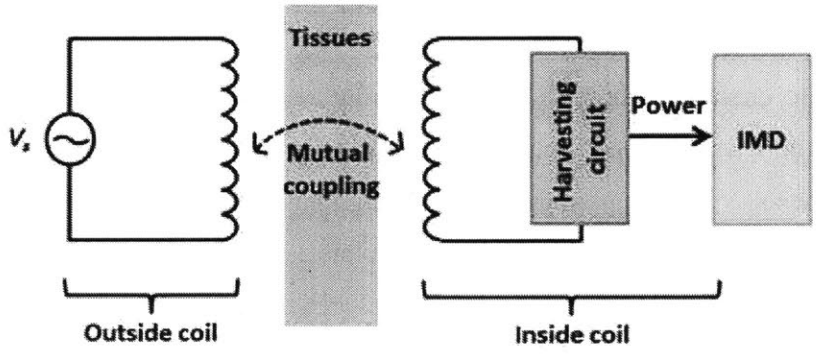

Figure 4. Schematic of inductive coupling to charge an implantable medical device (IMD) [10].

There are several implant packages that allow RF transmission. One technique is to use the metal can design and make the sides of the can extremely thin. Bulk metal is not RF transparent. However, RF waves can transmit through thin metal with acceptable signal loss. If the can is made thin enough, enough of the signal will be able to reach the internal electronics of the implant. Although this is not the most efficient package for RF transmission, it is still commonly used due to the strength of the metal material and the simplicity of the packaging which reduces the time and cost to manufacture the package.

Packages that require efficient RF transmission generally incorporate RF transparent materials into the package design. Current materials that are known to be RF transparent, biocompatible, and can create hermetic seals are ceramics and glass. Biocompatible ceramics include alumina, zirconia, and hydroxyapatite [4]. Hydroxyapatite is bioactive, meaning tissue can grow on its surface, while alumina and zirconia are bioinert. Therefore, because alumina and zirconia are bioinert, they are generally better choices for electronic packages than bioactive hydroxyapatite.

Many packages that incorporate ceramic or glass into their design for RF transparency still use metal as the main package material due to the advantages of metals such as high strength, ductility, and easier manufacturing methods. The ceramic or glass components are incorporated into these designs as windows.

There are many methods that can be used to incorporate glass windows into metal packages. One manufacturing technique places the glass component within the metal frame and then this assembly is heated up past the glass softening point to allow for the glass to bond to the metal frame. At these high temperatures, the finish of the glass may be affected. Therefore post-process grinding and polishing may be required to achieve the finish that is needed [11]. Alternatively, glass windows can be soldered to the frame with metal-alloy solder or solder-glass materials. Images acquired from SCHOTT of a glass window placement in a metal package can be seen below in Figure 5 [8].

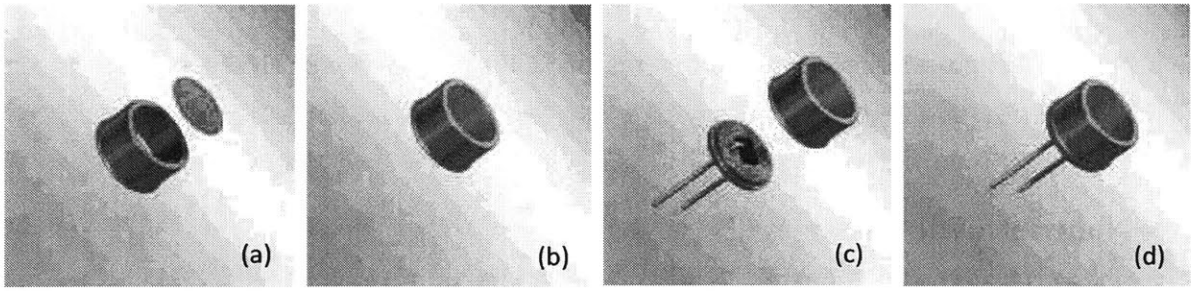

Figure 5. (a-b) A glass window is bonded to the metal cap. Then the (c) metal cap and baseplate are laser welded together to form the (d) final product. Images reprinted with permission of SCHOTT AG [8]. SCHOTT produced and owns all images.

Ceramic windows are placed in metal packages in a very similar way as glass windows. However, the bonding between the ceramic component and the metal can is usually done with a brazing processes. In Figure 3(a) you can see gold brazed between the alumina base plate and the titanium flange [9].

When an implant is small, needs efficient RF transmission, and is not expected to be subjected to substantial stresses, packages made entirely out of glass are good enclosure options. Glass packages are a popular choice for smaller electronics, such as radio-frequency identification (RFID) tags. Images acquired from SCHOTT's *Hermetic Packaging and Sealing* document can be seen in Figure 6 below [8]. These images show the process of enclosing electronics within a glass package. This package starts off as a hollow glass tube. The electronics are placed inside and then both ends of the tube are melted to enclose the electronics with a hermetic seal. The ends of the tubes are melted with a light-only source, such as a laser. Using a lighting source rather than a flame ensures that no impurities will enter the package [8].

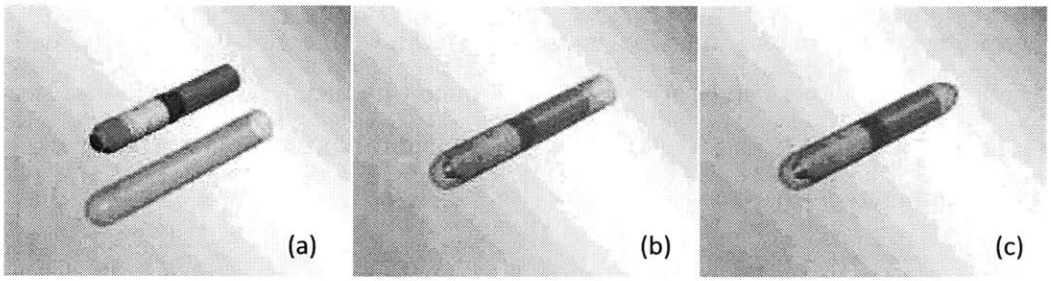

Figure 6. (a) The electronics and glass can be seen side by side before assemble. (b) The electronics are placed within the glass tubing. (c) The open end of the glass tube is heated up by a laser to seal the enclosure. Images reprinted with permission of SCHOTT AG [8]. SCHOTT produced and owns all images.

1.1.4 Non-Hermetic Packages

The materials and manufacturing processes to create hermetic packages can be costly, and time and labor intensive. Moreover, current packages are generally rigid and large. In order to address these limitations of current packaging techniques, alternatives using non-hermetic packages have also been explored. Many biocompatible polymers have been explored for implant

packages. However, most are unsuitable since the water absorption of the polymers are too high, which leads to an increase in the enclosure's humidity and consequently early failure of the electronics. Current medical electronic implants do use polymers, such as polyurethane and silicone rubber, for connector blocks where leads plug in (see the top of the pacemaker in Figure 1), for insulation around leads, for seals, and to over-mold implants. These polymers are used in current implants when either insulation, flexibility, or a softer material is necessary. However, generally polymers aren't utilized to package the core electronics due to their water absorption properties. However, new research has been exploring the possibility of using polymers to package the electronics.

The most promising research on packaging with polymers has been looking at using liquid crystal polymers (LCP) [2], [12]. LCPs have good mechanical properties and water absorption between 2% and 4% (percent mass increase when placed in water) which is lower than many other biocompatible polymers [2]. Although the water absorption is low, over long periods of time water absorption can lead to increased humidity within the package, causing the electronic components to fail. In order to test the long-term reliability of electronics packaged in LCP, accelerated soak tests have been conducted. One research paper reported functional electronics within a LCP encapsulation after 300 days in a PBS soak test [13]. Researchers from Seoul National University, Kangnam Sacred Heart Hospital, and Seoul National University College of Medicine ran calculations to determine the amount of time that will pass before the internal cavity of a LCP enclosure in saline reaches a relative humidity of 63%. The research found an estimated time of 15.3 years and 64.3 years for LCP encapsulations that were 25 μm and 100 μm thick, respectively [12]. Therefore, depending on the electronics' sensitivity to humidity, the desired lifetime of the electronic implant, and the strength needed in the implant packaging, LCP packages may or may not be an acceptable packaging alternative.

If LCP is found to be an acceptable alternative to traditional hermetic packaging, it can result in lower material cost and simpler manufacturing. One research paper describes the following manufacturing processes to create a LCP package. The two sides of the implant package can be thermoformed from high temperature LCP into a desired shape. A low temperature LCP can be placed between the two LCP thermoformed parts. Then, these parts can be pressed together with high pressure and heat to melt the low temperature LCP and create a hermetic seal. Water

cooling is also used during the pressing step to prevent overheating of the internal electronics [13]. Figure 7 illustrates this manufacturing process [13].

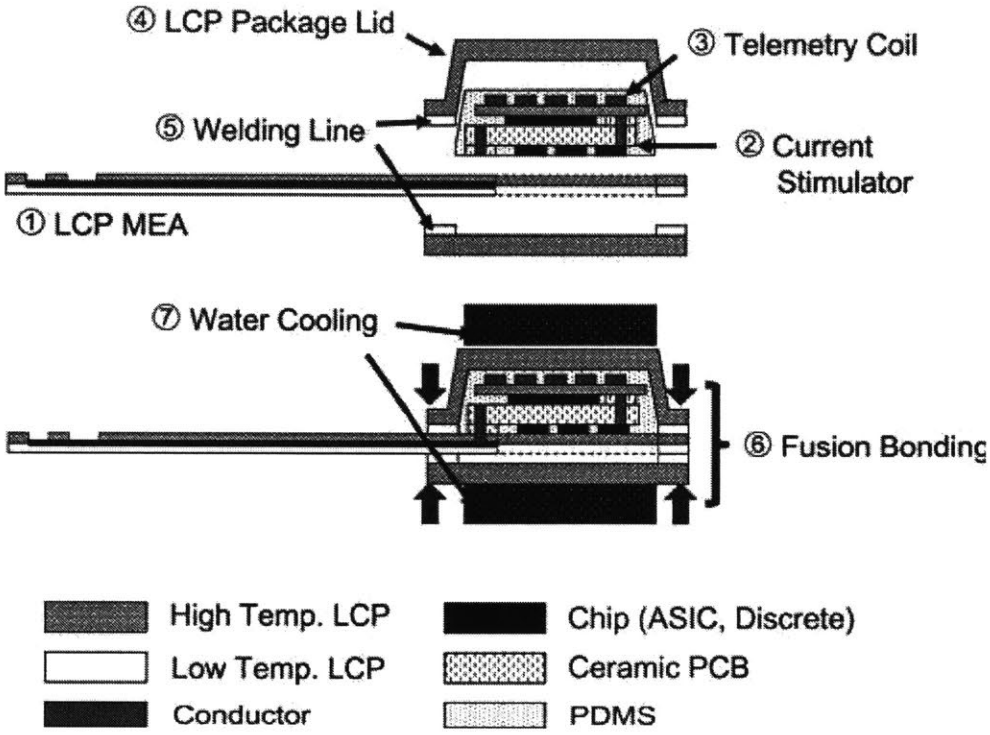

Figure 7. Example of manufacturing processes used to create a LCP package for implants [13]. © 2011 IEEE.

Another method to hermetically seal electronics transitions from having a hermetic seal at the system-level, Figure 8 (a), to a hermetic seal at the component-level, Figure 8 (b) [14]. In component-level hermetic packaging, silicone rubber is usually molded over the electronics to create a non-hermetic seal to prevent corrosion and water condensation on the electronic components [14]. Therefore good adhesion between this polymer layer and the underlying electronics is necessary.

As can be seen in the images of Figure 8, for similar electronics, system-level hermetic packages are generally larger than component-level hermetic packages due to wasted space within the one large hermetic package. The component-level hermetic packaging with the conformal silicone encapsulation can result in much smaller final implant dimensions. This is what makes this packaging technique so attractive. However, the success of this packaging technique depends

on whether the small components can be designed in their own hermetic packages. Additionally, it adds complexity since it requires a hermetic package for each individual component and insulation on wires running between components. Moreover, since each individual component must be individually hermetically sealed, each component can act as a point of failure to the device. Therefore, with more possible points of failure, it raises the overall failure rate of the device. Some research has also looked at creating encapsulations without hermetically sealing the internal components. With a 75 μm thick LCP coating rather than an LCP enclosure, it can take 3.5 years before the internal components reach 63% humidity [12]. Therefore, this may be an option if the implant needs to be small in size and only needs to function in the body for a few years or less.

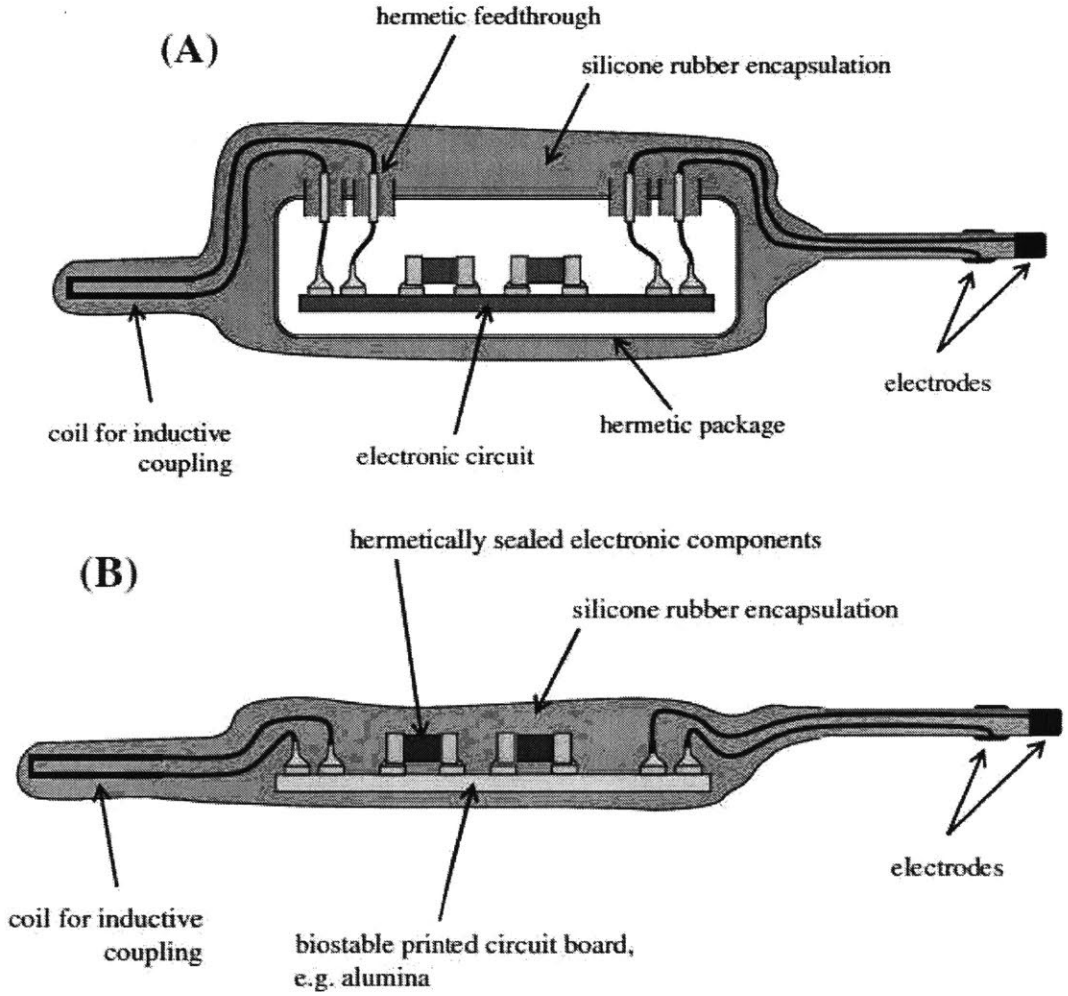

Figure 8. (a) System level hermetic packaging. (b) Component-level hermetic packaging. Modified from T. Stieglitz [14]. © 2010 Springer.

1.1.5 Summary of Packaging Methods for Electronic Implants

Several types of packages can be used to hermetically seal electronic implants. The simplest and most widely used is the metal can design. This packaging technique is a good choice since it results in a high strength package and has lower manufacturing costs. However, when efficient RF transmission is required, the metal can design may not be an appropriate choice since RF waves will be attenuated through the metal. Efficient RF transmission can occur through glass packages, and ceramic or glass windows in metal packages. Moreover, when direct connections between the electronic implant and components external to the package are needed, feedthrough pins must be incorporated into the package. Feedthrough pins can complicate a package design since many wires must come out of the package while keeping a hermetic seal. Additionally, the wires must be electrically insulated from any other metal that is a part of the package.

Recent research has also looked at using non-hermetic polymer packaging of electronic implants in order to either reduce costs, increase flexibility, and/or reduce the size of implant. Although all polymers absorb some amount of water, the research suggests that non-hermetic polymer packaging may be an acceptable alternative in specific applications. If the electronics in an implant can withstand higher humidity levels or if the implant is intended for short-term use, polymers may be an acceptable and lower cost alternative to traditional hermetic packages.

Additionally, an alternative to traditional system-level hermetic packaging is component-level hermetic packaging with a polymer encapsulation. This packaging technique can significantly reduce the overall dimensions of electronic implants. However, this technique adds complexity to the design since each component must be hermetically sealed and wires between components must be properly insulated. In this design, each component may be a source of failure, therefore this results in higher failure rates than system-level packages that contain fewer hermetic seals. Therefore, this packaging technique may not be a good choice unless it is crucial for the dimensions of the implant to be as small as possible. Polymer encapsulations with no hermetic seals can also be used but this significantly reduces the number of years the implant can function before it fails from high humidity levels around the electronics.

Each packaging technique has its advantages and disadvantages. The best package for a specific electronic implant is highly dependent on requirements such as strength, RF transparency, number of feedthrough pins needed, size, and the expected lifetime of the implant.

1.2 Drawbacks of Current Packaging Techniques

Although many packages successfully seal electronics from the environment, there is still room to improve upon current packaging designs and process techniques. Conventional implant packages such as the metal can packages are bulky which limits the miniaturization of implants, therefore also limiting where they can fit within the human body due to size constraints. Additionally, current packaging techniques can be expensive, and time and labor intensive.

Electronic implant packages generally do not follow the contours of the device since this would take more time to design and would be more expensive to manufacture. Therefore, instead of being conformal packages, the packages are generally made large enough to incorporate the largest component of the electronics and battery. This type of packaging is therefore larger than it needs to be to fully surround the electronics. Additionally, some implantable electronics require multiple components in the package such as RF transparent windows or feedthrough pins. These additional components can increase the dimensions of the final package and increase the manufacturing cost.

Due to improvements in electronics manufacturing, electronic implants keep decreasing in size and are moving towards integrated-circuit (IC) based designs. As implant electronics become significantly smaller with the use of ICs, the traditional packages become a limiting factor on implant miniaturization.

Another drawback of current packaging techniques for medical implants is the time and labor intensive processes. Building electronic packages can require mamy materials, multiple machines, and several manufacturing steps. Another major expense to creating these sealed packages is the amount of time and man hours needed just to design the package in the first place. Implants for different applications will have different electronic components, different battery sizes, different amounts of feedthrough pins, and different needs in general. Therefore, with each

new implant product, generally a new package must be designed by engineers which adds on to the man hours spent creating the package, consequently increasing the overall cost of the implant.

1.3 Cold Spray Process to Package Medical Electronics

In order to address many of these drawbacks seen in conventional medical device packages, a manufacturing process called cold spray was investigated as a new packaging method. The Army Research Laboratory has worked with the cold spray process for a period of decades and continues to explore new applications for this technology. Cold spray has previously been researched for use in passive implants [15]. However, there has not been research on cold spray being used to seal active electronic implants. Using cold spray to package electronic implants has several possible advantages over traditional packaging techniques. Cold spraying electronics would create conformal coatings, therefore leading to the smallest possible package. Hermetic seals are likely possible since cold sprayed materials have resulted in dense coatings. This manufacturing method would also be simpler and streamlined. To create the package, implants would be set under the cold spray machine and the coating would be sprayed on as the nozzle traverses back and forth over the implant. One other major advantage would be the significant reduction or possibly even elimination of package design time.

In order to investigate the possibility of using cold spray to package electronic implants, the Army Research lab provided funding to Draper. For this research, Draper connected with VRC Metal Systems, L.L.C. (VRC) to cold spray samples. VRC has several years of experience with the cold spray manufacturing process. VRC contributed their expertise in the cold spray process and Draper contributed thorough knowledge of integrated circuits and implant design for the research. Additionally, Northeastern University was involved in this research. Professor Sinan Müftü and post-doc Ozan Ozdemir from Northeastern University worked with Draper to select biocompatible powders to use with the cold spray system. Ozan Ozdemir also contributed to this research by running computational fluid dynamic (CFD) models of the cold spray process for specific powder and substrate materials. Initial process parameters for the cold spray experiments were selected from the outputs of the CFD model.

2 Cold Spray Process and Cold Sprayed Biocompatible Materials

2.1 Overview of the Cold Spray Manufacturing Process

The cold spray process accelerates feedstock powder to supersonic speeds with highly pressurized process gas. These high-speed particles are sprayed out of a nozzle as it scans back and forth above the substrate surface. When the particles contact the substrate, the high-speed impact causes the particles and substrate to deform and mechanically bond to one another. A particle will only adhere to the substrate if the particle's velocity is at or above a specific velocity called the critical velocity. The critical velocity is dependent on the particle material properties, size, and the substrate material. Since the cold spray process keeps the powder material in the solid state while it is deposited, it minimizes oxidation and phase transformations of the feedstock material which are issues that can occur with other thermal spray processes that melt the powder, such as plasma spray and high-velocity oxy-fuel (HVOF) [15], [16]. A schematic of the cold spay manufacturing process can be seen in Figure 9.

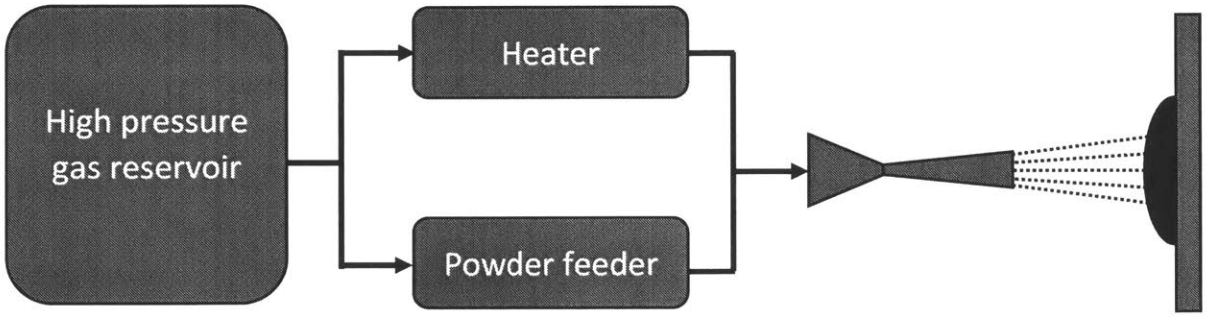

Figure 9. Simplified model of a cold spray system.

Some cold spray systems are manual. With these systems, the nozzle is manipulated by someone that moves it back and forth over the substrate. Manual systems have the advantage of

allowing complex movements of the nozzle over the substrate. Complex movements might be needed when cold spray is used to fill cracks in material or the system needs to build up original geometries. Automated systems have been built using a robot arm to move the spray nozzle. This automated system can keep a constant stand-off distance and traverse speed as it scans across the substrate. This leads to reliable and consistent coatings across samples. More advanced robotic systems can also spray coatings with multiple different nozzle angles rather than just perpendicular to the substrate. In the current research, VRC's cold spray system was used. Their cold spray system is automated and their robotic system is shown in Figure 10.

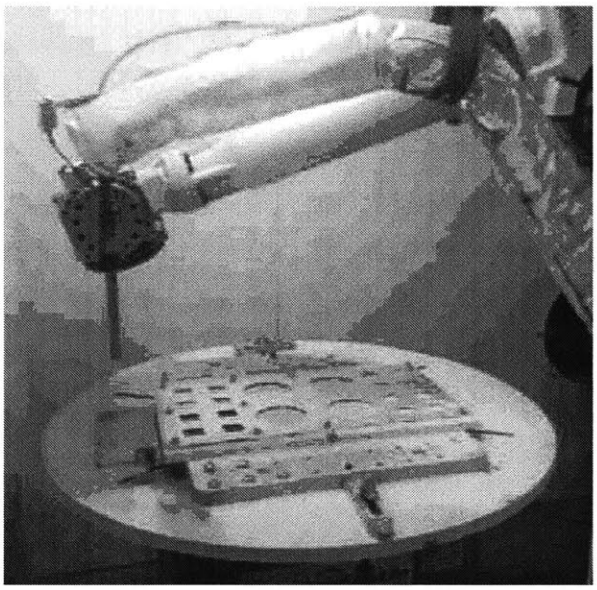

Figure 10. VRC's robotic cold spray system.

2.2 Overview of Biocompatible Materials that have been Cold Sprayed

Recent research has been using the cold spray process to deposit biocompatible materials. Most of this research has been conducted within the last ten years. This section is a review of long-term biocompatible materials that have been cold sprayed: stainless steel, titanium, tantalum, titanium dioxide (TiO_2), hydroxyapatite (HA), and ultra-high molecular weight polyethylene (UHMWPE). The review discusses porosity values found in the cold sprayed materials as well as any corrosion, biocompatibility, and cytotoxicity tests that have been conducted on them.

2.2.1 Stainless Steel Coatings

Density of Stainless Steel Coatings

Dense coatings of stainless steel have been achieved with the cold spray process. Porosity values range from 0.2% to 8.5% depending on powder particle shape and size, substrate material, and process parameters [17]–[21]. Spencer et al. tested 316L SS powder with particle sizes of -22 μm, -10 μm, and -5 μm (these are powders where the particles were small enough to pass through a 22 μm, 10 μm, and 5 μm mesh, respectively), and showed that as the particle size got smaller, the coating became more homogeneous and porosity decreased. Although the very fine particle size created extremely dense coatings, it did cause inconsistent feed rates in the flow and caused the nozzle to clog, making it difficult to create thick coatings. Spencer et al. also realized that with a combination of two monosized powders of different sizes, the packing density of the powder can be improved. Therefore, Spencer et al. also created two mixed powder feedstocks: 50/50 vol.% of -22 μm and -5 μm particles and 50/50 vol.% of -10 μm and -5 μm particles. The coating from the mixture of -22 μm and -5 μm particles still had visible porosity while the coating from the mixture of -10 μm and -5 μm particles had a density similar to the -5 μm particle coating, without the negative effects of inconsistent feeding and nozzle clogging [18].

Sova et al. also analyzed material porosity due to particle size. Powders with d50 of 18 μm, 28 μm, and 36 μm were used and the resulting porosities were 5%, 5.5%, and 8.5%, respectively [20]. Sova et al. also observed that at high traverse speeds the porosity appeared to be the highest between layers, forming layers of high porosity parallel to the surface. At low traverse speeds the porosity appeared to be in layers angled at approximately 30° from the substrate. This 30° angle was most likely due to the velocity profile of the particles coming out of the nozzle with the highest velocity particles near the center of the nozzle and lower velocity particles near the edges. Sova et al. also performed a laser post treatment on the cold sprayed material that came from the coarsest powder. This was done in order to reduce the porosity near the surface. This laser treatment ended up affecting the coating from the surface to a depth of ~200 μm. Within the laser treated region the porosity was reduced from 8.5% to less than 1% due to the melting and bonding of these particles [20]. This reduction in surface porosity also drastically improved the corrosion properties of the coating and this is further discussed in the next section on corrosion properties of cold sprayed stainless steel coatings.

In other work done by AL-Mangour et al. (2014), both helium and nitrogen gas were used. Both of the gas systems were set to the highest possible temperature that did not cause clogging of the nozzle. The results showed that helium gas created denser coatings of 316L SS than those created by nitrogen gas most probably due to the higher particle velocities (996 ± 138 m/s compared to 838 ± 84 m/s) and therefore greater plastic deformation of the particles upon impact [19]. AL-Mangour et al. (2014), also showed that annealing both the nitrogen and helium coatings caused a decrease in the coating porosities and annealing at temperatures of 800°C and above resulted in porosities of 0.2% or less for both coatings [19]. This is in agreement with other work that has also shown that heat treatments reduce the porosity of cold sprayed materials [21].

Research done by Villa et al. analyzed how changes in pressure and temperature inputs to the cold spray process affected the quality of 316L SS coatings. The coatings were sprayed with temperatures between 600°C and 800°C and pressures between 20 bar and 40 bar [22]. The optimal coating was determined after analyzing three characteristics of the coatings: deposition efficiency, thickness, and porosity. Through the experiment, Villa et al. found that the coating created with the highest temperature and pressure resulted in the optimal coating with a low porosity, the highest deposition efficiency, and the greatest thickness. Villa at al. also observed that as the temperature increased, it consistently increased the coating quality. On the other hand, an increase in pressure did not necessarily always correlate with a better coating. Increasing pressure would increase the particle velocity and could therefore increase the plastic deformation of the particles upon impact. However, if the temperature was low with high pressure, it caused erosion of the substrate. Therefore, thermal softening of the particles appeared to be necessary for the binding of the particles to the substrate.

Corrosion Properties of Stainless Steel Coatings

Research on corrosion properties of cold sprayed stainless steel have been promising. Work by Spencer et al. showed that for a 4% porous coating, as the thickness of the coating increased from 40 μm to 305 μm, the corrosion protection increased and the corrosion properties became closer to that of bulk 316L SS [18]. In another piece of work, 316L SS powder was combined with L605 chromium alloy powder to increase the corrosion resistance of cold sprayed stainless steel.

Mixtures were made with 316L SS powder combined with 25%, 33%, or 50% L605 chromium alloy powder by volume. The actual coatings contained 23%, 31%, and 33% of the chromium alloy for the powder mixtures containing 25%, 33%, and 50% of L605 respectively [17]. The coatings obtained with the 25% and 33% L605 powders resulted in porosities below 2% while the 50% L605 powder coating resulted in a porosity of approximately 4.5% and it also contained cracks [17]. Corrosion properties of the coatings were analyzed with a potentio-dynamic polarization test. The 50% L605 powder mixture had poor corrosion properties. However, the 25% and 33% L605 powder coatings had better corrosion resistance than cold sprayed pure stainless steel, and both had a corrosion rate close to bulk stainless steel [17]. Annealing of the coatings further deceased the corrosion rate. Additionally, it was found that after annealing the cold sprayed pure stainless steel coating at 1100°C for one hour, its corrosion properties became close to that of bulk stainless steel as well [17]. Other work has also shown that heat treatments of cold sprayed 316L SS results in a significant decrease in corrosion rate, bringing the corrosion rate much closer to that of bulk 316L SS [21].

Another approach to improve the corrosion properties of cold sprayed coatings is by using a laser post-treatment. Corrosion properties of cold sprayed coatings depend on the overall porosity and the quality of interparticle bonding. Laser post-treatment causes localized melting in the surface of the coating which significantly decreases porosity and causes better bonding of the particles in that region. Therefore, with these properties at the surface of the coating, it can significantly improve the corrosion properties of the whole coating. In work by Sova et al., a laser treated coarse particle coating, an as-sprayed coarse particle coating, an as-sprayed fine particle coating, and bulk 316L SS were subjected to an anodic polarization corrosion test following the ASTM G 5-94 standard. The as-sprayed coarse coating had the worst corrosion properties and had the highest corrosion current density. The finer particle coating had a slightly reduced corrosion current density. The laser treated coarse coating had a significantly lower current density that was close to bulk 316L SS corrosion properties [20]. Table 1 includes the cold spray process parameters used to create different stainless steel coatings.

Table 1. Process inputs and coating properties of cold sprayed 316L SS.

Cold Sprayed 316L SS from the Literature

Author	Powder	Powder shape	Particle diameter: avg. or ranges (µm)	Substrate	Gas	Gas temperature (°C)	Gas pressure (bar)	Standoff distance (mm)	Traverse speed (mm/s)	Deposition thickness (µm)	Post-processing steps	Porosity (%)
AL-Mangour et al. (2013)	75% 316L SS + 25% L605 chromium alloy	316L SS: irregular, L605 chromium alloy: spherical	316L SS: 23.9, L605 chromium alloy: 33.5	mild steel	N2	700	40	80	300	3400	-	1.2
											Heat treated at 400 °C for 1 hr.	1
											Heat treated at 800 °C for 1 hr.	1
											Heat treated at 1000 °C for 1 hr.	<1
											Heat treated at 1100 °C for 1 hr.	<1
	66.6% 316L SS + 33.3% L605 chromium alloy									2500	-	0.81
											Heat treated at 400 °C for 1 hr.	<0.8
											Heat treated at 800 °C for 1 hr.	<0.8
											Heat treated at 1000 °C for 1 hr.	<0.8
											Heat treated at 1100 °C for 1 hr.	<0.8
	50% 316L SS + 50% L605 chromium alloy									470	-	4.45
											Heat treated at 400 °C for 1 hr.	4
											Heat treated at 800 °C for 1 hr.	3.2
											Heat treated at 1000 °C for 1 hr.	2.5
											Heat treated at 1100 °C for 1 hr.	2.5
AL-Mangour et al. (2014)	316L SS	irregular	-45 + 15	mild carbon steel	N2	700	40	80	300	3000	-	1.6
											Heat treated at 400 °C for 1 hr.	0.8
											Heat treated at 800 °C for 1 hr.	≤ 0.2
											Heat treated at 1000 °C for 1 hr.	≤ 0.2
											Heat treated at 1100 °C for 1 hr.	≤ 0.2
					He	350					-	0.2
											Heat treated at 400 °C for 1 hr.	≤ 0.2
											Heat treated at 800 °C for 1 hr.	≤ 0.2
											Heat treated at 1000 °C for 1 hr.	≤ 0.2
											Heat treated at 1100 °C for 1 hr.	≤ 0.2
K. Spencer et al.	316L SS	spherical	-22 µm	cast AZ91 E alloy	He	320	6.2	12	50	<50 to 305	-	4
			-10 µm							-		<1
			-5 µm							-		<1
			50%: -22, 50%: -5							-		-
			50%: -10, 50%: -5							-		<1
M. Villa et al.	316L SS	spherical	31.5	Al-7075-T6	N2	High: 600 - 800	Low: 20 - 40	40	500	463 ± 20	-	-
						High: 600 - 800	Medium: 20 - 40			458 ± 17		-
						High: 600 - 800	High: 20 - 40			495 ± 17		-
						Medium: 600 - 800	Low: 20 - 40			463 ± 32		-
						Medium: 600 - 800	Medium: 20 - 40			479 ± 19		-
						Medium: 600 - 800	High: 20 - 40			474 ± 18		-
						Low: 600 - 800	Low: 20 - 40			336 ± 33		-
						Low: 600 - 800	Medium: 20 - 40			-		-
						Low: 600 - 800	High: 20 - 40			-		-
Sova et al.	316L SS	spherical	18	aluminum	N2	500	40	50	120	1900 and 3800	-	5
									30	1900 and 3800		
			28			600			120	1900 and 3800		5.5
									30	1900 and 3800		
			36			720			120	1900 and 3800		8.5
										1900	Laser treatment on coating	Top: <1
									30	1900 and 3800		
										1900	Laser treatment on coating	Top: <1
Sundararajan et al.	316L SS	-	-45 +15 um	mild steel	Air	475	20	15	-	-	-	0.8
										-	Heat treated at 400 °C for 1 hr.	0.76
										-	Heat treated at 800 °C for 1 hr.	0.36
										-	Heat treated at 1100 °C for 1 hr.	0.2

2.2.2 Titanium Coatings

Density of Titanium Coatings

A wide range of titanium coating porosities have been accomplished through the cold spray process. Commercially pure titanium and Ti-6Al-4V feedstock powder have resulted in porosities ranging from almost no porosity to 22.3% [16], [23]–[27]. Additionally, Hamweendo et al. added nickel to titanium feedstock powder in order to improve the mechanical properties of the coating. This titanium-nickel coating resulted in a porosity between 17% and 30% [26]. In almost all the research found in the literature, titanium was sprayed on metal substrates, but work by Gardon et al. successfully sprayed titanium on Polyetheretherketone (PEEK), a bioinert material, in order to increase the substrate's bioactivity. Gardon et al. was able to deposit titanium powder on PEEK when lower energetic spraying parameters were used; more energetic spraying parameters caused thermal softening of the substrate which caused titanium particles to become embedded in the substrate rather than building up on the substrate to form a coating [28].

In work by Wong et al., titanium was deposited on substrates with both helium and nitrogen. In order to compare the gases, the particle velocities were matched by changing the input pressure and temperature for each gas. At higher particle velocities, the nitrogen coatings were much denser than those achieved by helium. This was probably due to the higher gas temperatures used for the nitrogen coatings. Higher temperatures would have thermally softened the powder particles and the substrate. This thermal softening most likely allowed more plastic deformation and better bonding between the particles and the substrate. After observing this effect from high gas temperatures, Wong et al. sprayed coatings with nitrogen gas at 800°C and a slower traverse speed of 5 mm/s to heat up the substrate even more. This coating resulted in a porosity of approximately 0.1% and oxidation of the substrate around the spraying area was seen. Then nitrogen was sprayed at 800°C and a traverse speed of 150 mm/s and the porosity was found to still be very low, at 0.9%, and no oxidation was seen on the substrate. Additionally, Wong et al. also sprayed a coating with helium gas with an input temperature of 350°C and a pressure of 4 MPa. With these input parameters, a very high particle velocity of 1173 m/s was achieved. The coating that resulted had no detectable porosity. Zahiri et al. also found that using helium instead of nitrogen gas resulted in denser coatings. This work also found that shorter stand-off distances and smaller particles resulted in lower porosities [29].

Other research found that when the powder material and the substrate had similar strength, it resulted in a critical velocity higher than if there was a mismatch in strength between the powder material and substrate. Additionally, when the powder was soft and the substrate hard, it resulted in critical velocities lower than if the powder was hard and the substrate was soft [30]. Research by Christoulis et al. also showed the importance of the substrate and powder combination. This research looked at creating dense coatings on five different substrates with the same coarse titanium powder. These substrates included aluminum AISI 1050-H16, aluminum AISI 2017-T4, copper, stainless steel AISI 304L, and Ti-6Al-4V. The particles that were sprayed on AISI 1050 with nitrogen gas penetrated far into the substrate and many of these particles still appeared to be spherical in shape and the substrate experienced a large amount of deformation. The copper substrate also had significant deformation but less than the AISI 1050 substrate. With the higher strength stainless steel 304L substrate, both the substrate and the particles deformed. With the very hard Ti-6Al-4V substrate, there was minimal deformation in the substrate and substantial plastic deformation in the particles. With nitrogen gas, no coating was formed on the AISI 2017 material. This was most likely due to a thick oxidation layer on the metal. However, when helium gas was used, a coating was formed since this oxidation layer was ruptured with the higher velocity of the particles. The copper, steel, and Ti-6Al-4V substrates were also sprayed with helium gas which resulted in coatings with lower porosities due to the higher impact velocities achieved [31].

As was just discussed, dense coatings of titanium have been created with the cold spray process. Other research though has specifically looked at creating porous coatings which would be beneficial for osseointigration on orthopedic implants. To create these extremely porous coatings, researchers spray titanium with a secondary material and then the secondary material is removed after the cold spray process. Sun et al. sprayed magnesium with titanium and then the magnesium was removed through sintering which resulted in a titanium coating porosity of 48.6% [24]. In other research, Qiu et al. sprayed aluminum with titanium and then the aluminum was removed through alkaline leaching, resulting in a coating porosity of 48 ± 3% [25].

Corrosion Properties of Titanium Coatings

Research by Zhou et al. looked at the corrosion properties of as-sprayed titanium coatings and titanium coatings that had been heat treated at 850°C for 5 hours in Argon with 5% hydrogen.

A potentiodynamic polarization test was run on these coatings, bulk titanium, and heat treated bulk titanium. The results from the test showed that the heat treatment of the cold sprayed coating substantially decreased the corrosion rate, increased the corrosion potential, and stabilized the coating at high potentials. Zhou et al. also averaged the corrosion potential and corrosion current from the polarization curves. The heat treated coating had a decrease in corrosion current (0.45 ± 0.05 $\mu A/cm^2$ compared to 1.37 ± 0.09 $\mu A/cm^2$) and an increase in corrosion potential (-445 mV compared to -376 mV) [32]. This indicated that the heat treatment significantly improved the corrosion properties of the coating. This heat treated coating had a comparable corrosion potential to the bulk titanium that had a corrosion potential of -326 mV [32]. However, the heat treated coating still had a much higher corrosion current compared to bulk titanium (0.13± 0.03 $\mu A/cm^2$) and heat treated bulk titanium (0.14± 0.05 $\mu A/cm^2$) [32].

Titanium-hydroxyapatite coatings and bioactivity and cytotoxicity tests

Research papers have also looked at adding hydroxyapatite (HA) to titanium coatings for osseointegration. Choudhuri et al., used 20% and 50% HA mixed with either commercially pure titanium (CP-titanium) or sponge titanium to create coatings. Any HA mixture with the spherical titanium could not be built up on the substrate. However, with the sponge titanium, the 20% HA mixture resulted in a dense coating while the 50% HA mixture resulted in a coating with broken HA particles and a limited coating thickness [33]. As stated earlier, Qui et al. used the technique of spraying aluminum with titanium and then removed the aluminum through alkaline leaching to create porous coatings. Qui et al. also sprayed three-part mixtures of titanium, aluminum, and HA to create coatings that could help initiate osseointegration. Powder mixtures of 50% Ti, 45% Al, and 5% HA and mixtures of 50% Ti, 40% Al, and 10% HA were used with two different HA powders to create four different mixtures with HA. All of the coatings produced with HA resulted in porosities greater than 60% [25]. Also in this research, an in vitro biological test was done in simulated body fluid (SBF) which showed that the HA coatings had significantly more Ca^{2+} mineralization than the coating without HA, and the 10% HA coatings had approximately twice as much mineralization as the 5% HA coatings [25]. Qui et al. also performed a cytotoxicity test for 48 hours on the 10% HA coatings and the HA-free coating. All of the coatings either maintained the same number of cells or there was an increase in cell viability, which indicated that the coatings

were not toxic to the cells [25]. A table of the cold spray parameters used for titanium coatings can be seen in Table 2.

Table 2. Process inputs and coating properties of cold sprayed titanium.

Cold Sprayed Titanium from the Literature												
Author	Powder	Powder shape	Particle diameter: avg. or ranges (μm)	Substrate	Gas	Gas temperature (°C)	Gas pressure (bar)	Standoff distance (mm)	Traverse speed (mm/s)	Deposition thickness (μm)	Post-processing steps	Final porosity (%)
Choudhuri et al. [33]	Ti	spherical	45	Ti and Al	N2	500	25	25	400	-	-	-
						500	35		400	-		-
						500	35		100	-		-
	80% Ti + 20% HA	Ti: spherical HA: spherical	Ti: 45, HA: -			700	38		between 50 and 400	10		-
	Ti	sponge	45			500	35			-		-
	80% Ti + 20% HA	Ti: sponge HA: spherical	Ti: 45, HA: -			600	35			-		-
	50% Ti + 50% HA					700	30			200		-
Christoulis et al. [31]	Ti	spherical	60, -70 + 45	aluminum: AISI 1050-H16	N2	550	30	40	100	660	-	10.1
					He	450				-		-
				aluminum: AISI 2017-T4	N2	550				0		-
					He	450				1400		1.2
				copper	N2	550				700		10.4
					He	450				1400		0.8
				stainless steel: AISI 304L	N2	550				661		10.3
					He	450				1360		1.8
				Ti-6Al-4V	N2	550				589		13.2
					He	450				1320		3.0
Cizek et al. [16]	Ti	irregular	5 to 29	Ti-6Al-4V	He	260	16.7	12	40	650	-	2.7
Gardon et al. [28]	Ti	angular	20 to 90	PEEK	N2	-	-	-	-	1000	-	-
						-	-	-		-		-
						-	-	-		-		-
						-	-	-		-		-
Hamweendo et al. [26]	50% Ti + 50% Ni	Ti: angular Ni: irregular	-	steel	Air	-	-	-	10	-	-	-
				copper		-	-	-		-		17.0 to 30.0
	Ti	angular				-	-	-		-		-
Li et al. [23]	Ti	angular	22.4	Ti-6Al-4V	Air	520	28	30	-	-	-	5.4
										-	Vacuum heat treatment at 850°C for 4 hr.	21.6
	Ti-6Al-4V	spherical	47							-	-	22.3
										-	Vacuum heat treatment at 850°C for 4 hr.	29.7

Table 2 continued. Process inputs and coating properties of cold sprayed titanium.

Cold Sprayed Titanium from the Literature

Author	Powder	Powder shape	Particle diameter: avg. or ranges (μm)	Substrate	Gas	Gas temperature (°C)	Gas pressure (bar)	Standoff distance (mm)	Traverse speed (mm/s)	Deposition thickness (μm)	Post-processing steps	Final porosity (%)
Qiu et al. [25]	50% Ti+ 50% Al	Ti: irregular Al: irregular	Ti: <20, Al: 75 to 105	annealed grade 2 CP-Ti	He	370	6.9	12.5	1.67	-	Al removed by alkaline leaching. Vacuum heat treatment at 1200°C for 2 hr.	48
	50% Ti + 45% Al + 5% HA	Ti: irregular Al: irregular HA: spherical	Ti: <20, Al: 75 to 105 , HA: 15							-	Al removed by alkaline leaching. Vacuum heat treatment at 800°C for 16 hr.	61
	50% Ti + 40% Al + 10% HA									-		63
	50% Ti + 45% Al + 5% HA	Ti: irregular Al: irregular HA: spherical	Ti: <20, Al: 75 to 105 , HA: 25							-		66
	50% Ti + 40% Al + 10% HA									-		65
Sun et al. [24]	25% Ti + 75% Mg	spherical	Ti: 10 to 45 Mg: 63 to 73	Ti	He	340	10	-	-	-	Vacuum sintering at 1250°C for 1 hr. Mg completely removed by evaporation.	48.6
Wong et al. [27]	Ti	spherical	29	mild carbon seel	N2	300	30	40	330	605	-	Top= 20.6 Bottom=19.5
					He	100	5			797		Top= 14.6 Bottom=10.8
					N2	600	30			1344		Top= 7.8 Bottom=5.0
					He	70	7.5			1030		Top= 13.2 Bottom=10.2
					N2	800	40			1172		Top= 1.9 Bottom=1.7
					He	50	14			1064		Top= 10.1 Bottom=7.0
					N2	800	40		150	-		0.9
					N2	800	40		5	-		0.1
					He	350	40	8	330	-		0.0
Zahiri et al. [29]	Ti	angular	22	aluminum	N2	600	24	20	1.667	-	-	9.5
							24	50		-		10.0
							24	80		-		12.5
							24	100		-		14.0
							24	20		-		8.0
			16							-		0.5
					He		15	20		-	Heat treatment at 450°C for 30 min.	-
Zhou et al. [32]	Ti	irregular	-325	wrought Ti	N2	500	35	15	-	600	-	-
											Heat treated at 850°C in Argon with 5% hydrogen for 5 hr.	-

2.2.3 Tantalum Coatings

Density of Tantalum Coatings

Cold sprayed tantalum has resulted in very dense coatings. In work by Kumar et al. the porosity of as-sprayed tantalum with compressed air was less than 0.3%, while coatings that had a post-spraying heat treatment for 2 hours at 500°C resulted in less than 0.2% porosity and heat treatments at 750°C and above resulted in less than 0.1% porosity [34]. Work by Texler et al. optimized process inputs to spray tantalum coatings. The optimized coatings with nitrogen gas had comparable coating quality to coatings created by more expensive helium gas. Coating densities and tensile strengths were very comparable between the coatings created from the two gases [35].

Corrosion Properties of Tantalum Coatings

Corrosion studies on cold sprayed tantalum coatings have also been performed. Koivuluoto et al. compared on older cold spray system to a new model which allowed higher input pressures and temperatures to see the difference in the corrosion properties of the coatings from the two systems. The older system used a temperature of 530°C and a pressure of 32 bar while the newer system used 800°C and 38 bar. Koivuluoto et al. also used a finer particle size with the newer spraying system (-30+10 μm compared to -38+10 μm). Open-cell potential measurements were taken and the coating created from the older system had a potential close to that of the substrate, while the coating from the newer system had a potential close to that of bulk tantalum [36]. This result suggests that the coating created from the older system had through porosity to the substrate while the coating from the new system did not have through porosity from the surface to the substrate. A salt spray fog test was also done on the newer system coating and no changes were seen on the surface suggesting that the coating was dense [36]. Koivuluoto et al. also performed polarization corrosion tests in a 3.5 wt% NaCl and 40 wt.% H_2SO_4 solution. The results showed that the newer system coating and bulk tantalum had corrosion current densities very similar to each other in both solutions while the coating created from the older system had a much higher corrosion current density [36].

In another piece of work, Kumar et al. conducted a polarization test in a 1 M KOH solution for bulk tantalum, an as-sprayed tantalum coating, and tantalum coatings heat treated at 500, 750, 1000, 1250, and 1500°C. This paper showed that as the heat treatment temperature increased, the corrosion current density decreased from 7.184 $\mu A/cm^2$ to 0.703 $\mu A/cm^2$, approaching the corrosion current density of bulk tantalum which is 0.528 $\mu A/cm^2$ [34]. Therefore, higher heat treatments helped improve the corrosion properties of cold sprayed tantalum. A table of the cold spray parameters used for tantalum coatings can be seen in Table 3.

Table 3. Process inputs and coating properties of cold sprayed tantalum.

Cold Sprayed Tantalum from the Literature												
Author	**Powder**	**Powder shape**	**Particle diameter: avg. or ranges (µm)**	**Substrate**	**Gas**	**Gas temperature (°C)**	**Gas pressure (bar)**	**Standoff distance (mm)**	**Traverse speed (mm/s)**	**Deposition thickness (µm)**	**Post-processing steps**	**Porosity (%)**
Koivuluoto et al. [36]	Ta	angular	-38 + 10	carbon steel: Fe52	N2	530	32	-	-	470	-	-
			-30 + 10			800	38			450		-
Kumar et al. [34]	Ta	sponge	15 - 45	steel	Air	450	20	15	10	800	-	< 0.3
											Vacuum heat treated at 500°C for 2 hr.	< 0.2
											Vacuum heat treated at 750°C for 2 hr.	< 0.1
											Vacuum heat treated at 1000°C for 2 hr.	< 0.1
											Vacuum heat treated at 1250°C for 2 hr.	< 0.1
											Vacuum heat treated at 1500°C for 2 hr.	< 0.1
Trexler et al. [35]	Ta	angular	< 40	aluminum	N2	-	-	-	-	-	-	-
					He					-	-	-
					N2					-	annealed	-
					He					-	annealed	-

2.2.4 Hydroxyapatite Coatings

Density of Hydroxyapatite Coatings

Hydroxyapatite is a very common material used on the surfaces of dental and orthopedic implants to promote osseointegration. Plasma spray is the most commonly used process to deposit HA. However, the high temperatures of this process can cause the HA to change into other calcium phosphate phases. Therefore, depositing HA with the cold spray process could eliminate this problem since it uses much lower temperatures. Cold spray systems using room temperature compressed air and preheated substrates have resulted in dense HA coating between 10 μm and 50 μm thick [37], [38]. A fractional factorial experimental design was created by Hasniyati et al. to optimize cold sprayed HA. From those experiments, the standoff distance, surface roughness, and substrate heating temperature were found to be significant factors for the thickness, nanohardness, and elastic modulus of the coatings [37].

Bioactivity of Hydroxyapatite Coatings

In work done by Noorakma et al., a magnesium alloy was cold sprayed with a hydroxyapatite coating and tests were run in simulated body fluid (SBF). The average thickness of the HA coatings were 25 μm. Parts were placed in SBF for 14 days and the solution pH was monitored. Coatings were checked at day 0, 1, 4, 10, and 14. At day 10, HA coatings showed apatite formation and continued apatite formation through day 14 [38]. This coated magnesium alloy proved to be both biodegradable and bioactive, two good qualities that are needed in many medical applications. A table of the cold spray parameters used for hydroxyapetite coatings can be seen in Table 4.

Table 4. Process inputs and coating properties of cold sprayed hydroxyapatite.

Cold Sprayed Hydroxyapetite from the Literature										
Author	Powder	Average particle diameter (µm)	Substrate	Gas	Substrate preheated temperature (°C)	Substrate surface roughness (grit of sandpaper)	Gas temperature (°C)	Gas pressure (bar)	Standoff distance (mm)	Deposition thickness (µm)
Hasniyati et al. [37]	HA	5	magnesium	Air	550	2000	room temp	10	40	21.96
					350	2000			20	18.73
					350	2000			20	18.19
					350	2000			40	13.03
					550	240			40	23.56
					550	240			40	24.43
					550	2000			40	21.84
					350	240			40	20.31
					550	2000			20	32.63
					350	2000			40	17.48
					550	240			20	49.77
					350	240			40	21.48
					550	240			20	39.08
					350	240			20	35.09
					350	240			20	38.97
					550	2000			20	25.58
Noorakma et al. [38]	HA	4	magnesium alloy: AZ51	Air	400	1000	room temp	10	40	25

2.2.5 UHMWPE Coatings

Cold spray systems have also been used to deposit the biocompatible polymer UHMWPE. Work done by Ravi et al. showed that UHMWPE coatings, from 60 μm particles, could be deposited with coating thicknesses of 3 mm and 1 mm for aluminum and polypropylene substrates, respectively. When trying to spray with a converging-diverging nozzle followed by a 100 mm diverging nozzle, UHMWPE coatings could not be created. However, after adding on a second diverging nozzle to the end of the first, it created a discontinuity of the stream between the two nozzles, therefore allowing the gas particles to decelerate and increase the temperature of the stream. This addition of the second diverging nozzle allowed for thermal softening of the particles which would help increase the particles' plastic deformation upon impact. This setup resulted in a monolayer being formed on the aluminum substrate but caused erosion on the polypropylene substrate. In order to improve the coatings, Ravi et al. added 4% nano-alumina to the feedstock [39]. This nano-alumina could then bind to the surface of the UHMWPE particles and increase the UHMWPE-UHMWPE particle bonding. With this mixture, 3-4 mm thick coatings were deposited on aluminum when the input temperature was 350°C and the input pressure was between 3 bar and 4 bar. With the polypropylene substrate, 1 mm thick coatings were achieved when the input temperature was 170°C and the input pressure was between 3 bar and 4 bar. Additionally, the UHMWPE coating on the aluminum substrate showed signs of delamination so the coating was heated at 200°C for 10 minutes to improve the bond. The deposited and rebounded particles were also analyzed with differential scanning calorimetry. The particles in the coating showed signs of melting and recrystallizing while the particles that were rebounded did not melt during the cold spray process. This melting may be essential to the deposition of the UHMWPE particles onto the substrate. Table 5 includes the cold spray process parameters used to create the UHMWPE coatings.

2.2.6 TiO_2 Coatings

Some less conventional cold spray feedstock powders, such as TiO_2 have been researched for medical applications as well. Kliemann et al. cold sprayed TiO_2 onto four different substrates: pure titanium, stainless steel, copper, and aluminum. All coatings of TiO_2 were minimal and

deposition efficiencies were less than 6% [40]. TiO_2 coatings could only be produced on the most ductile of substrates, and even then, the particles of TiO_2 on the substrate were crushed. Additionally, the coating could not build up past a first initial layer, because new ceramic particles bounced off the thin, non-ductile ceramic coating already present on the substrate. Table 5 includes the process inputs used for the TiO_2 coatings.

Table 5. Process inputs and coating properties of cold sprayed UHMWPE and TiO_2.

Cold Sprayed UHMWPE and TiO2 from the Literature												
Author	**Powder**	**Powder shape**	**Particle diameter: avg. or ranges (μm)**	**Substrate**	**Accelerating gas**	**Gas temperature (°C)**	**Gas pressure (bar)**	**Standoff distance (mm)**	**Traverse speed (mm/s)**	**Deposition thickness (μm)**	**Deposition efficiency (%)**	**Post-processing steps**
Ravi et al. [39]	UHMWPE	UHMWPE: irregular	60	aluminum	Air	350-380	3 to 4	5-20 mm	-	45	-	
				polypropylene						No coating. Errosion of surface.	-	
	96% UHMWPE + 4% nano-alumina	UHMWPE: irregular, nano-alumina: -	UHMWPE: 60, alumina: -	aluminum		350				3000 to 4000	-	Heat treated at 200°C for 10 min.
				polypropylene		170				1000	-	
Kliemann et al. [40]	TiO2	spherical	3 to 50	titanium	N2	800	40	60	320	-	>5 on first pass	-
				stainless steel: AISI 304						-	~5 on first pass	
				copper						-	>3 on first pass	
				aluminum alloy: AlMg3						-	>2 on first pass	

2.2.7 Cold Sprayed Biocompatible Materials Conclusion

Several different biocompatible coatings have been created with the cold spray process. Dense coatings of stainless steel, titanium, tantalum, HA, and UHMWPE have been accomplished. Furthermore, research on cold sprayed metals showed that post-spray heat treatments can decrease coating porosity. In general, coating porosity decreased and coating thickness increased with an increase in input gas temperature and pressure. However, high pressures without a significant amount of heat can cause erosion of the substrate. Additionally, lower porosity coatings could be achieved when the powder had smaller particle sizes. Very porous coatings of titanium were also accomplished through several methods, some of which included secondary materials in the powder feedstock that were removed after the cold spray process. Although successful coatings have been accomplished for some biomaterials, good quality TiO_2 coatings have not been accomplished due to the material's low ductility and brittle nature. Corrosion properties tended to improve with increased coating thickness, reduced porosity, and improved metallurgic bonds. For highly dense coatings with strong metallurgic bonds, corrosion properties are similar to bulk material.

Bioactivity and cytotoxicity tests have also been performed on titanium coatings and titanium coatings with HA. The results showed that the titanium coatings with HA had significant Ca2+ mineralization and did not appear to be toxic to the cells. Pure HA coatings have also been tested in SBF and showed good bioactive properties.

2.3 Mechanical Properties of Cold Sprayed Biocompatible Materials

Many cold sprayed biocompatible materials have also had different tests conducted on them in order to document the mechanical properties of the coatings. The types of mechanical tests are wide ranging: adhesion and cohesion strength tests, three-point bending tests, compression strength tests, lug shear tests, fatigue tests, hardness tests, tensile strength tests, and abrasion tests. The following section is a review of the mechanical properties found for biocompatible coatings created by the cold spray process. The mechanical properties of dense coatings are compared to that of bulk material and porous coatings are compared to that of bulk material as well as porous coatings achieved through other thermal spray methods.

2.3.1 Mechanical Properties of Stainless Steel Coatings

As was discussed earlier in section 2.2.1, Villa et al. varied cold spray process parameters for 316L SS feedstock with nitrogen gas temperatures between 600°C and 800°C and pressures between 20 bar and 40 bar. Hardness tests were conducted on the materials resulting from each varied input. The tests were performed according to the ASTM E38 standard. Hardness values ranged from 310 ± 61 HV to 358 ± 36 HV, depending on process parameters [22]. Also, Villa et al. tested the hardness of the feedstock powder and found a hardness value of 180 ± 45 HV. Bulk medical grade 316L SS has a hardness value generally ranging from 170 HV to 220 HV [4]. The tested powder was in this range but the coating had a much higher hardness value. The higher hardness values seen in the coatings were probably due to work hardening of the material during the cold spray process.

Sova et al. also measured high hardness in 316L SS cold sprayed coatings which would indicate work hardening. The smallest particle size distribution resulted in ~290 HV and the largest particle size distribution resulted in ~330 HV [20]. A laser post-treatment was also conducted on the coarse particle coating. The laser treated area had a reduced hardness of ~170 HV [20]. Sova et al. also tested the adhesion strength of these coatings to their aluminum substrates and found for all coatings the adhesion strength was between 80 MPa and 85 MPa [20].

Further work by Villa et al. analyzed the wear resistance of a cold sprayed 316L SS coating and found a wear rate of $0.9*10^{-4}$ mm^3/Nm, which was a similar wear rate to coatings obtained through the high-velocity oxy-fuel (HVOF) process, with values ranging from $1.15*10^{-4}$ mm^3/Nm to $1.60*10^{-4}$ mm^3/Nm [41].

As mentioned earlier, AL-Mangour et al. (2014) conducted heat treatments on cold sprayed coatings and saw a reduction in coating porosity. Additionally, how the heat treatments affected the mechanical properties of the coatings was analyzed as well. These properties were analyzed for nitrogen and helium process gas. The results showed that the as-sprayed coatings resulted in hardness values of 393 ± 14 HV and 452 ± 16 HV for the nitrogen gas and helium gas, respectively [19]. The hardness of the coatings were much higher than the hardness of the as-received powder and that of bulk material. Again, this would suggest a work hardening effect on the particles from the cold spray process. The coatings showed an increase in hardness after annealing at 400°C and

a decrease in hardness after annealing at temperatures 700°C and above. Annealing at 1100°C lowered the coating hardness for both nitrogen and helium gas coatings to a value close to that of the as-received powder (185 ± 15 HV) [19]. The nitrogen coating annealed at 1100°C resulted in a hardness values of ~175 HV, while the helium coating annealed at 1100°C resulted in a hardness value of ~195 HV [19]. Other work by Sundararajan et al. found that heat treatments between 400 °C and 1100°C consistently decreased the hardness of their coatings and substantially increased the elastic modulus. As sprayed specimens had an elastic modulus of 98.43 GPa while heat treated specimens at 1100 °C had an elastic modulus of 164.42 GPa [21].

AL-Mangour et al. (2014) also tested the tensile strength of their coatings, following the ASTM E8 standard with rectangular specimens. AL-Mangour et al. (2014) conducted two tensile tests for as-sprayed nitrogen samples and nitrogen samples annealed at 400, 800, 1000, and 1100°C and only one sample was tensile tested for the as-sprayed helium and helium samples annealed at 1000, and 1100°C. The tensile strength of the as-sprayed helium coating, 230 MPa, was approximately twice that of the as-sprayed nitrogen coating at 113 ± 5 MPa [19]. Annealing of the nitrogen coatings at 800°C and above caused an increase in the tensile strength with a maximum strength of 571 ± 50 MPa after a heat treatment at 1000°C [19]. However, annealing of the helium coating at 1000°C or 1100°C showed no increase in the tensile strength of the coating, possibly due to the formation of small pore defects along the boundaries of the interconnected particles after annealing. For both coatings, the annealing process generally increased the ductility of the coatings [19]. AL-Mangour et al. (2014) also tensile tested bulk 316L SS and found a tensile strength of 1048 ± 6 MPa and it had an elongation of 91 ± 11%. According to the ASM Medical Materials Database, bulk 316L SS for medical applications generally has a tensile strength of 341 MPa to 1007 MPa and an elongation of 22.3 to 57.7% [4]. Therefore, the tensile strengths from the as-sprayed coatings were well below the value seen in bulk material. However, the nitrogen coating annealed at 1000°C led to a tensile strength of 571 ± 50 MPa and an elongation of 14.2 ± 1.1% which was a major improvement from the as-sprayed coatings. This tensile strength is also much closer to the bulk material in the experiment and the tensile strength is within the range listed for 316L SS in the ASM Medical Materials Database although the ductility was still limited.

As was discussed earlier, other work by AL-Mangour e-t al. (2013) created thick coatings from 316L SS feedstock with an added chromium alloy, L605, to improve the strength of the

coating. Hardness values for these coatings included 432.8 HV, 440.3 HV, and 301 HV for 25%, 33%, and 50% L605 feedstock powder, respectively [17]. Additionally, tensile tests were conducted with the ASTM E8 standard on the 25% and 33% L605 feedstock coatings. The tensile strengths were ~150 MPa and ~180 MPa for the as-sprayed 25% and 33% L605 feedstock coatings, respectively [17]. Annealing at 400, 800, 1000, and 1100°C continually increased the tensile strength and ductility of the coatings. The 33% L605 coating reached a maximum tensile strength of 685 MPa and a ductility of ~19% after being annealed at 1100°C [17]. The mechanical properties of cold sprayed 316L SS can be seen in Table 6.

Table 6. Mechanical properties of cold sprayed 316L SS.

Cold Sprayed 316L SS from the Literature

Author	Powder	Substrate	Post-processing steps	Mechanical strength test	Elongation (%)	Elastic Modulus (GPa)	Tensile strength (MPa)	Adhesion strength (MPa)	Other mechanical tests	Other mechanical test results
AL-Mangour et al. (2013) [17]	75% 316L SS + 25% L605 chromium alloy	mild steel	-	ASTM E8 standard	~5	-	~150	-	Vickers microhardness test	432.8 HV
			Heat treated at 400 °C for 1 hr.		~5	-	~150	-		-
			Heat treated at 800 °C for 1 hr.		~8	-	~500	-		-
			Heat treated at 1000 °C for 1 hr.		~13	-	~610	-		-
			Heat treated at 1100 °C for 1 hr.		~19	-	~660	-		-
	66.6% 316L SS + 33.3% L605 chromium alloy		-		~3	-	~180	-		440.3 HV
			Heat treated at 400 °C for 1 hr.		~2	-	~200	-		-
			Heat treated at 800 °C for 1 hr.		~4	-	~450	-		-
			Heat treated at 1000 °C for 1 hr.		~11	-	~640	-		-
			Heat treated at 1100 °C for 1 hr.		~19	-	~685	-		-
	50% 316L SS + 50% L605 chromium alloy		-		-	-	-	-		301 HV
			Heat treated at 400 °C for 1 hr.		-	-	-	-		-
			Heat treated at 800 °C for 1 hr.		-	-	-	-		-
			Heat treated at 1000 °C for 1 hr.		-	-	-	-		-
			Heat treated at 1100 °C for 1 hr.		-	-	-	-		-
AL-Mangour et al. (2014) [19]	316L SS	mild carbon steel	-	MTS 810 at room temp. ASTM E8 standard for rectangular specimens.	1.3 ± 0.1	-	113 ± 5	-	Vickers microhardness test	~393 ± 14 HV
			Heat treated at 400 °C for 1 hr.		1 ± 0.1	-	91 ± 9	-		~425 HV
			Heat treated at 800 °C for 1 hr.		3.7 ± 1.0	-	349 ± 56	-		~225 HV
			Heat treated at 1000 °C for 1 hr.		14.2 ± 1.1	-	571 ± 50	-		~190 HV
			Heat treated at 1100 °C for 1 hr.		22.7 ± 3.6	-	433 ± 39	-		~175 HV
			-		-	-	230	-		~452 ± 16 HV
			Heat treated at 400 °C for 1 hr.		-	-	-	-		~460 HV
			Heat treated at 800 °C for 1 hr.		-	-	-	-		~260 HV
			Heat treated at 1000 °C for 1 hr.		10.6	-	202	-		~235 HV
			Heat treated at 1100 °C for 1 hr.		12.8	-	230	-		~195 HV
M. Villa et al. [22]	316L SS	Al-7075-T6	-	-	-	-	-	-	Vickers microhardness test. Abrassive wear test following the ASTM G65-04 standard.	338 ± 44 HV
					-	-	-	-		340 ± 66 HV
					-	-	-	-		358 ± 36 HV; wear rate of
					-	-	-	-		353 ± 36 HV
					-	-	-	-		314 ± 58 HV
					-	-	-	-		333 ± 57 HV
					-	-	-	-		310 ± 61 HV
					-	-	-	-		-
					-	-	-	-		-
Sova et al. [20]	316L SS	aluminum	-	Coating adhesion strength test using the pin method	-	-	-	82	Vickers microhardness test	~290 HV
			-		-	-	-			
			-		-	-	-			
			-		-	-	-			
			-		-	-	-	80		~300 HV
			-		-	-	-			
			-		-	-	-			
			-		-	-	-			
			Laser treatment on coating		-	-	-	80		~330 HV for normal area of coating and ~170 HV for the laser treated section
			-		-	-	-	85		
			Laser treatment on coating		-	-	-	80		
Sundararajan et al. [21]	316L SS	mild steel	-	Elastic modulus from nanoindent	-	98.43	-	-	Vicers microhardness test	2.924 Gpa; 98.43 Gpa
			Heat treated at 400 °C for 1 hr.		-	104.89	-	-		2.604 Gpa, 104.89 Gpa
			Heat treated at 800 °C for 1 hr.		-	161.8	-	-		2.202 Gpa, 161.80 Gpa
			Heat treated at 1100 °C for 1 hr.		-	164..42	-	-		2.114 Gpa, 164.42 Gpa

2.3.2 Mechanical Properties of Titanium Coatings

Dense as well as very porous coatings of titanium have been created with the cold spray process. In work by Choudhuri et al., the strength of multiple titanium coatings were tested with a pull-off adhesion/cohesion test. The coatings tested included coatings from spherical titanium feedstock, sponge titanium feedstock, and coatings with a mixed feedstock of sponge titanium and HA. The cohesion strength for spherical titanium coatings were 15.3 MPa and 47.4 MPa for transverse speeds of 400 mm/s and 100 mm/s respectively [33]. For the sponge titanium coatings, failure of the tests were within the epoxy, suggesting that the adhesion and cohesion strength of the coating was greater than that of the epoxy that had a strength of ~65 MPa [33]. The spherical titanium cohesion strength was well below the tensile strength of bulk titanium which ranges from 240 MPa to 670 MPa [4], [42]. Since the sponge titanium coating adhesion test failed in the epoxy, its tensile strength could not be determined. However, the tensile strength must be greater than 65 MPa. The coatings of sponge titanium with hydroxyapatite failed in cohesion as well at 24.45 MPa and 18.2 MPa for 20% and 50% hydroxyapatite in the powder feedstock, respectively [33]. Choudhuri et al. also mentions that these adhesion/cohesion strengths of the coatings are comparable or better than results given in the literature for plasma sprayed HA coatings at ~10-15 MPa.

Wong et al. also looked at mechanical properties of dense titanium coatings. These coatings were sprayed with both helium and nitrogen. Hardness measurements were similar for coatings created from helium and nitrogen gas. The hardness measurements ranged from 161 HV to 218 HV on these coatings [27]. Also, this research showed consistently higher hardness values near the substrate and lower hardness values near the surface of the coating. A similar trend in hardness for as-sprayed titanium coatings was seen in work by Zhou et al. In that work, the hardness at the surface was 172 ± 22 HV while the hardness near the substrate was 221 ± 18 HV [32]. This trend in hardness can be attributed to the coating being denser near the substrate and more porous near the surface. The denser coating is created near the substrate due to more deformation in the particles. These particles are deformed when they deposit and then they are deformed again by other particles impacting on them. The particles near the surface of the coating however are only deformed when they deposit since no following particles impact on them. This added deformation in the particles near the substrate causes this section of the coating to be harder. In both the work

by Wong et al. and the work by Zhou et al., the resulting hardness values are below that of two recorded hardness values of bulk material, 264 ± 14 HV [9] and 200.26 ± 5.43 HV [10]. This is contradictory to what has been found in other cold spray research. Other research has shown work hardening of the particles during the deposition process [19], [22], [34], [35]. Zhou et al. contributed the observed lower hardness to the sponge titanium powder that was used. However, this same theory would not be able to be applied to the work done by Wong et al. since spherical particles were used. Wong et al. did notice that the particles and substrate that experienced the highest temperature led to the lowest hardness value. This could be due to thermal effects that softened the coating. [29]. Additionally, Zhou et al. annealed the coatings in their research which caused an increase in the hardness, the opposite of what is usually seen after annealing cold sprayed coatings. Again, Zhou et al. attributes this to a more homogenous coating being formed and removing the defects seen in sponge titanium. This may be further supported by other research by Zahiri et al. which found that hardness values increased with lower porosity in the cold sprayed material. In the work by Zahiri et al., a large range of hardness values were obtained depending on the coating porosity. When the porosity was low enough, it resulted in hardness values greater than that seen in bulk material, again suggesting a work hardening effect from the cold spray process. When the least porous coating (less than 0.5%) was heat treated, this did result in a decrease in the coating hardness to a hardness value close to annealed grade 2 CP titanium [29].

In another piece of work, Cizek et al. cold sprayed Ti-6Al-4V substrates with pure titanium and then fatigue tested the specimens. The cold sprayed specimens had a shorter fatigue life compared to plasma sprayed, grit blasted, and as received Ti-6Al-4V substrates. Cizek et al. mentions that this short fatigue life may be due to the direction that the cracks formed and propagated (orthogonal to the coating surface). Additionally, Cizek at al. calculated the elastic modulus from the resonance frequencies from the fatigue experiments. The cold sprayed coating had an elastic modulus of 31.2 GPa, which Cizek et al. mentions is 31.6% of the elastic modulus of bulk titanium which is 116 GPa [16]. This value for bulk titanium that Cizek et al. uses is close to that found in the ASM Medical Materials Database which has the elastic modulus ranging from 99 to 111 GPa [4]. Therefore, the as-sprayed coating had an elastic modulus significantly lower than that of bulk titanium.

As described earlier, Sun et al. created very porous coatings of titanium by spraying titanium with magnesium and then later removing the magnesium through a sintering process. Sun et al. tested this 48.6% porous coating with an adhesion and cohesion test following the ASTM C633 standard and failure occurred at 42 MPa. Most of the failure occurred in the epoxy which indicated that both the cohesion and adhesion strength were greater than 42 MPa [24]. This adhesion strength is greater than the adhesion strength achieved for porous titanium coatings created from plasma spray which failed at <10 MPa [44].

Sun et al. also conducted a three-point bending test and a compression test on the coatings. The resulting bending modulus was 14.47 ± 1.21 GPa and the bending strength was 106.93 ± 10.79 MPa [24]. The compressive modulus and compressive yield strength were 3.99 ± 0.12 GPa and 178.66 ± 13.20 MPa, respectively [24]. Sun et al. mentions that bulk titanium implants have a bending and compressive modulus around 105 GPa, which is much higher than what was seen in these coatings. However, Sun et al. mentions that the lower modulus and strength values could be beneficial for orthopedic implants. Many orthopedic implants that are placed in bones have high modulus values which causes them to take a significant amount of the load placed on the bone. This causes the bone around the implant to experience less stress. This absence of stress in the bone causes the bone to become less dense and weaker. Therefore, this porous material that Sun et al. created could allow for better bone ingrowth because of the porous nature and the lower modulus of the material would help avoid significant stress shielding in the bone.

The other research conducted by Qui et al. also created porous titanium coatings. Qui et al. cold spraying 50% titanium, 40% aluminum, and 10% HA for two different HA particles. Qui et al. then removed the aluminum with alkaline leaching and the coatings were then annealed at 800°C for 16 hours. Lug shear tests resulted in a shear strength of 20 MPa for the coatings, which was half of the shear strength that the coatings had before the removal of the aluminum [25]. Since this was a very porous coating, the shear strength was expected to be well below the bulk titanium shear strength of 290 MPa [4]. A table of the cold sprayed titanium materials and their mechanical properties can be seen in Table 7.

Table 7. Mechanical properties of cold sprayed titanium.

Cold SprayedTitanium from the Literature									
Author	Powder	Substrate	Post-processing steps	Mechanical strength test	Elastic Modulus (GPa)	Yield strength (Mpa)	Tensile strength (MPa)	Other mechanical tests	Other mechanical test results
Choudhuri et al. [33]	Ti	Ti and Al	-	Pull-of adhesion bond test	-	-	-	-	-
					-	-	15.3		-
					-	-	47.4		-
	80% Ti + 20% HA				-	-	-		-
	Ti				-	-	>65		-
	80% Ti + 20% HA				-	-	24.45		-
	50% Ti + 50% HA				-	-	18.2		-
Cizek et al. [16]	Ti	Ti-6Al-4V	-	Elastic modulus calculated from resonance frequency of material	36.7	-	-	Fatigue test. Result is listed as life cycles compared to as-received substrate.	0.91
Qiu et al. [25]	50% Ti+ 50% Al	annealed grade 2 CP-Ti	Al removed by alkaline leaching. Vacuum heat treatment at 1200°C	-	-	-	-	Lug shear test	-
	50% Ti + 45% Al + 5% HA (15 µm)				-	-	-		-
	50% Ti + 40% Al + 10% HA (15 µm)		Al removed by alkaline leaching. Vacuum heat treatment at 800°C for 16 hr.		-	-	-		20 MPa
	50% Ti + 45% Al + 5% HA (25 µm)				-	-	-		-
	50% Ti + 40% Al + 10% HA (25 µm)				-	-	-		18 MPa
Sun et al. [24]	25% Ti + 75% Mg	Ti	Vacuum sintering at 1250°C for 1 hr. Mg completely removed by evaporation.	Adhesion/cohesion test according to ASTM-C633	-	-	42	Three-point bending test. Compression test.	Bending Young's modulus: 14.47±1.21 Gpa; bending strength: 106.93± 10.79 Mpa. Compressive Young's modulus: 3.99 ± 0.12 GPa; compressive yield strength:178.66± 13.20 Mpa.
Wong et al. [27]	Ti	mild carbon seel	-	-	-	-	-	Vickers microhardness test	Top=190 HV; Bottom=192 HV
					-	-	-		Top=187 HV; Bottom=188 HV
					-	-	-		Top=187 HV; Bottom=203 HV
					-	-	-		Top=188 HV; Bottom=194 HV
					-	-	-		Top=205 HV; Bottom=218 HV
					-	-	-		Top=188 HV; Bottom=198 HV
					-	-	-		207 HV
					-	-	-		161 HV
					-	-	-		Top=189; Bottom=206 HV
Zahiri et al. [29]	Ti	aluminum	-	-	-	-	-	Vickers microhardness test	~150 HV
					-	-	-		~140 HV
					-	-	-		~125 HV
					-	-	-		100 HV
					-	-	-		~185 HV
					-	-	-		300 HV
			Heat treatment at 450°C for 30 min.		-	-	-		230 HV
Zhou et al. [32]	Ti	wrought Ti	-	-	-	-	-	Vickers microhardness test	Top: 172 ± 22 HV Middle: 207 ± 30 Bottom: 221 ± 18
			Heat treated at 850°C in Argon with 5% hydrogen for 5 hr.		-	-	-		Top: 258 ± 68 HV Middle: 251 ± 89 Bottom: 210 ± 30

2.3.3 Mechanical Properties of Tantalum Coatings

Cold sprayed tantalum coatings tend to be very dense with low porosity. Trexler et al. created coatings with hardness values in the range of 238 HV and 245 HV before annealing, and 225 HV and 226 HV after annealing (hardness units given in the paper were converted from HRC to HV). The average hardness of bulk tantalum ranges from 65.1 HV to 235 HV [4]. Therefore, the as-sprayed coatings created by Trexler et al. are near the higher end of hardness values seen in bulk tantalum. This could possibly indicate work hardening during the cold spray process, which has been observed in other studies. Additionally, Trexler et al. performed tensile tests according to the ASTM E8 standard. Coatings created with nitrogen as the carrier gas used rectangular cross sections, while coatings created with helium used round cross sections for the tensile test. As-sprayed coatings resulted in tensile strengths of 7.7 MPa and 13.3 MPa for the nitrogen and helium gases, respectively [35]. After the annealing process, the tensile strengths of the coatings were 10.8 MPa and 10.9 MPa and the elongation values were 42% and 35% for the nitrogen and helium gas, respectively [35]. This was a significant increase in the ductility compared to less than 1% ductility seen in the as-sprayed coatings. Although Trexler et al. proved that very comparable coatings of tantalum could be created with nitrogen and helium gas, the tensile strength of both coatings were much lower than the tensile strength of bulk tantalum that ranges from 170 MPa to 650 MPa [42].

Research by Kumar et al. was able to accomplish significantly higher tensile strengths for tantalum. Kumar et al. used air as the process gas and the as-sprayed coating had a tensile strength of 48.49 MPa and with a 1500°C heat treatment, the tensile strength increased to 320 MPa [34]. The as-sprayed coating by Kumar et al. was much stronger than what was seen by Trexler et al. Additionally, after the annealing processes, the tensile strength of the coating was increased to a value similar to what is seen in bulk tantalum. Kumar et al. also measured the elastic moduli of the coatings from nanoindentation measurements. As the temperature of the heat treatment increased, not only did the tensile strength increase, but the elastic modulus generally increased as well. The as-sprayed coating had an elastic modulus of ~100 GPa while the coating heat treated at 1500°C resulted in an elastic modulus of ~125 GPa [34]. Although the elastic modulus increased with the heat treatment, the value was still below that seen in bulk titanium which ranges from 180 GPa to 188 GPa [4].

Also, Kumar et al. showed that increasing the annealing temperature decreased the hardness of the coatings. As-sprayed, the coating hardness was ~375 HV and after annealing at 1500°C the hardness was ~200 HV [34]. Again, these high hardness values seen from cold spray suggest work hardening during the coating process. The heat treatments reduced the hardness of the coatings and brought the hardness value within the range seen in bulk tantalum, 65.1 HV to 235 HV [4]. A scratch test was also conducted on these coatings to find the critical load before debonding occurred. The critical load increased with the temperature of the annealing treatment. The as-sprayed coating had ~4 N critical load, and the coating treated at 1500°C had a critical load of ~31 N [34]. A table of cold sprayed tantalum coatings and their mechanical properties can be seen in Table 8.

Table 8. Mechanical properties of cold sprayed tantalum.

Cold Sprayed Tantalum from the Literature										
Author	**Powder**	**Substrate**	**Gas**	**Post-processing steps**	**Mechanical strength test**	**Elongation (%)**	**Elastic Modulus (GPa)**	**Tensile strength (MPa)**	**Other mechanical tests**	**Other mechanical test results**
Kumar et al. [34]	Ta	steel	Air	-	Elastic modulus from nanoindenter. 3-kN microtensile testing machine.	-	~100	48.49	Vickers microhardness test. Scratch test.	~375 HV0.1; ~4N
				Vacuum heat treated at 500°C for 2 hr.		-	~115	-		~350 HV; ~8N
				Vacuum heat treated at 750°C for 2 hr.		-	~120	-		~325 HV; ~9N
				Vacuum heat treated at 1000°C for 2 hr.		-	~140	-		~325 HV; ~8N
				Vacuum heat treated at 1250°C for 2 hr.		-	~125	-		~300 HV; ~10N
				Vacuum heat treated at 1500°C for 2 hr.		-	~125	320		~200 HV; ~31N
Trexler et al. [35]	Ta	aluminum	N2	-	ASTM E8-04 for rectangular specimens	0.285	-	7.7	Rockwell C hardness measurement	19.85 HRC
			He	-	ASTM Standard E8-04 for round axial specimens	0.296	-	13.3		21.3 HRC
			N2	annealed	ASTM E8-04 for rectangular specimens	42	-	10.8		14.18 HRC
			He	annealed	ASTM Standard E8-04 for round axial specimens	35	-	10.9		14.9 HRC

2.3.4 Mechanical Properties of Hydroxyapatite Coatings

Dense hydroxyapatite coatings have been created on magnesium substrates with the cold spray process. Two different pieces of literature have documented elastic modulus and hardness values for hydroxyapatite coatings on magnesium [37], [38]. The research from both of these papers had similar input parameters, such as room temperature compressed air with preheated magnesium substrates.

In one of these papers, Noorakma et al. achieved 25 μm thick hydroxyapatite coatings. The elastic modulus and hardness of the coating was determined from a nanoindentation test. From these tests, Noorakma et al. found an elastic modulus of 9 GPa and hardness of 90 MPa [38]. Similar values were found in research done by Hasniyati et al. from nanoindentation tests on hydroxyapatite coatings with different process inputs. Elastic modulus values ranged from 9.09 GPa to 45.69 GPa and the hardness ranged from 35.01 MPa to 462.61 MPa. Bulk hydroxyapatite has an elastic modulus between 73 GPa to 117 GPa and a hardness value around 3.43 GPa [4]. Therefore, the coatings in these papers had elastic moduli well below that of bulk hydroxyapatite. Moreover, the hardness values of the coatings appeared to be significantly lower than that of bulk hydroxyapatite. This lower hardness is the opposite of what is usually found will metal coatings from the cold spray process.

Hasniyati et al. used the steepest ascent method from a DOE to determine the input parameters needed to create the best hydroxyapatite coating. The input parameters that were manipulated were the surface roughness, standoff distance, substrate temperature, and number of coating layers. The output parameters that were recorded for the coatings were the thickness of the coating, elastic modulus, and hardness. After analysis, Hasniyati et al. found that the number of coating layers was an insignificant factor on the resulting mechanical properties, however all other inputs were found to be significant [37]. For the tested range of inputs, it was found that a decrease in standoff distance, and an increase in both temperature and roughness (decrease in sandpaper grit number) resulted in coatings with higher hardness and elastic modulus values [37]. A table of cold sprayed hydroxyapatite coatings and their mechanical properties can be seen in Table 9.

Table 9. Mechanical properties of cold sprayed hydroxyapatite.

Cold Sprayed Hydroxyapetite from the Literature										
Author	**Powder**	**Substrate**	**Substrate preheated temperature (°C)**	**Substrate surface roughness (grit of sandpaper)**	**Standoff distance (mm)**	**Deposition thickness (µm)**	**Mechanical strength test**	**Elastic Modulus (GPa)**	**Other mechanical tests**	**Other mechanical test results**
Hasniyati et al. [37]	HA	magnesium	550	2000	40	21.96	Elastic modulus from nanoindenter	13.96	Nanoindentation test to measure hardness	69.49 Mpa
			350	2000	20	18.73		16.81		47.58 MPa
			350	2000	20	18.19		15.26		39.12 MPa
			350	2000	40	13.03		9.09		36.82 MPa
			550	240	40	23.56		23.46		156.87 MPa
			550	240	40	24.43		19.3		73.6 MPa
			550	2000	40	21.84		14.7		67.72 MPa
			350	240	40	20.31		13.8		67.23 MPa
			550	2000	20	32.63		30.73		197.65 MPa
			350	2000	40	17.48		11.08		35.01 MPa
			550	240	20	49.77		45.69		462.61 MPa
			350	240	40	21.48		16.32		65.61 MPa
			550	240	20	39.08		43.06		429.02 MPa
			350	240	20	35.09		33.26		255.92 MPa
			350	240	20	38.97		36.33		323.71 Mpa
			550	2000	20	25.58		23.46		156.87 Mpa
Noorakma et al. [38]	HA	magnesium alloy: AZ51	400	1000	40	25	Elastic modulus from nanoindenter	9	Nanoindentation test to measure hardness	0.09 GPa

2.3.5 Cold Sprayed Biocompatible Materials Mechanical Properties Conclusion

The cold spray process has been used with many biocompatible materials and some research has looked at the mechanical properties of these coatings. Mechanical properties can drastically change depending on the initial powder, the processing parameters, and post processing steps. From the research, it can be generalized that cold sprayed coatings tend to have hardness values greater than that of the bulk material, suggesting that the particles experience work hardening during the cold spray process. However, in two pieces of work with titanium coatings, the hardness of the coating was actually less than that of bulk material possibly due to the powder properties or the thermal conditions of the process.

Additionally, the tensile strength and elastic modulus of as-sprayed coatings tend to be well below that of the bulk materials. Moreover, the as-sprayed coatings tend to act in a brittle nature with lower ductility than bulk material. However, high heat treatments around 800°C to 1500°C on the coatings can decrease the hardness and porosity and drastically increase the tensile strength, elastic modulus, and ductility of the coatings.

3 Selection of Substrates and Powders for Cold Spray Experiments

3.1 Substrate Material Selection

In order to test the applicability of the cold spray manufacturing process to coat ICs, the test substrates needed to mimic the materials appearing in ICs as closely as possible. ICs are built up layer by layer and a simplified version of one of Draper's ICs can be seen in Figure 11 (not drawn to scale).

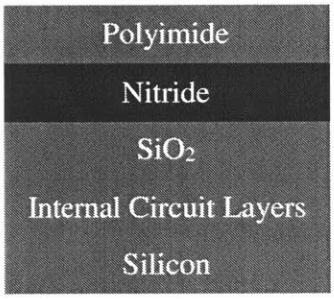

Figure 11. Simplified model of an IC cross-section.

ICs are very thin and the bottom layer is generally silicon and the top layer polyimide. Therefore to coat completely around ICs, the cold spray process would need to deposit a coating on both silicon and polyimide material. Hence, these two materials were chosen as substrates for the experiments.

3.2 Cold Spray Powder Material Selection

Electronic implant packages have many requirements to be successful in the body. The packages must be sealed, biocompatible, and must protect the underlying electronics from outside forces. Many packages also need RF transparency to allow for communication to an outside source

or to allow for battery charging. All of these requirements were taken into account when choosing what material should be used for the cold sprayed conformal packaging.

One of the most important aspects of electronic implant packages is biocompatibility. A list of long-term biocompatible materials was created from the ASM Medical Materials database. This list was then reduced to materials that have been previously cold sprayed in dense coatings. Materials that have already been proven to be compatible with the cold spray manufacturing process were chosen in order to reduce the time needed to optimize cold spray parameters for the specific powder. From the literature, it was found that the long-term biocompatible materials that have been successfully cold sprayed in dense coatings include 316L stainless steel (316L SS), commercially pure (CP) titanium, grade 5 titanium (Ti-6Al-4V), tantalum, and UHMWPE [16]–[21], [23], [27]–[29], [31]–[36], [39]. A description of these cold sprayed coating properties was included in the previous chapter, Chapter 2: Cold Spray Process and Cold Sprayed Biocompatible Materials.

From these possible coating materials, UHMWPE was chosen to test as a packaging material in this research. UHWMPE was selected since the cost is significantly lower than the other material options and it was the only material that was RF transparent. RF transparency would allow for communication or charging of the electronic implant from a source external to the body. UHMWPE is also non-conductive and is softer than metals, which are advantages of the material. Since the material is non-conductive, it would be possible to spray all components of the IC directly, even wires that will carry electricity, such as feedthrough pins. Also, since the UHMWPE package would be a softer package material than metal, it could be placed in more sensitive tissue areas.

UHMWPE has many advantages over metal packaging, however it has much lower material strength compared to metals. For specific implants, strong packaging may be necessary to protect the internal implant components from external forces and shocks. Moreover, UHMWPE packages would be non-hermetic and therefore would only be a good choice for shorter term implants. Metal packaging would be stronger and could result in fully hermetic seals. Therefore, metal coating options were investigated as well. Of the long-term biocompatible metals that have been successfully cold sprayed in the literature, tantalum is the softest. Since tantalum is such a soft metal, cold sprayed tantalum is dense with very low porosity. However, the cost of tantalum

powder is substantially higher than that of titanium or stainless steel alloys. The high cost of the tantalum powder makes it a poor choice for implant packaging. Therefore, the next softest metal, CP titanium, was chosen since it was a less expensive option and sufficient data demonstrated dense coatings.

4 Preparation of Substrates and Creation of Fixture to Hold Substrates

4.1 Substrate Preparation

Substrates of polyimide and silicon were prepared to be sprayed. Standard 100 mm diameter single side polished silicon wafers were diced into four equal quarter-wafer pieces. The non-polished side of the silicon wafers were used as the surface to be cold sprayed.

The polyimide layers in Draper ICs are created by spin-on polyimide. However, in this research adhesive polyimide was used instead of spin-on polyimide since the adhesive version was easier to obtain, inexpensive, and allowed for quicker substrate preparation. Five inch wide 1 mil Kapton tape was acquired and used for these experiments. This tape included a 1 mil thick polyimide layer on top of a 1.5 mil thick silicone adhesive layer. To create the substrate samples, the Kapton tape was placed on top of the polished side of the silicon quarter-wafer pieces and the excess tape around the substrate was cut away.

4.2 Design and Build of Fixture Device to Hold Substrates

Since the substrates were thin and brittle in nature, they needed to be held down securely with a fixture. VRC had previous experience with brittle substrates and found that if air flow was able to get under the substrates then this could cause them to flex upward and then break. Therefore, a fixture device was designed to hold down the substrates while also allowing air to flow away from the substrates.

The fixture device, shown in Figures 12-16, included a base plate and a mask and was designed to hold 4 full wafers and 16 quarter wafer pieces. In order to prevent air flow under the substrates, areas were machined into the base plate for the substrates to be placed in. The compartments were designed so that when the substrates were placed in them, the substrates would stick out higher than the top of the base plate to allow for the metal mask plate to make contact

with the substrates and hold them firmly to the baseplate. The plain silicon wafers were the thinnest samples chosen for testing, at 500 μm to 550 μm, so the indents in the holder were machined down 250 μm. This design allowed the substrates to be taller than the machined out component. The SolidWorks model of the base plate can be seen in Figure 12. The base plate also had curved sections machined down on the corners of the quarter wafer pieces and on both sides of the full wafers. These areas were machined so the substrates could easily be removed from the base plate. Additionally, the two curved cutouts on either side of the base plate are there so that bolts can hold the base plate to the table. Lastly, six threaded holes were machined in the base plate so that screws and nuts could be used to attach the mask plate on top.

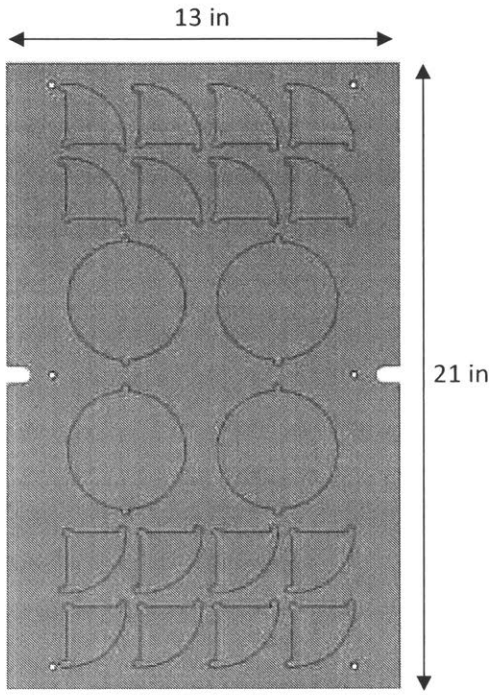

Figure 12. Base plate to set wafer substrates in.

The mask plate was designed to hold down the delicate wafers on the base plate during the cold spray process. In order to prevent the adherence of the mask to the substrates, the mask was elevated and not in direct contact with the substrates near the mask cutouts. Moreover, 1.5 mm deep vertical and horizonal rectangles were machined out of the bottom of the mask plate in order to create paths where the air flow could escape during the cold spray process. The top and bottom view of the mask plate can be seen in Figure 13.

The SolidWorks assembly of the mask plate, base plate, and substrates is shown in Figure 14. This figure shows the normal assembly and also the assembly with the mask plate made transparent to show how the mask plate geometry sits on the base plate and substrates.

A cross-section of the fixture assembly, through one of the quarter-wafer substrates pieces, can be seen in Figure 15. To give a better perspective of the contact points between the mask plate and the substrates, Figure 16 shows the cross-section viewed at an angle.

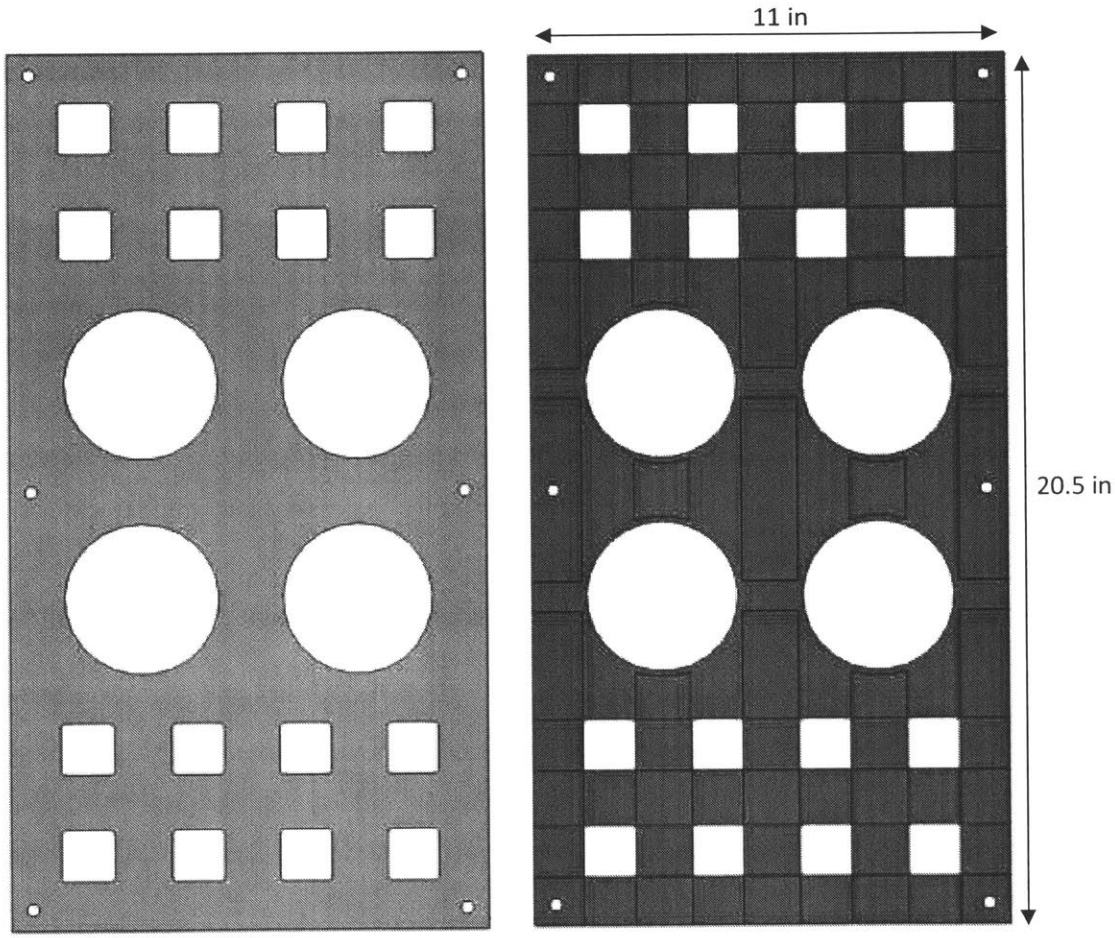

Figure 13. Mask plate component of fixture. On the left is the top view of the mask plate and on the right is the bottom view of the mask plate.

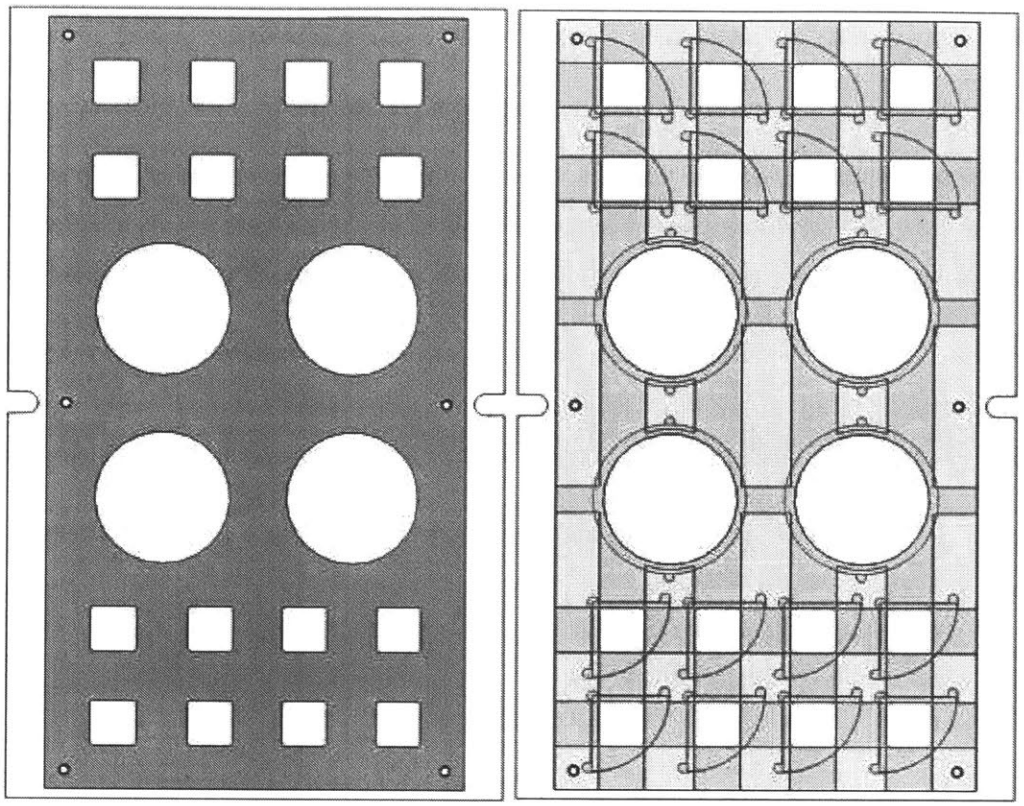

Figure 14. Assembly of fixture device to hold wafer substrates. On the left shows the full assembly and on the right is the full assembly with the top mask plate made transparent.

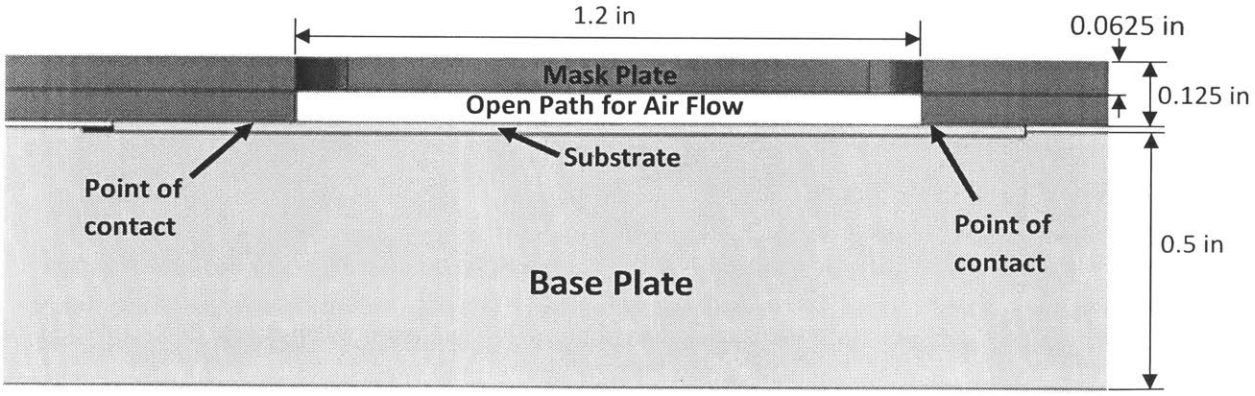

Figure 15. Cross-section of base plate, substrate, and mask assembly through one of the quarter wafer substrate pieces.

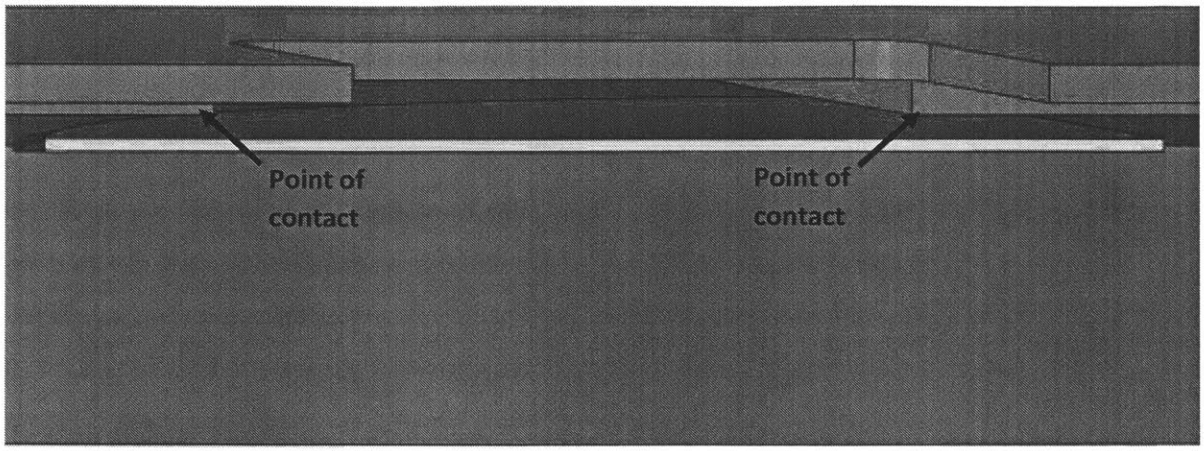

Figure 16. Angled image of cross-section in Figure 15.

5 Experiments Cold Spraying UHMWPE onto Substrates

5.1 Methods and Results for UHMWPE Coatings

Spherical UHMWPE powder, MIPELON™ XM-220, was obtained from Mitsui Chemicals, Inc. (Rye Brook, New York, USA). This powder distribution contained 10% of particles under 20 μm, 35% between 20 and 30 μm, 35% between 30 and 40 μm, and 20% greater than 40 μm. The average particle size from the distribution was 30 μm.

With the UHMWPE powder information, Ozan Ozdemir, a postdoctoral researcher at Northeastern University, ran his Cold Spray Interactive© computational fluid dynamics (CFD) simulation. The simulation calculated the velocity of different sized particles upon impact and compared it to the critical velocity of the particles. The ratio of the particle velocity to its critical velocity is defined by the variable η. If η is greater than 1, then deposition is expected since the particle velocity is greater than the critical velocity it needs to deposit. Additionally, higher η values would be expected to lead to higher plastic deformation of the particles and improved coating properties, such as lower porosity. An ideal η value would be at least 1.5 to obtain good dense coatings. The calculations assume that the substrate material and the powder material are the same. Therefore, these calculations work well when the substrate and powder are the same material or when building up a coating on already deposited powder. However, it may not be an accurate calculation to estimate when particles will adhere to substrates when the substrate is a different material than the powder. With dissimilar materials, there is not enough data to generalize when adhesion will occur, but qualitative predictions can be made. For example, if a calculation resulted in an η value of 0.95 for homogenous materials, and the actual substrate is of a stronger material than was in the simulation, the powder would be expected to deform more at impact, resulting in a η value greater than 1. With an η value greater than 1, you would expect deposition.

This simulation was run for UHMWPE powder with different particle sizes and a range of input temperatures and pressures. The maximum gas input temperature was set to 130°C since the melting temperature of the UHMWPE powder was 136°C. Moreover, the maximum pressure input

was chosen to match the upper end that the cold spray system could handle. The standoff distance was kept constant at 25 mm and nitrogen was used as the process gas. The results of the simulation can be seen in Table 10. The outputs in the table show that the η value increased with an increase in input temperature, an increase in the particle size, and a decrease in pressure. Usually an increase in the pressure will increase particle velocity, therefore increasing the η value. Yet in this scenario, an increase in the pressure increased the bow shock at the surface. The bow shock decreases the velocity of particles heading to the surface and affects smaller, less dense, particles the most. The bow shock effect is common in cold spray when the standoff distance is short [45].

The results in Table 10 show that none of the η values were greater than 1. However, the substrates (polyimide and silicon) have much higher tensile strength than UHMWPE, so it was expected that this would increase the η values. Additionally, UHMWPE had been cold sprayed on a polymer before, polypropylene, in other research with a low pressure cold spray system [39]. In this research, with access to a higher pressure cold spray system, it would be expected to help with the deposition of the material.

Table 10. Eta (η) value outputs from CFD analysis for UHMWPE powder and 25 mm standoff. Powder particle sizes, temperature inputs, and pressure inputs are varied. A larger η value generally means better powder deposition.

Particle size dependent η upon impact															
diameter (um)	31 (bar) & 20 (C)	31 (bar) & 47.5 (C)	31 (bar) & 75 (C)	31 (bar) & 102.5 (C)	31 (bar) & 130 (C)	41 (bar) & 20 (C)	41 (bar) & 47.5 (C)	41 (bar) & 75 (C)	41 (bar) & 102.5 (C)	41 (bar) & 130 (C)	51 (bar) & 20 (C)	51 (bar) & 47.5 (C)	51 (bar) & 75 (C)	51 (bar) & 102.5 (C)	51 (bar) & 130 (C)
5	0.273	0.338	0.410	0.490	0.579	0.198	0.256	0.324	0.404	0.499	0.147	0.196	0.257	0.334	0.433
10	0.502	0.562	0.622	0.683	0.745	0.441	0.501	0.562	0.625	0.689	0.387	0.447	0.508	0.571	0.636
15	0.582	0.637	0.693	0.749	0.806	0.537	0.593	0.650	0.707	0.765	0.495	0.552	0.609	0.667	0.726
20	0.621	0.674	0.728	0.782	0.837	0.587	0.641	0.695	0.750	0.806	0.508	0.563	0.619	0.675	0.740
25	0.644	0.696	0.749	0.802	0.858	0.583	0.637	0.691	0.752	0.808	0.547	0.601	0.656	0.712	0.768
30	0.638	0.694	0.751	0.805	0.867	0.606	0.660	0.713	0.768	0.825	0.575	0.629	0.683	0.739	0.796
35	0.650	0.702	0.756	0.811	0.871	0.623	0.677	0.731	0.786	0.844	0.596	0.650	0.705	0.761	0.818
40	0.660	0.712	0.766	0.822	0.881	0.637	0.690	0.745	0.801	0.860	0.613	0.667	0.722	0.779	0.837
45	0.668	0.721	0.775	0.832	0.893	0.648	0.702	0.757	0.814	0.874	0.627	0.681	0.737	0.795	0.855
50	0.674	0.728	0.783	0.842	0.904	0.657	0.712	0.768	0.826	0.888	0.639	0.694	0.750	0.809	0.870
55	0.680	0.734	0.791	0.851	0.915	0.666	0.721	0.778	0.837	0.901	0.649	0.705	0.762	0.822	0.885
60	0.685	0.740	0.798	0.859	0.925	0.673	0.729	0.787	0.848	0.914	0.658	0.714	0.773	0.834	0.900
70	0.694	0.751	0.811	0.875	0.945	0.685	0.743	0.803	0.867	0.937	0.674	0.732	0.792	0.857	0.926
80	0.702	0.760	0.822	0.889	0.964	0.696	0.755	0.818	0.885	0.960	0.687	0.746	0.809	0.877	0.951
90	0.708	0.768	0.832	0.903	0.982	0.705	0.766	0.831	0.902	0.981	0.698	0.760	0.825	0.896	0.975

Legend: Color ranges from red to green as the value increases	
	Values below the 50th percentile
	50th percentile value
	Values above the 50th percentile

An experimental design of input temperatures and pressures was created to test the deposition of UHMWPE on the substrates. Using the results from the CFD simulation, higher temperatures were chosen since it was clear that higher temperatures would result in a higher η value. The η value fluctuated less with pressure changes and therefore a wide range of pressure inputs were chosen. For the initial experiments, nitrogen was used as the process gas, the standoff distance was kept at 25 mm, the traverse speed at 250 mm/s, and 5 scans across the surface area were completed. The temperature inputs ranged from 100°C to 130°C and the pressure ranged from 30 bar to 50 bar. These substrates were sprayed and no significant buildup of the coating was observed. Therefore, input parameters were varied to see if any build up could be observed. The standoff distance was increased to reduce the bow shock effect and the traverse speed was decreased to allow for more particles to impact on top of each other. Additionally, for some parts the temperature was increased to soften the particles and the pressure was lowered to decrease the bow shock effect. Even with the input changes, no coating buildup was observed. The process inputs for these experiments can be seen in Table 11.

Table 11. Cold spray process inputs for first experiments with UHMWPE powder.

#	Substrate Material	Temperature (°C)	Pressure (bar)	Stand off Distance (mm)	Traverse Speed (mm/s)	# layers
1	Polyimide	100	30	25	250	5
2	Polyimide	100	50	25	250	5
3	Polyimide	115	40	25	250	5
4	Polyimide	130	30	25	250	5
5	Polyimide	130	50	25	250	5
6	Polyimide	120	20	100	Held	-
7	Polyimide	140	20	100	100	5
8	Polyimide	140	50	100	Held	-
9	Silicon	100	30	25	250	5
10	Silicon	100	50	25	250	5
11	Silicon	115	40	25	250	5
12	Silicon	140	20	100	100	5

None of the silicon substrates had any coating deposition nor was substrate erosion observed. With the polyimide substrates, it was unclear whether the substrates had a thin coating

of material on them or if the change in the surface appearance was due to erosion. Therefore, the surfaces were analyzed under a scanning electron microscope (SEM). The substrate surfaces all looked very similar for parts 1 through 5. The surface of substrate 5 is shown in Figure 17. Additionally, the substrates where the traverse speed was reduced or the nozzle was held over the substrate, similar surfaces were seen compared to parts 1 through 5 except that more erosion was also observed. The surface of one of these substrates, substrate 6, is shown in Figure 18. From these results for all the parts, it appeared that the particles were not reaching their critical velocity since no deposition was found on the silicon substrates and only wear was observed on the polyimide substrates. Moreover, the UHMWPE particles did not appear to have any significant deformation.

Since no deposition was obtained, further experiments were conducted. The input temperature was increased which would soften the particles and increase the particle velocity. The pressure was kept at 30 bar and the standoff distance was placed at 50 mm since any closer standoff distance was hard to keep without the risk of breaking the fragile substrates. Additionally, the increased standoff would reduce the bow shock effect. The traverse speed was kept at 100 mm/s. The process inputs for these experiments are show in Table 12.

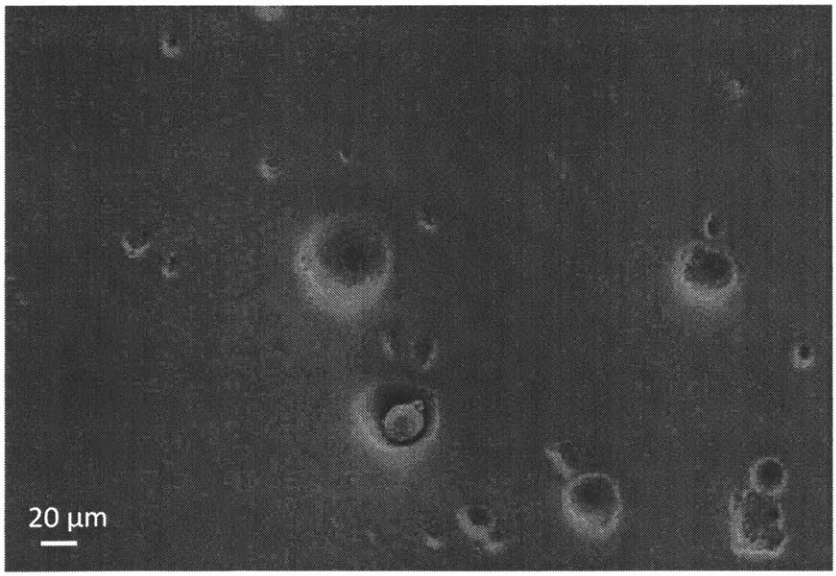

Figure 17. Surface image of substrate number 5 obtained from an SEM. No significant UHMWPE deposition is shown on the polyimide substrate. Process inputs: 130°C temperature, 50 bar pressure, 25 mm standoff, 250 mm/s traverse speed, and 5 passes.

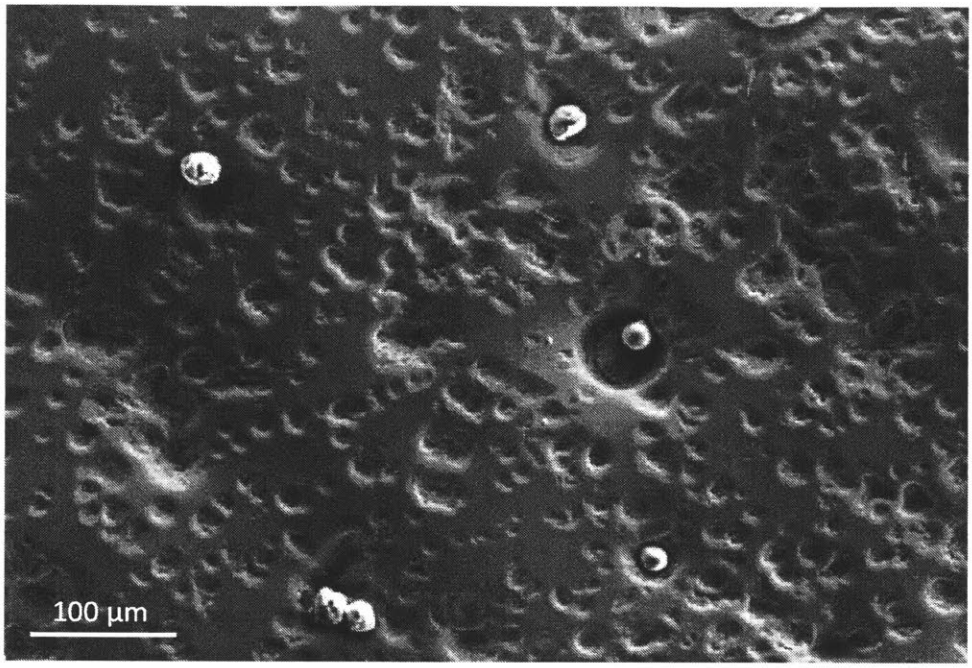

Figure 18. Surface image of substrate number 6 obtained from an SEM with backscatter detector. No significant UHMWPE deposition was seen on the polyimide substrate. Process inputs: 120°C temperature, 20 bar pressure, 100 mm standoff, and the nozzle was held in the same spot over the substrate.

Table 12. Cold spray process inputs for second run of experiments with UHMWPE powder.

#	Substrate Material	Temperature (°C)	Pressure (bar)	Stand off Distance (mm)	Traverse Speed (mm/s)	# layers
13	Polyimide	150	30	50	100	5
14	Polyimide	180	30	50	100	5
15	Polyimide	200	30	50	100	5
16	Polyimide	210	30	50	100	5
17	Silicon	210	30	50	100	5

Similar results were found from these experiments. There appeared to be no significant or noticeable difference between these experiments and the previous ones. As an example, an image of the surface of substrate 16 is shown in Figure 19.

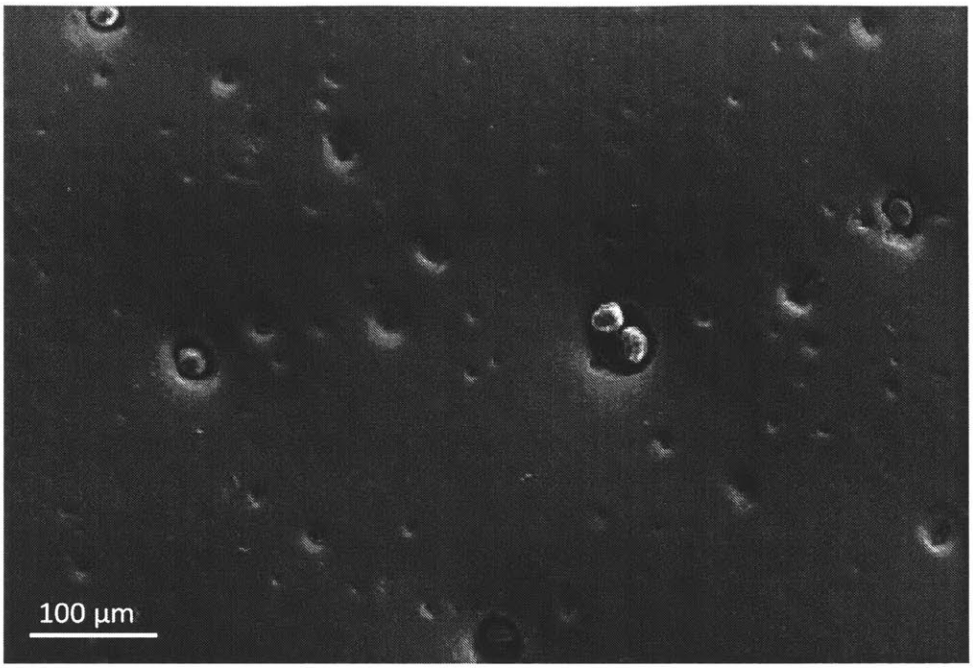

Figure 19. Surface image of substrate number 16 obtained from an SEM with backscatter detector. No significant UHMWPE deposition was seen on the polymide substrate. Process inputs: 210°C temperature, 30 bar pressure, 50 mm standoff, 100 mm/s traverse speed, and 5 passes.

5.2 Discussion of UHMWPE Experiments

None of the experiments resulted in significant UHMWPE deposition even though the experiments conducted in this research used pressures that were approximately ten times the pressures used in other research that successfully deposited thick coatings of UHMWPE [39]. The other research conducted by Ravi et al. however included nano-alumina particles in the UHMWPE feedstock in order to build up the coating. With the pure UHMWPE powder in Ravi et al.'s research, only thin layers of UHMWPE could be deposited on the substrates. In this current research, it was not possible to include nano-alumina particles since alumina particles under 1 µm can be harmful inside the human body [4]. The research by Ravi et al. also had to make modifications to the nozzle to allow for more heat to be exchanged to the particles and it was observed that the particles did not deposit unless the particles were sufficiently heated. Therefore, in this research perhaps the lower heat energy in the particles could have been one of the reasons for a lack of deposition.

As was stated earlier, higher pressure inputs for cold spray increases the velocity of the particles and therefore better deposition usually results with metal powders. However, more recent research investigating the deposition of high density polyethylene (HDPE) on different substrates discovered that the erosion velocity of HDPE can be very low for specific substrates [46]. Some substrates had erosion velocities below 250m/s [46]. In this research the UHMWPE particle velocities were more than twice that at the 25mm standoff distance according to the CFD model. Therefore, the velocities of the particles in this research may have been above the erosion velocity, therefore they only eroded the substrate rather than depositing on it.

Additionally, this research used significantly higher pressure inputs than two other papers that successfully deposited either UHMWPE or HDPE [39], [46]. Higher pressures can increase the particle velocity, therefore resulting in good deposition. However, with higher pressure inputs, it could have created a greater bow shock effect that either slowed down or deflected the incoming UHMWPE particles.

5.3 Conclusion and Next Steps for UHMWPE Experiments

In this research, UHMWPE deposition and buildup was not seen on the polyimide or silicon substrates. Future research needs to be conducted to see if UHMWPE coatings are possible on silicon or polyimide substrates. The use of a modified nozzle to increase the temperature of the particles before impact may need to be tested. Moreover, it was unknown if the particles were reaching the critical velocity needed for deposition since no deposition was observed and no particle deformation was seen. This research used higher pressures than other research that successfully deposited UHMWPE or HDPE [39], [46]. Higher pressures generally result in greater particle velocities. However, the higher pressure could have created a bow shock at the surface of the substrate, therefore slowing down particles before they reached the substrate. On the other hand, other research has found very low erosion velocities for polymers, so in this research the particles may have been over the erosion velocity as well [46]. Although this is a possibility, it may be more likely that the particles were not reaching their critical velocity since the particles did not appear to have any plastic deformation. A wider range of inputs to create varying particle velocities may need to be tested.

6 Experiments Cold Spraying Titanium onto Substrates

6.1 Methods and Results for Titanium Coatings

For the titanium coatings, additional substrates were chosen to be tested. Figure 11 in section 3.1 showed a simplified model of a Draper IC with a bottom layer of silicon and a top layer of polyimide. Since silicon is such a hard material, it was expected to be difficult to cold spray metal powder on it. The silicon substrate would have little to no deformation when metal particles impact with it. Between the substrate and the particles, only the titanium particles would be deforming, therefore poor mechanical bonding at the surface would be expected. Additionally, since polyimide is a polymer and is very soft compared to the titanium powder, the titanium particles may become embedded in the polyimide rather than build up on it. It was suggested by the partners at Northeastern University and VRC to add an intermediate layer between the substrate and the cold spray which would allow for better adhesion of the cold spray coating. Moreover, they suggested a metal interlayer that would both be strong against impacting particles and that would also deform and mechanically bond with the impacting particles from cold spray. Therefore, a sputtered titanium layer was used as an interlayer since Draper had the capability to sputter titanium onto the substrates at a maximum thickness of 1 μm layer (1 μm thick Ti is not thick enough to create a strong, hermetic package so cold spraying more titanium to create a thicker coating is essential). A layer thickness of 1 μm would be thin compared to the particle sizes in the powder (-20 μm titanium powder). Hence, the substrate material under the sputtered titanium layer would be important as well, especially if cold sprayed particles were able to penetrate through the sputtered layer.

For the initial experiments, four different substrates were chosen. Silicon and polyimide substrates were kept as the standard substrates to test. Additionally, two more substrates were included. These were the substrates you would get if you directly sputtered both sides of a Draper IC. The first was a silicon substrate with a 1 μm thick sputtered Ti. The other substrate was the

silicon wafer with polyimide tape (1 mil thick polyimide layer on top of a 1.5 mil thick silicone adhesive layer) on top and then a final 1 μm sputtered Ti layer on top of that.

Angular (crushed from sponge powder) CP-Titanium powder, TI-101, was obtained from Atlantic Equipment Engineers. The powder was a -20 μm powder (all particles in the powder are able to pass through a 20 μm mesh) with 99.7% purity. This powder had a higher purity than Grade 1 CP Ti which is 99.5% pure. As a titanium powder becomes more pure, it tends to have a lower tensile strength [4]. Therefore, the tensile strength of this powder was expected to be less than that of Grade 1 Ti which is 240 MPa. This was an advantage of the powder since lower tensile strength results in a lower critical velocity for the particles.

The list of input parameters for the cold spray experiments can be seen in Table 13. All parts in this table that have the word "broken" rather than a part number means that the substrate shattered during the spraying process. The first substrate was cold sprayed with a standoff distance of 50 mm. However, at this close distance, it caused significant bowing and eventual failure of the substrate. Therefore, the standoff distance was increased to 150 mm for the remaining experiments. Throughout the experiments, the traverse speed was kept at 250 mm/s which is a fairly common speed with metal deposition.

For the sputtered titanium on silicon substrates, parts 1 through 3, it appeared that the sputtered titanium layer was removed by the high pressure and therefore wasn't acting as an intermediate layer to the incoming cold sprayed titanium particles. Additionally, with these parts, the cold sprayed titanium eroded the surface and there was so much erosion that there was a visible indent in the material in the area that was cold sprayed.

Next, parts 4 and 5 were cold sprayed. Deposition was observed but the titanium did not build up. To test whether buildup would occur, parts 6-9 were sprayed at the same parameters as parts 4 and 5 but with twice as many layers. For the titanium sputtered on polyimide substrates, the sputtered layer appeared to be stripped off by the high pressure before any cold spray particles deposited on the polyimide, which is a similar result to what was found with the sputtered layer on the silicon substrate. Parts 6-9 had titanium deposited on them, but the deposition did not appear to be any thicker than the deposition on parts 4 and 5.

Although titanium deposited on parts 4 through 9, no titanium coating buildup was observed. In order to better understand the titanium deposition with different temperature and pressure inputs, a DOE was designed. After spraying part 9, there were just enough titanium sputtered polyimide substrates left to get data points for a full 2^2 DOE with 3 center points if the previous part 7 was included. Although there were not enough polyimide substrates left to get a full DOE with them as well, as many data points as possible were collected. Table 14 shows the data points for the DOE. Near the end of the experiments, some silicon substrates were attempted to be sprayed at similar conditions, but this only caused the silicon substrates to shatter.

Table 13. Cold spray process inputs for first round of experiments with titanium powder.

Part #	Substrate Material	Temperature (°C)	Pressure (bar)	Stand off Distance (mm)	Traverse Speed (mm/s)	# layers
Broken	Sputtered Ti	500	34.5	50	250	-
1	Sputtered Ti	400	34.5	150	250	3
2	Sputtered Ti	500	37.9	150	250	3
3	Sputtered Ti	400	34.5	150	250	6
4	Polyimide	350	34.5	150	250	6
5	Polyimide	300	34.5	150	250	6
6	Polyimide	350	34.5	150	250	12
7	Polyimide + Sputtered Ti	350	34.5	150	250	12
8	Polyimide	300	34.5	150	250	12
9	Polyimide + Sputtered Ti	300	34.5	150	250	12
10	Polyimide	400	48.3	150	250	12
11	Polyimide + Sputtered Ti	400	48.3	150	250	12
12	Polyimide	375	41.4	150	250	12
13	Polyimide + Sputtered Ti	375	41.4	150	250	12
14	Polyimide	375	41.4	150	250	12
15	Polyimide + Sputtered Ti	375	41.4	150	250	12
16	Polyimide	350	48.3	150	250	12
17	Polyimide + Sputtered Ti	350	48.3	150	250	12
18	Polyimide + Sputtered Ti	375	41.4	150	250	12
Broken	Silicon	375	41.4	150	250	-
19	Polyimide + Sputtered Ti	400	34.5	150	250	12
Broken	Silicon	400	34.5	150	250	-

Table 14. Cold spray process inputs for data points in DOE and the corresponding substrate numbers.

DOE Analysis Inputs			Wafer Number	
DOE data point	Temp	Pressure	Polyimide + Sputtered Ti	Polyimide
(1)	350	34.5	7	6
a	400	34.5	19	-
b	350	48.3	17	16
ab	400	48.3	11	10
centerpoint	375	41.4	13	12
centerpoint	375	41.4	15	14
centerpoint	375	41.4	18	-

The surfaces of the substrates from the DOE were analyzed under a SEM microscope. All the surfaces looked very similar and indistinguishable from each another. The surface images of part 15 can be seen in Figure 20 and Figure 21.

The surface was rock-like in appearance which would suggest that a porous coating had been formed. To better analyze the substrates, cross-sections were taken. Many papers have taken cross-sections of cold sprayed material in order to analyze the percentage of porosity [18], [20], [28]. Being able to analyze the porosity from the DOE parts would give valuable information for optimizing the input parameters to create the densest coating. Each part was diced into four sections. One of the diced components was then potted in epoxy, ground, and polished for analysis on the SEM. Unfortunately, the porosity of the cold sprayed titanium could not be determined since none of the sprayed parts had a dense titanium coating. All of the cross-sections from the parts in the DOE looked very similar and no significant difference was seen between them. The part 11 cross-section images are shown in Figure 22, Figure 23, and Figure 24 as examples.

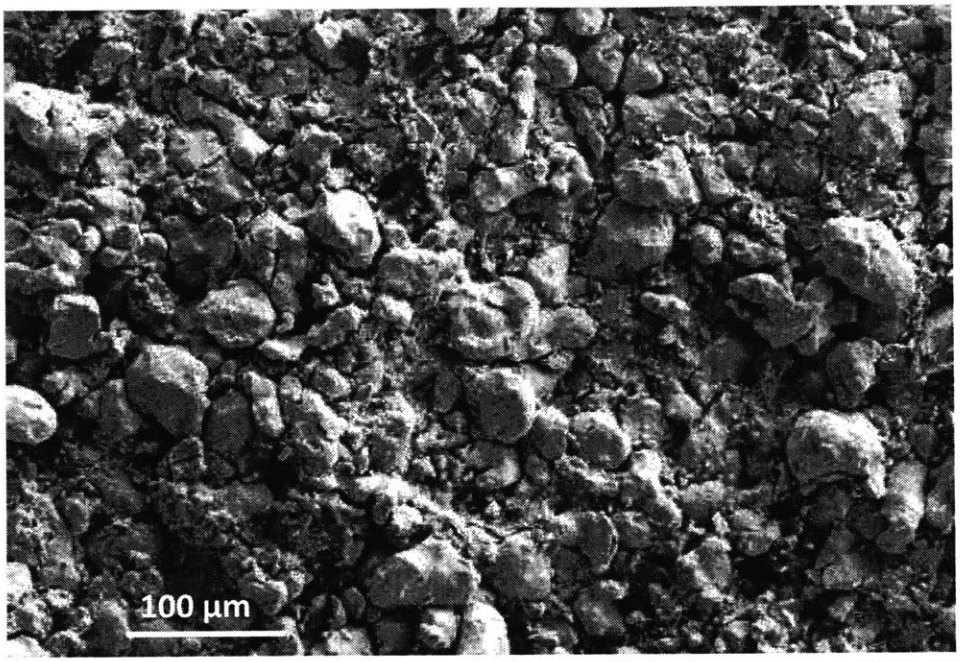

Figure 20. Surface image of titanium coating on substrate 15 obtained from an SEM. This type of surface was seen for both the titanium sprayed on polyimide and polyimide + sputtered Ti substrates.

Figure 21. Magnified image of Figure 20.

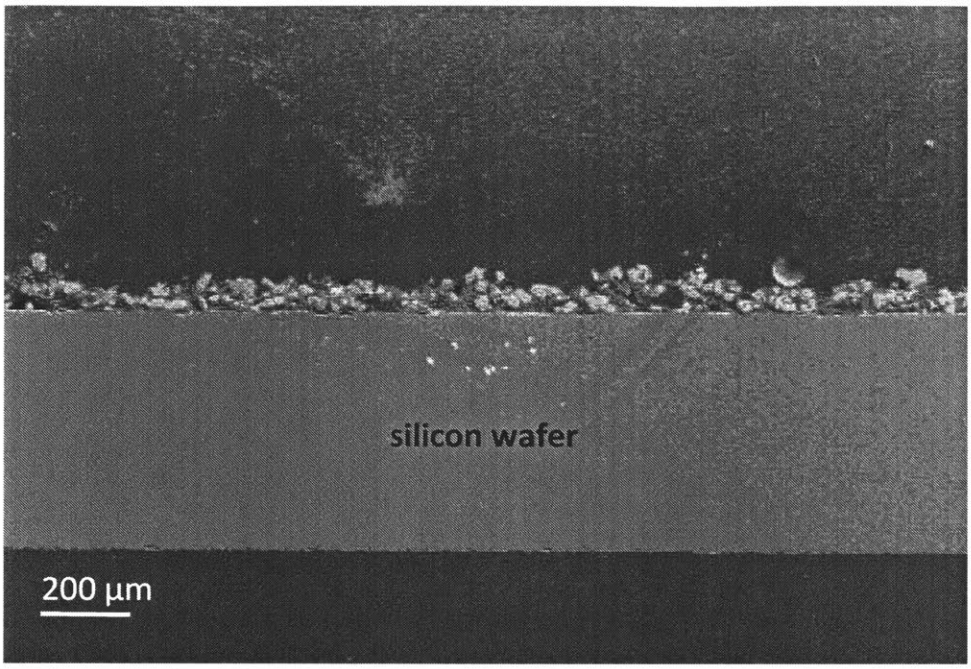

Figure 22. Cross section of part 11. Titanium cold sprayed on a single polyimide tape layer on top of a silicon wafer. Buildup of the coating isn't seen.

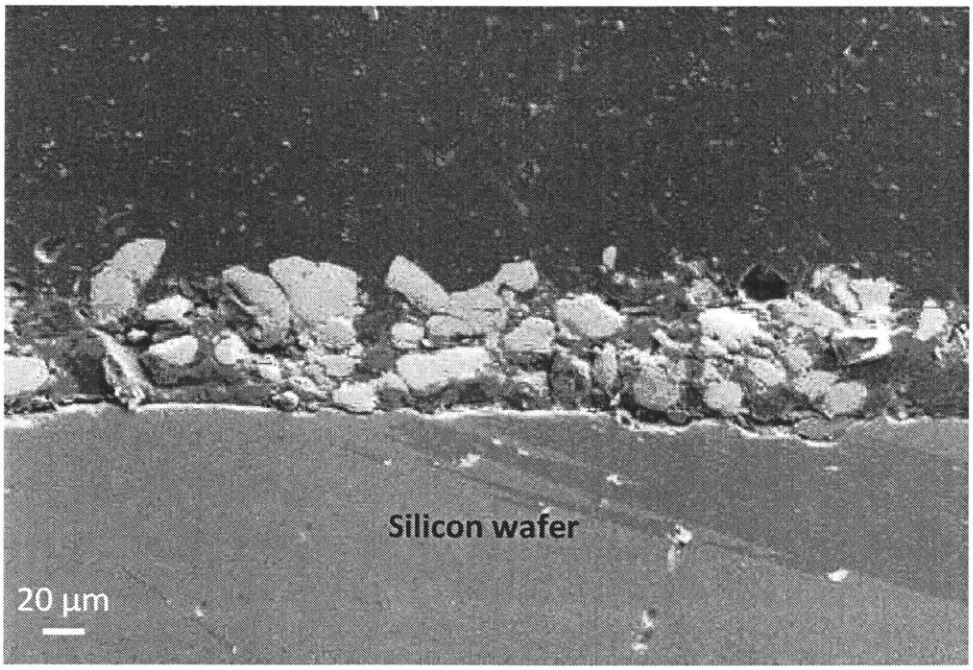

Figure 23. Magnified image of Figure 22.

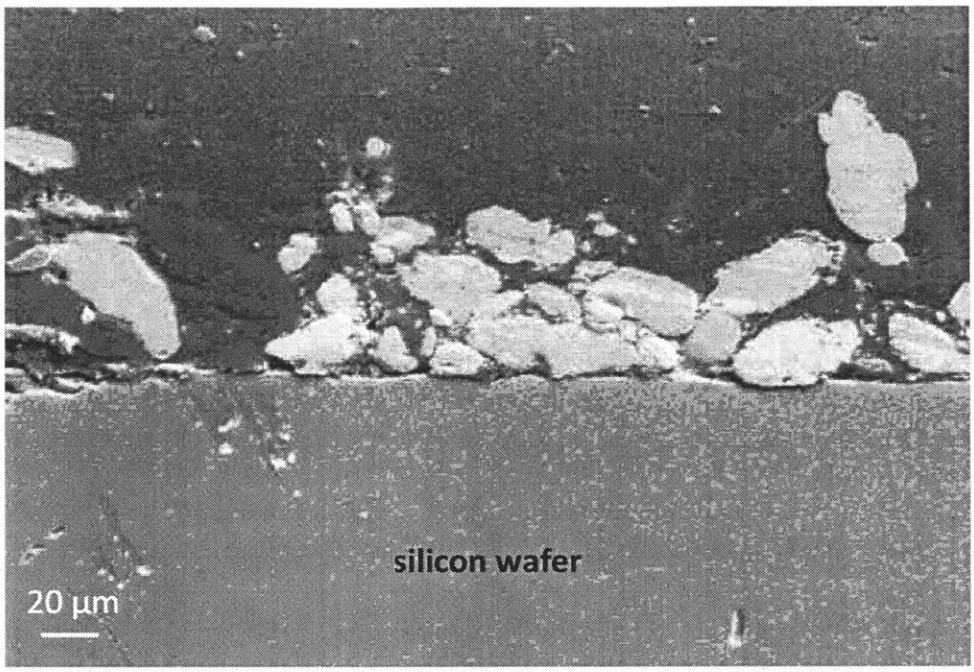

Figure 24. Another magnified image of Figure 22.

From the cross-sections it was clear that dense coatings were not formed. Some of the titanium particles were even making it all the way through the polyimide and silicone adhesive layers and down to the silicon substrate. Since all parts had multiple passes of the cold spray nozzle over the substrate, there was no way to know if the particles were reaching the substrate during the first pass or if the impact of particles on the following passes were further embedding the particles. If the particles were continually pushed closer and closer to the substrate with each pass, then perhaps if the correct parameters were chosen then the coating would build up rather than embed the particles in the substrate. An increase in input temperature and pressure would increase the velocity of the particles and cause more deformation at impact, therefore possibly causing coating buildup.

However, if the particles were embedding during the first pass then perhaps the input parameters, temperature and pressure, were too high for the soft polyimide substrate. These high input parameters would significantly increase the velocity of the titanium particles, therefore possibly allowing the particles to embed far into the material. With these thoughts in mind, more substrates were sprayed with highly varying inputs to see if any changes in the input conditions could lead to a coating buildup. The input parameters for these tests are shown in Table 15.

Table 15. Cold spray process inputs for second round of experiments with titanium powder.

Part #	Substrate Material	Temperature (°C)	Pressure (bar)	Distance (mm)	Traverse Speed (mm/s)	# layers	Nozzle Angle
20	Polyimide	150	24.1	150	20	4	90
21	Polyimide	150	24.1	150	20	4	90
		400	34.5	150	250	-	90
22	Polyimide	150	24.1	150	20	4	90
		150	24.1	150	200	-	90
23	Polyimide	150	24.1	150	100	-	90
24	Polyimide	150	24.1	150	50	8	60
25	Polyimide	150	24.1	150	50	4	60
26	Polyimide	150	24.1	150	50	4	60
		350	27.6	150	50	4	90
27	Two Layers of Polyimide	150	24.1	150	50	2	60
		150	48.3	150	250	6	90
28*	Two Layers of Polyimide	150	24.1	150	50	2	60
		150	48.3	150	250	6	90
*This part was chilled for 30 minutes in a freezer before being sprayed.							

Throughout the experiments different input temperatures, pressures, traverse speeds, and nozzle angles were attempted. For part numbers that include two rows in Table 15, the second row of inputs were sprayed onto the substrates immediately after the first row of inputs. The two step spraying conditions were conducted since the spray conditions needed for a good initial deposition on the polyimide may differ from the inputs needed to get good coating buildup. For example, with part 21, the idea was to use low input parameters to get initial deposition on the soft polyimide followed by high input parameters in order to get the titanium particles to build up on the already deposited titanium. Additionally, on other parts, changing the traverse speed and nozzle angle between passes was attempted as well.

For parts 20 – 26 no coating buildup was observed. Most of these parts started off having similar depositions as the first experiments. However, after continual passes of the nozzle, the coating would soon disappear off of the substrate and expose the silicon substrate underneath. Hence, the process must have eroded away the polyimide and silicone adhesive layer to get down to the silicon underneath. With following passes, the silicon substrate would erode. Because this was observed, the process was carefully watched and as soon as a silicon substrate became visible, the process was stopped. Therefore, some of the boxes in the column "# layers" has "-" which

stands for an unknown amount of passes that were successfully deposited before the process was stopped.

For the final two parts, a double layer of the polyimide tape was placed on the silicon since erosion was commonly observed on the single layer. One part was chilled for 30 minutes in the freezer before being sprayed. This was done in order to harden the polyimide in an attempt to prevent the titanium particles form embedding in or eroding the polyimide. Once again however, no significant coating buildup was observed.

Parts 20 – 26 were cross-sectioned and the results looked very similar to all of the previous cold sprayed titanium cross-sections. However, these parts were cross sectioned in a certain way in order to show the edge of the sprayed section on the substrate. The two double layered polyimide substrates had very similar cross-sections to one another and no distinct differences were seen between the two. The single and double layered polyimide cross-sections revealed some interesting information. The cross-section of part 24 is shown in Figure 25 and the double layered polyimide part 27 is shown in Figure 26, Figure 27, and Figure 28.

Figure 25 shows that the sparse titanium layer is actually below the level of the polyimide layer of the polyimide tape. This was seen in all the single layer polyimide substrates. This suggested that the titanium deposition only appeared because particles were breaking through the polyimide layer and then adhering to the silicone adhesive. The double layered polyimide substrate cross-sections supported this idea as well. Figure 26 clearly shows the particles breaking through the topmost layer of polyimide and then staying in the topmost silicone adhesive layer. Figure 27 shows a more magnified image of the substrate where a small part of the top layer of polyimide of the double layered polyimide substrate was still left after cold spraying. This piece of the top layer of polyimide is outlined by the dashed line in Figure 27. However, most of the cross-sections for the double layered polyimide looked like Figure 28 where nothing of the topmost polyimide layer was visible and all of the particles stayed in the topmost silicone adhesive layer.

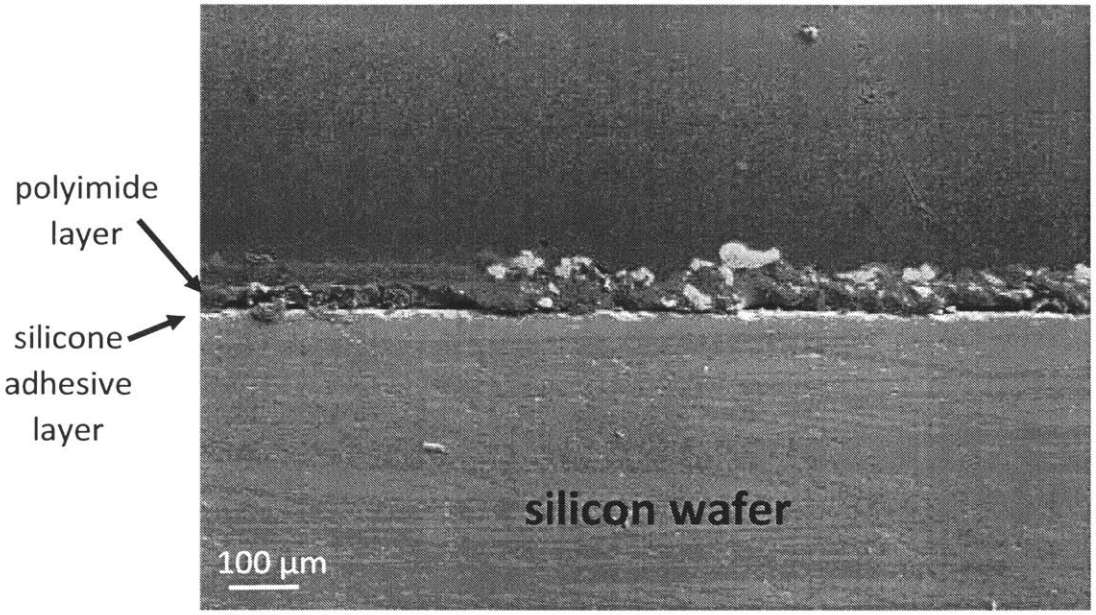

Figure 25. Cross section of part 24. Titanium was cold sprayed onto polyimide tape with inputs: 150°C temperature, 24.1 bar pressure, 150 mm standoff, 50 mm/s traverse speed, 8 passes, and 60° nozzle angle. The titanium particles broke through the layer of polyimide.

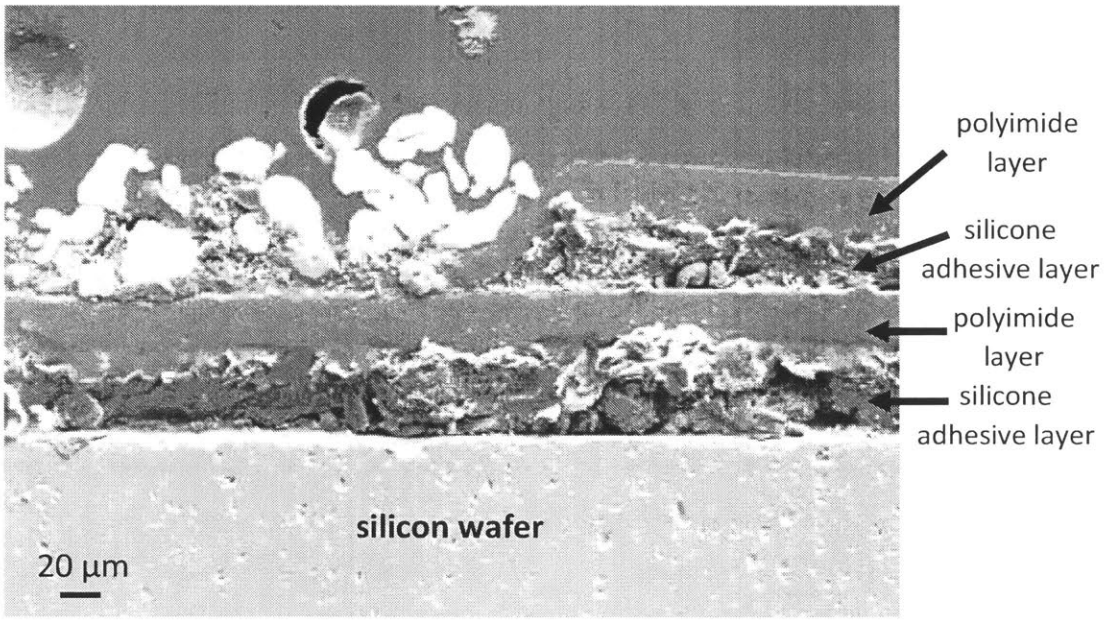

Figure 26. Cross section of part 27. Titanium cold sprayed onto a double layer of polyimide tape. Initial inputs of 150°C temperature, 24.1 bar pressure, 150 mm standoff, 50 mm/s traverse speed, 4 passes, and 60° nozzle angle. After this spray, a secondary spray was conducted with 150°C temperature, 48.3 bar pressure, 150 mm standoff, 50 mm/s traverse speed, 2 passes, and 90° nozzle angle. The titanium particles broke through the top polyimide layer and stayed in the first layer of silicon.

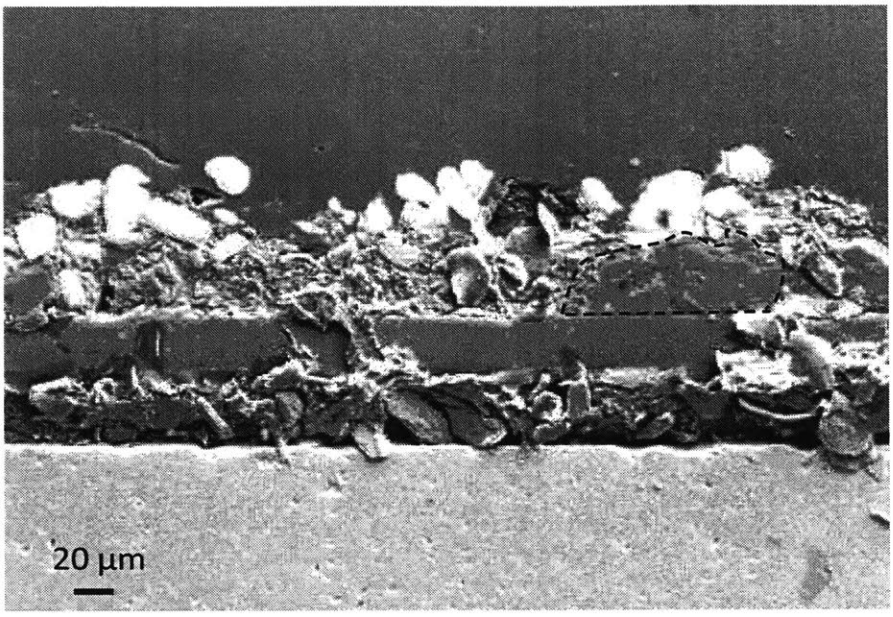

Figure 27. Cross section of part 27. Titanium was cold sprayed onto a double layer of polyimide placed on a silicon wafer. The topmost layer of polyimide was not visible in most of the cross section. However, a few pieces of the top layer of polyimide could be seen. One of these pieces is outlined in the figure by the dotted line.

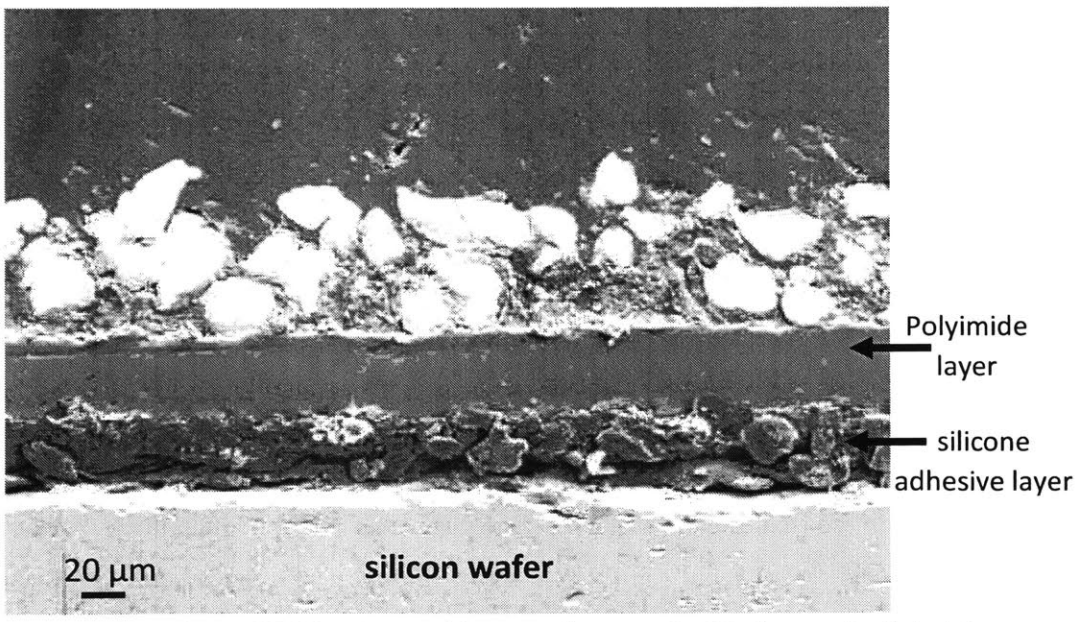

Figure 28. Cross section of part 27. Titanium cold sprayed onto a double layer of polyimide tape on a silicon wafer. The topmost layer of polyimide is no longer visible.

From these results, none of the coatings had formed on top of the polyimide surface but were actually appearing because the particles were sticking to the silicone adhesive underneath the polyimide. Therefore, the substrates were not a good representation of a polyimide substrate. The top layer of the polyimide was most likely too thin to handle the impact of the particles. For the next experiments, a thicker polyimide tape was obtained. This was a 4 mil polyimide tape which included a 4 mil thick polyimide layer with a 1.5 mil thick silicone adhesive layer underneath. This much thicker polyimide was chosen since it was expected to be thick enough to prevent any particles from breaking all the way through it to the silicone adhesive layer.

The thicker polyimide substrates were sprayed with several different input parameters as seen in Table 16. On all parts some deposition was seen but no buildup was formed, and with each cold spray pass the polyimide eroded.

Table 16. Cold spray process inputs for titanium powder with thick polyimide substrates.

Part #	Substrate Material	Temperature (°C)	Pressure (bar)	Standoff Distance (mm)	Traverse Speed (mm/s)	# layers	Angle
29	Thick Polyimide	150	24.1	150	100	4	60
		150	24.1	150	100	4	90
30	Thick Polyimide	400	48.3	150	200	4	60
		400	48.3	150	200	4	90
31	Thick Polyimide	400	31.0	150	200	4	60
		400	31.0	150	200	4	90
32	Thick Polyimide	400	31.0	150	200	4	90
33	Thick Polyimide	150	25.9	150	20	4	90

The deposition of many different types of metals on polymer substrates has been shown to be difficult in other research. Many papers will use a metal interlayer that is cold sprayed first before spraying the final metal [47], [48]. One paper was able to obtain thick copper coatings on polyvinyl chloride (PVC) only after first spraying spherical copper particles as the interlayer followed by dendritic copper particles [47]. Spherical copper particles or dendritic copper particles alone however could not be used to build up a coating. It was the combination of the particles and only in that order that allowed for coating buildup.

Using this knowledge, a similar approach was used in this research. Spherical copper particles were attempted to be cold sprayed first on the polyimide to act as an intermediate layer before spraying the angular titanium powder. The following process input parameters to cold spray copper on the substrates are shown in Table 17.

Table 17. Cold spray process inputs for spherical copper powder for metal interlayer.

Part #	Substrate Material	Temperature (°C)	Pressure (bar)	Standoff Distance (mm)	Traverse Speed (mm/s)	# layers	Nozzle Angle
Broken	Thick Polyimide	350	32.4	100	100	4	90
Broken	Polyimide	350	32.4	100	100	4	90
Broken	Silicon	350	32.4	100	100	4	90
Broken	Polished Silicon	350	32.4	100	100	4	90
34	Thick Polyimide	120	20.0	150	100	4	90
35	Polyimide	120	20.0	150	100	4	90
36	Silicon	120	20.0	150	100	4	90
37	Polished Silicon	120	20.0	150	100	4	90
38	Thick Polyimide	120	20.0	180	100	8	90
39	Polyimide	120	20.0	180	100	8	90
40	Polyimide	120	20.0	150	100	4	90
41	Polyimide	120	20.0	150	100	4	90
		350	31.0	150	100	4	90
42	Polyimide	120	20.0	150	100	4	90
		280	24.1	150	100	4	90
43	Polyimide	120	20.00	150	100	4	90
		200	24.1	150	100	4	90
		280	24.1	150	150	4	90
		280	24.1	150	150	4	90

The parts resulting from the copper sprays ended up having the same results as the experiments conducted to deposit titanium on the substrates. Erosion was observed on the silicon substrates, erosion occurred on the thick polyimide, and the thinner polyimide broke and some minor deposition was seen on the silicone adhesive layer.

The difficulty of depositing copper on polymers has been seen in other research as well and generally in these situations an even softer metal, tin, is used at the intermediate layer. Several papers have sprayed tin directly onto polymers and some have built up the tin coating successfully [47]–[49]. Additionally, some of those same papers used tin as an interlayer material and then a

higher strength metal was cold sprayed on top of it. Since tin is softer than spherical copper, tin may be an appropriate interlayer material to deposit directly on polyimide.

However, tin was not readily available, so another method was approached. Many ICs have something called glob tops which are put over semiconductors chips in order to protect against moisture and to electrically insulate the semiconductor. Glob tops are created from an epoxy that is placed over the semiconductor. Good glob top epoxies have minimal shrinkage while curing. Since placing epoxies onto ICs is already a standard in the industry, then an epoxy-like mixture used as an interlayer may be an easy additional manufacturing step. However, more than just a standard epoxy was used. A low shrinkage epoxy was mixed with titanium powder and then placed on top of the silicon or thick polyimide substrates. Since this mixture had a high percentage of titanium, it was expected that incoming cold sprayed titanium particles would make metallic bonds with this titanium, therefore initiating titanium bonding and coating build up. The process inputs for these experiments are shown in Table 18.

Table 18. Cold spray process inputs for deposition titanium powder on titanium/epoxy mixture substrates.

Part #	Substrate Material	Temperature (°C)	Pressure (bar)	Standoff Distance (mm)	Traverse Speed (mm/s)	# layers	Nozzle Angle
Broken	Ti/Epoxy Mix on Silicon	300	34.5	50	150	2	90
44	Ti/Epoxy Mix on Thick Polyimide	300	34.5	50	150	1	90
45	Ti/Epoxy Mix on Thick Polyimide	300	34.5	75	150	1	90
		300	34.5	75	20	1	90
46	Ti/Epoxy Mix on Silicon	300	34.5	75	20	1	90
47	Ti/Epoxy Mix on Silicon	300	34.5	75	20	1	90

For all the substrates in the areas that were sprayed, either the Ti/epoxy mixture was blown away by the high pressure or the spraying eroded away the Ti/epoxy mixture until the powder reached the substrate material underneath the Ti/epoxy layer. The first Ti/epoxy part that was cold sprayed had a standoff distance of 50 mm and high temperature and pressure inputs (300°C and 34.5 bar). The close standoff and high inputs were used since with the extra strength of the epoxy, it was expected that the substrate would be able to handle the higher particle velocities and pressure on the substrate. However, the first substrate broke soon after starting the spray. The second

substrate was tested at the same parameters. On this substrate, the epoxy was soon blown off, also pulling off some of the polyimide as well. Therefore, for the next substrate, the standoff distance was increased to 75 mm. Once again, the epoxy in the spraying area was blown off. However, this time the polyimide underneath remained. The traverse speed was slowed down to 20 mm/s to see if this would aid in building up the coating. After slowing down the traverse speed, a very obvious coating was formed. Although deposition efficiency wasn't measured, there appeared to be a high percentage of powder deposition. Just one pass across the total spraying area resulted in a 1/8 inch thick titanium coating, as shown in Figure 29. Since this resulted in a good coating, the same parameters were used on the last two substrates that had silicon underneath the Ti/epoxy layer. However, with these parts, the epoxy slowly eroded away to expose the silicon. Once the silicon was exposed, it was also eroded and eventually it eroded all the way through the silicon substrate.

Once the substrates were removed from the fixture, it was observed that part 44 also had some signifigant buildup on it before the epoxy blew off and ripped the polyimide. An image of this part can be seen in Figure 30.

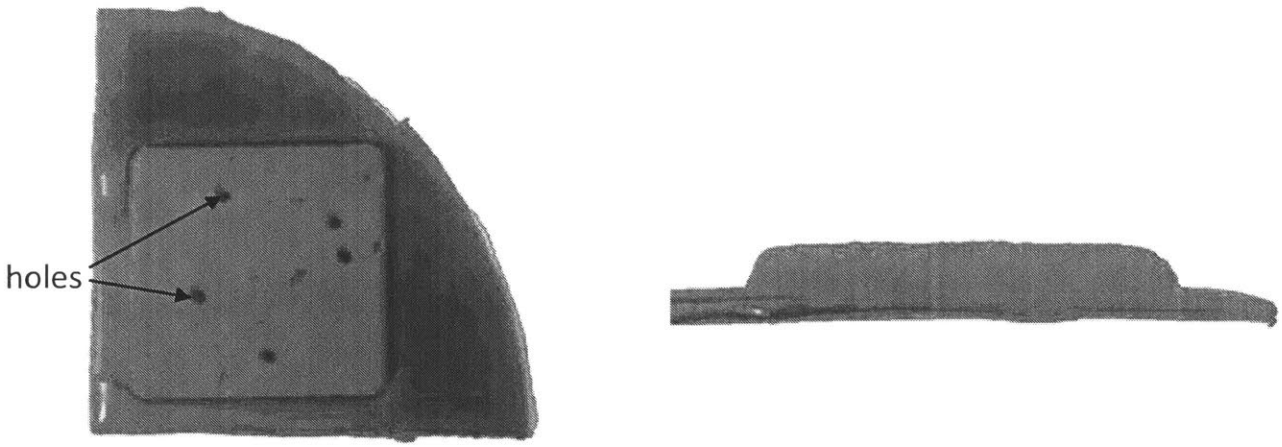

Figure 29. Images of part number 45, which had a 1/8" thick titainum coating deposited on polyimide. The image on the left is the top view and the image on the right is the side view. The image on the left also points out the large holes seen at the surface of the coating. This was created with an initial pass with process inputs: 300°C temperature, 34.5 bar pressure, 75 mm standoff, 150 mm/s traverse speed, and a 90° nozzle angle. This was then followed by a second pass will all the same parameters except for a change in the traverse speed to 20 mm/s.

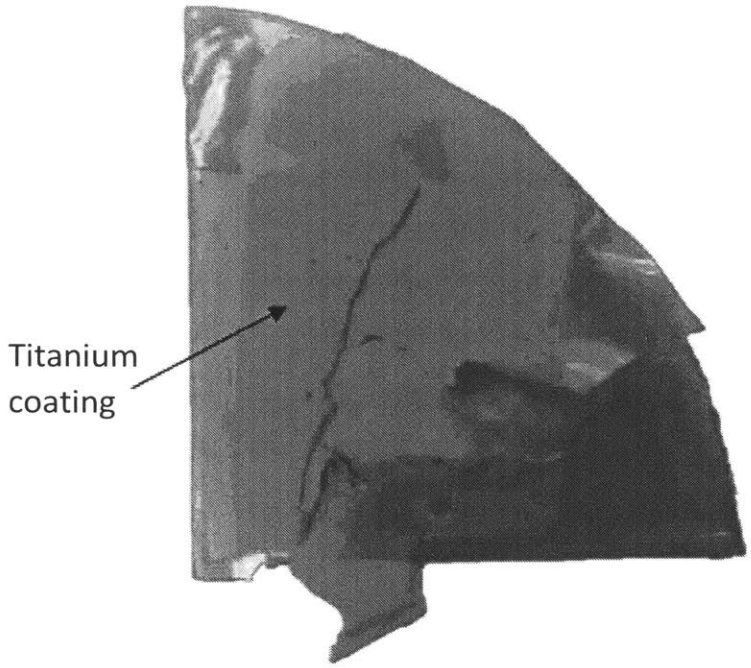

Figure 30. Top view of part 44. Some initial titanium coating was depositied before the polyimide tape ripped. This was achieved with process inputs: 300°C temperature, 34.5 bar pressure, 50 mm standoff, 150 mm/s traverse speed, 1 pass, and a 90° nozzle angle.

Parts 44 and 45 were taken to the SEM to view the surfaces of the titanium coatings. Both coating surfaces looked very similar and images of part 45 are shown in Figure 31 and Figure 32. Some particles showed significant deformation and bonding to other particles. However, the surface still appeared to have quite a bit of roughness to it from undeformed particles. Therefore, this would suggested that there may be some porosity within the coating due to the particles not completely flattening out. As pointed out in Figure 29, some visible large holes were seen on the surface of the coating. A view of one of these holes on the SEM is shown in Figure 33. The hole appeared large at the surface and smaller as it got closer to the substrate, creating s cone shape.

After imaging the surface, part number 45 was cut into four pieces. Cuting the piece was a two part process. A 1/8" end mill was used to machine down most of the way through the titanium coating. Then a diamond grinding wheel was used to cut the rest of the way through the part. The second step with the diamond griding wheel was necesarry because the silicon is very fragile. One of these sections after machining is shown in Figure 34. Two of the cut parts were then potted in epoxy and then ground and polished. The two parts were polished to specific areas in the coating.

The first was polished to a regular dense area of the coating. The other cross-section was polished down until the cross-section showed the middle of one of the large holes that had formed in the coating. The potted parts are shown in Figure 35.

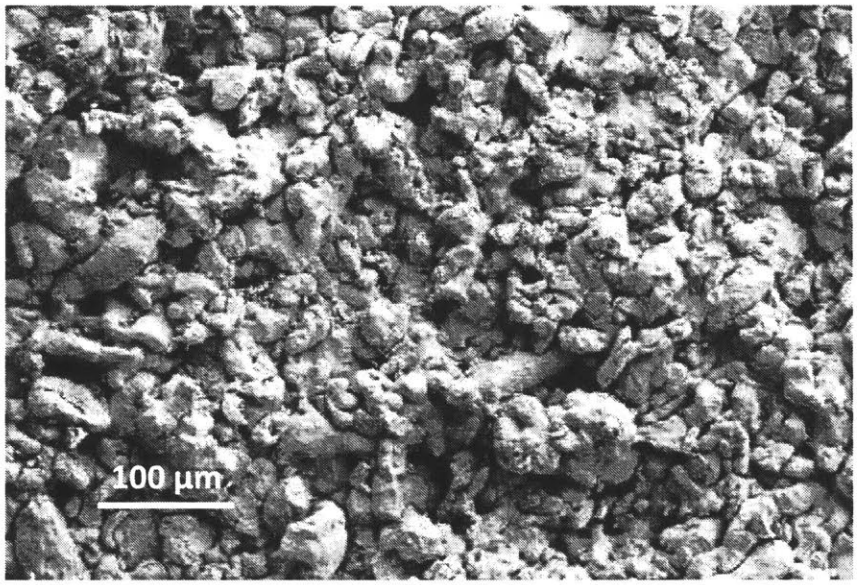

Figure 31. Surface image of part 45 obtained from an SEM. One pass of process inputs: 300°C temperature, 34.5 bar pressure, 75 mm standoff, 150 mm/s traverse speed, and a 90° nozzle angle. This was then followed by a second pass will all the same parameters except for a change in the traverse speed to 20 mm/s.

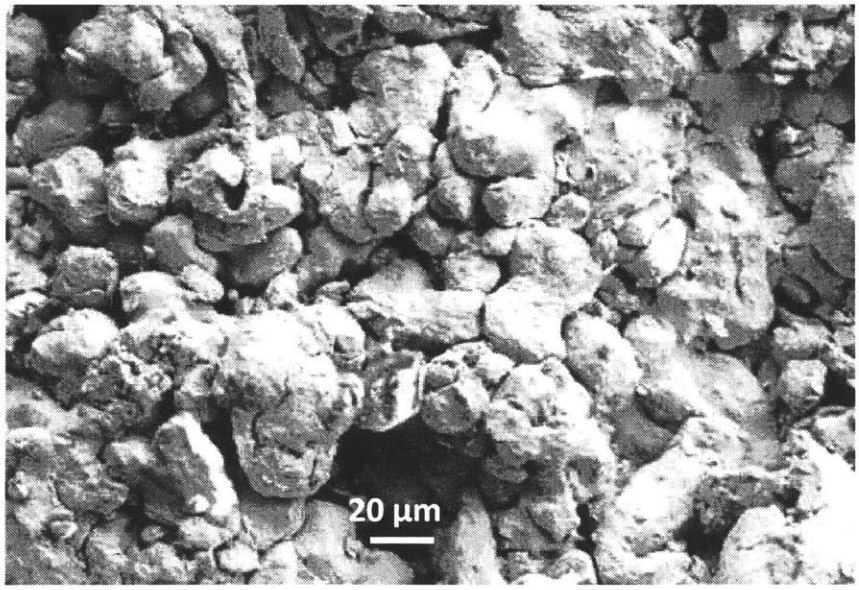

Figure 32. Magnified image of Figure 31.

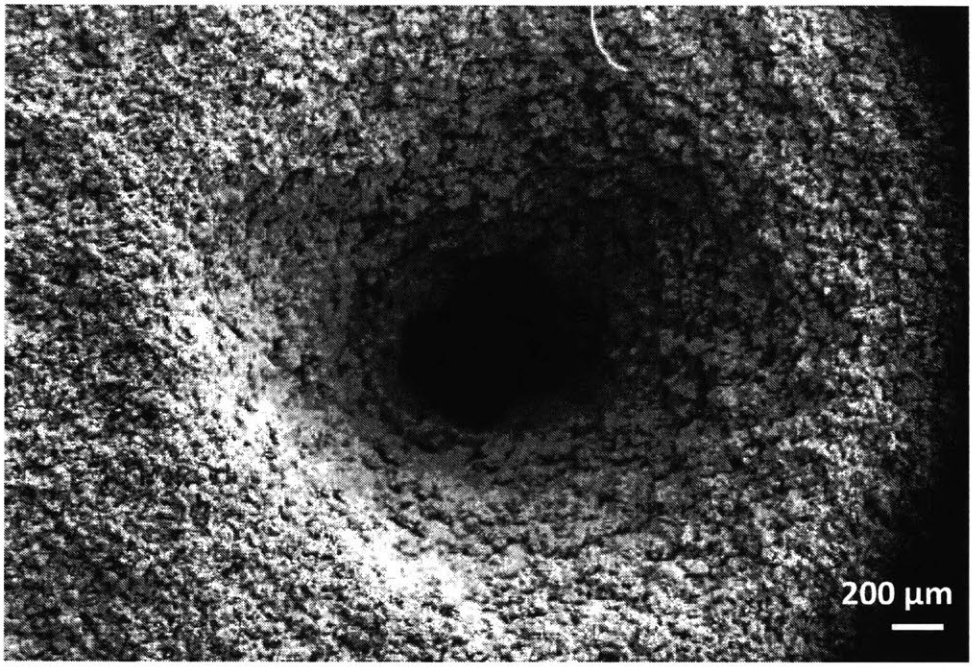

Figure 33. SEM image of one of the holes seen on the surface of part 45, as pointed out in Figure 29.

Figure 34. Cross-section of 1/8" thick titanium coating on polyimide substrate, part 45, after machining steps.

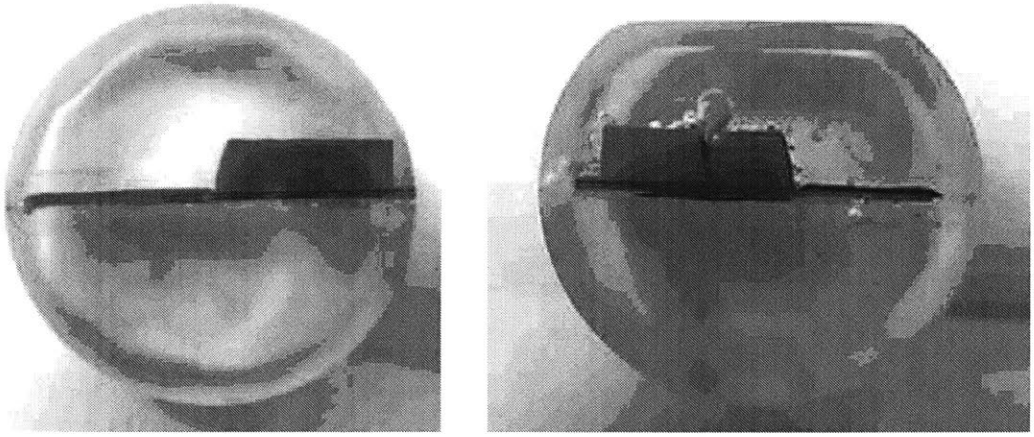

Figure 35. Potted cross-sections of thick titanium coating on substrates. The cross-section on the left is through a dense portion and the cross-section on the right was taken in the center of one of the large holes seen within the coating.

The cross-section image from the SEM shown in Figure 36 shows that the coating is very dense near the polyimide. Using ImageJ software (downloaded from https://imagej.nih.gov/ij/download.html; developer: NIH), a threshold procedure was done on three different images near the surface to estimate coating porosity. The coating porosity in this region was measured to be less than 2%. Figure 37 shows the titanium near the surface of the coating. In approximately the top 500 μm of the coating, a more porous area was observed. Porosity measurements were taken in this region again with the ImageJ software. Near the surface, the coating had approximately 6% porosity.

The bonding region between the cold sprayed titanium and the polyimide was investigated as well. Figure 38 shows this bonding region. The titanium particles had a good bond to the polyimide substrate and no gaps were seen between the polyimide and titanium. Also, while imaging the substrate, near the edges of the titanium coating, the Ti/epoxy mixture was visible, as shown in Figure 39. This Ti/epoxy mixture however was not seen between the polyimide and titanium coating. Therefore, the Ti/epoxy mixture most likely did not contribute to the titanium bonding and build up on the polyimide substrate.

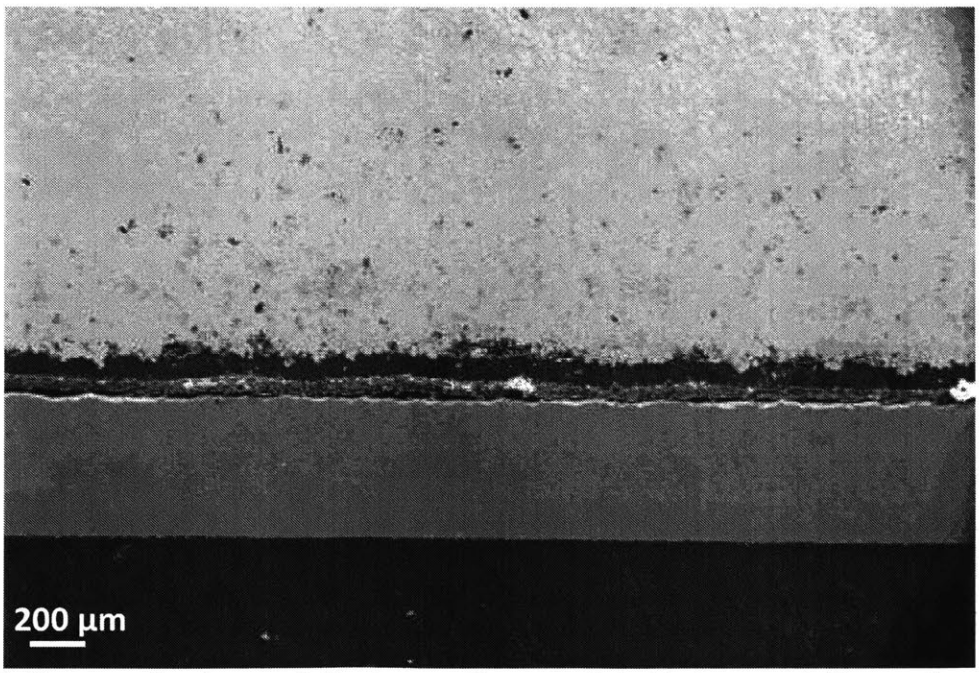

Figure 36. Cross-section image of titanium coating on polyimide tape, part 45, near the substrate.

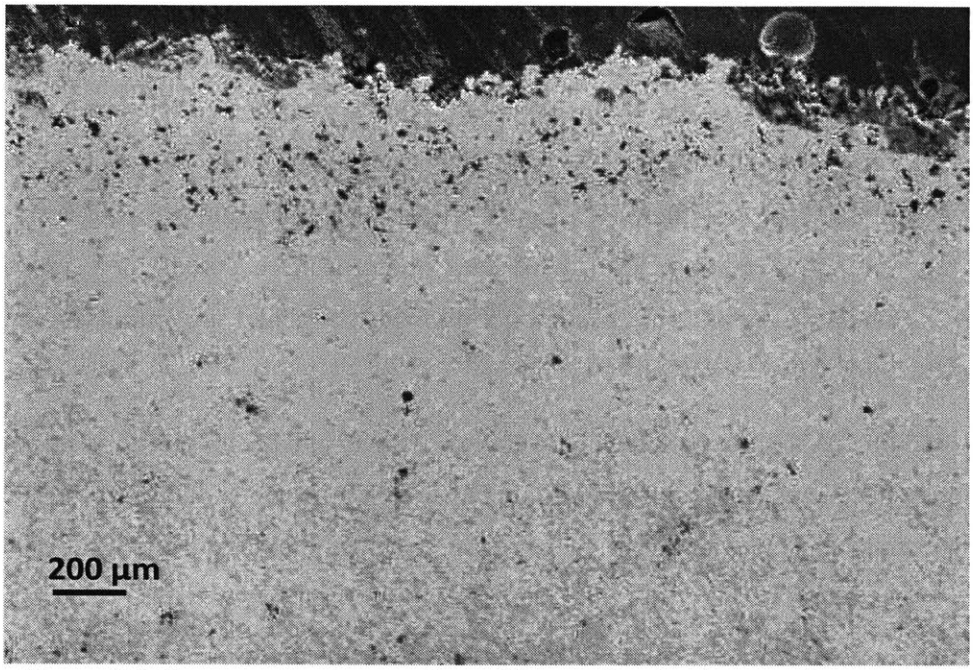

Figure 37. Cross-section image of part 45 near the titanium coating surface.

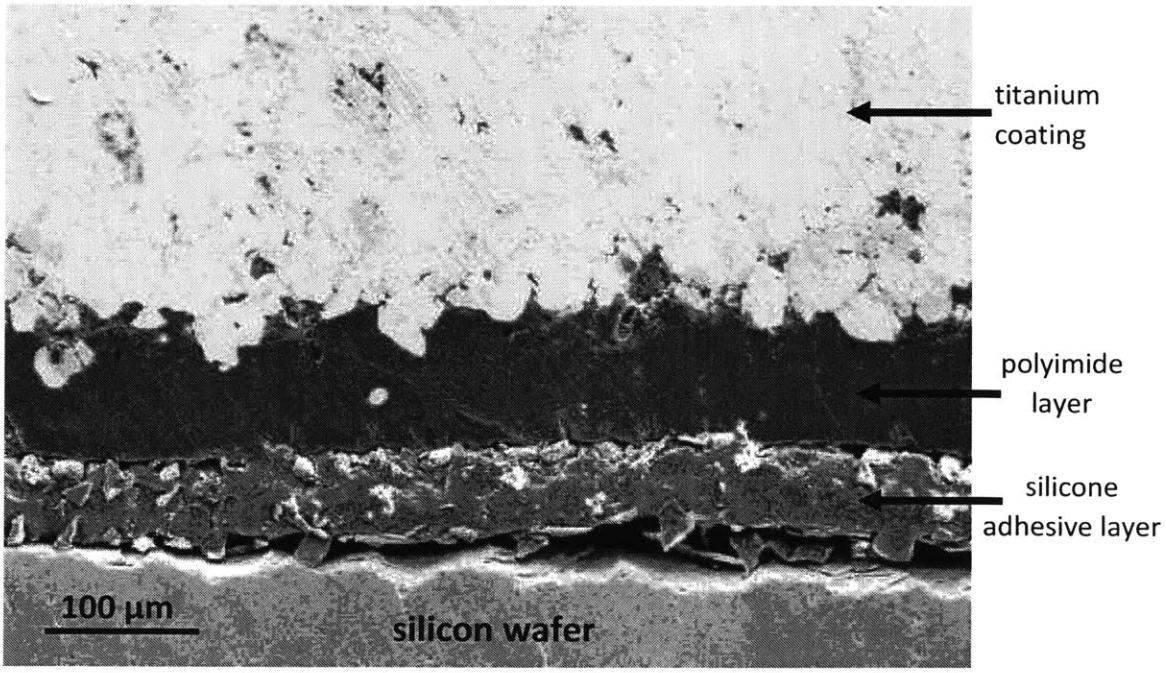

Figure 38. Cross-section image of part 45 showing the bonding of the titanium coating to the polyimide substrate.

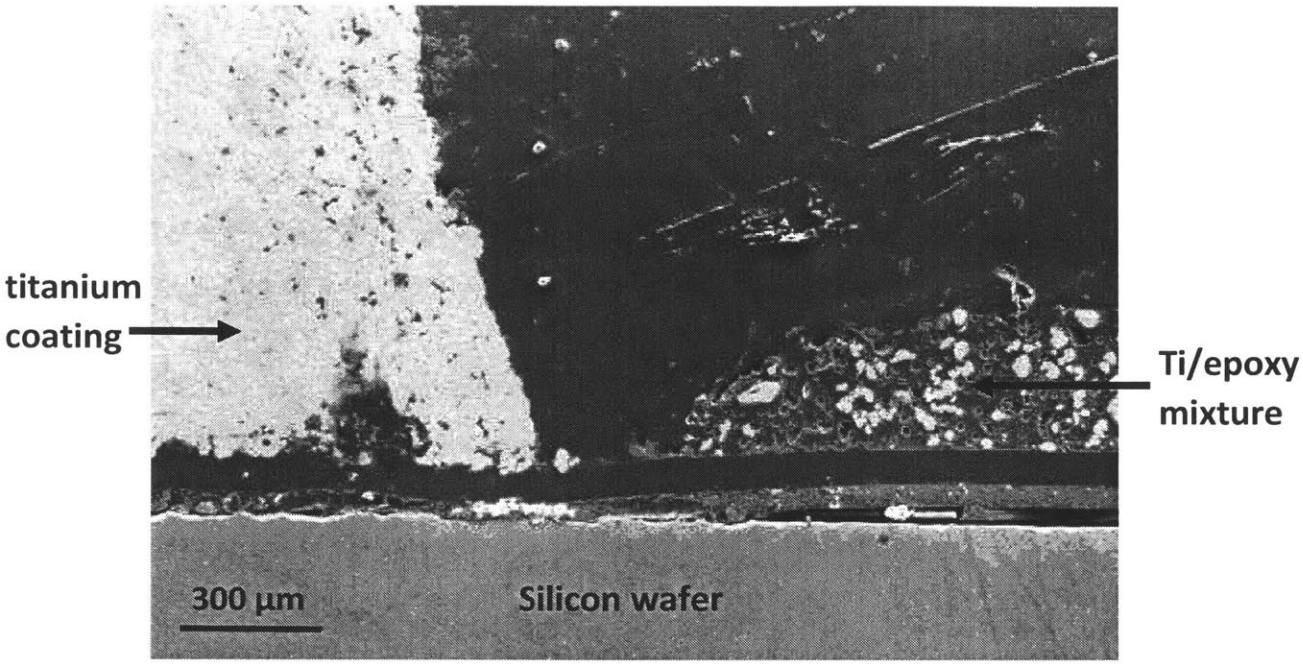

Figure 39. Image of part 45 near the edge of the titanium coating. The Ti/epoxy mixture appeared to have no effect on titanium buildup on the polyimide tape.

The other cross-section taken in the middle of one of the large holes was analyzed as well. Figure 40 shows the cross-section and a more magnified image near the polyimide substrate is shown in Figure 41. As the figures shows, the hole that was seen at the surface continued all the way down to the polyimide surface. It appeared that the hole in the titanium started off small at the polyimide surface and then progressively grew larger as the coating became thicker. On the polyimide surface, in the middle of the hole, there is an indent which could have resulted from a titanium particle that bonded with the polyimide and then dislodged. These type of holes have been observed in other cold spray research and Huang et al. conducted a computational simulation on impacting particles to investigate the reason for hole formation. The simulation resulted in holes when two different particles impacted too close to one another. Huang et al. suggested that a repellant force between the particles can result in the particles being deflected from one another and initiating a hole [50]. Since the particle feed rate was high and the traverse speed slow, in the small amount of time that the hole was formed, the particles around the hole site may have built up so far that it was difficult for other particles near the hole to build up. An image demonstrating this is shown in Figure 42. In this figure, particle 1 will hit the titanium coating and there will be a large area of contact with the coating, therefore its energy will cause the particle to deform and

bond to the coating. However, particle 2 in the figure will have a small area of contact with the coating, therefore a good bond will not be able to be formed between the particle and the coating. This effect most likely caused the cone shape of the hole as the coating built up.

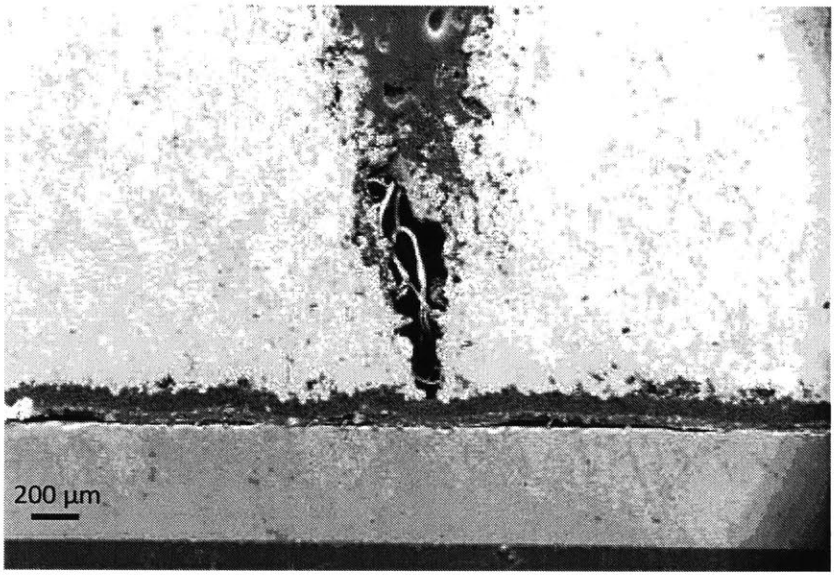

Figure 40. Cross-section through one of the holes in the titanium coating of part 45.

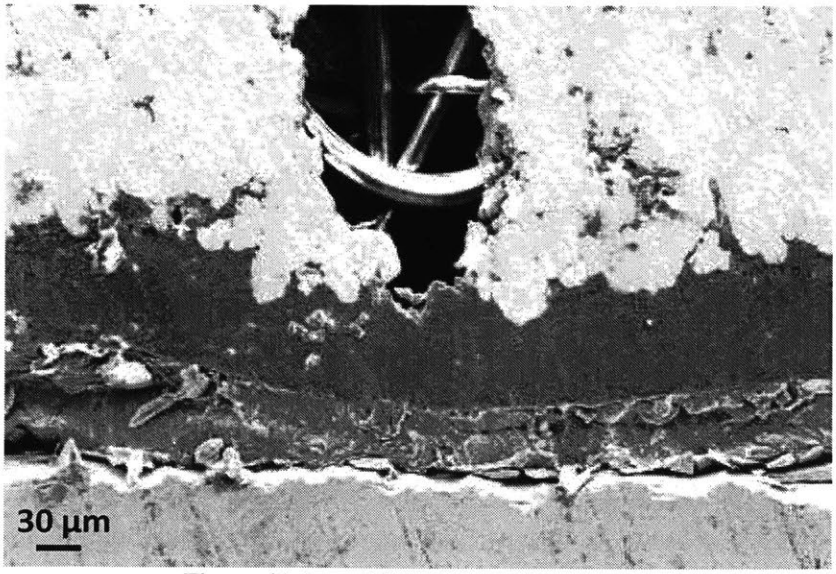

Figure 41. Magnified image of Figure 40.

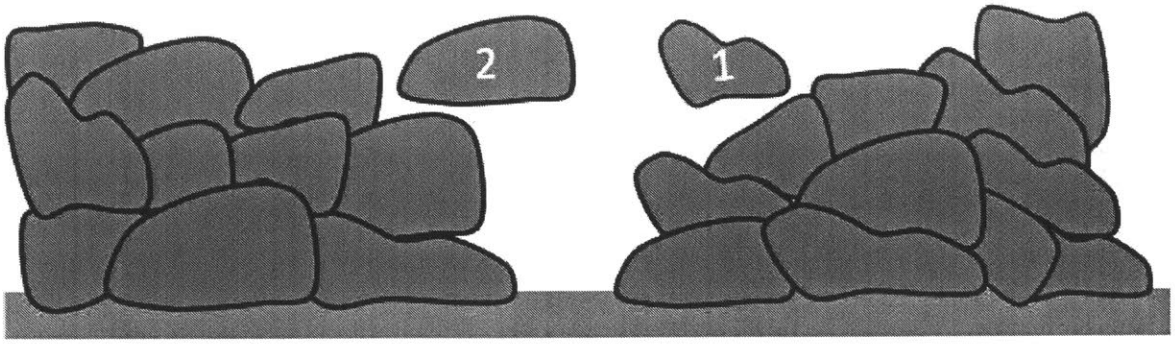

Figure 42. Model of proposed reason the hole grew as the titanium coating built up. Particle 1 will hit the titanium coating and there will be a large area of contact with the coating, therefore its energy will cause the particle to deform and bond to the coating. However, particle 2 in the figure will have a small area of contact with the coating, therefore a good bond will not be able to be formed between the particle and the coating.

One last experiment was conducted in this research. This last experiment was conducted since a major question still remained: did the Ti/epoxy mixture contribute at all to the coating deposition and buildup on the substrate? Since the previous substrates' top layer of Ti/epoxy appeared to either be blown away or eroded away before the titanium built up on the polyimide, it could be possible that the Ti/epoxy mixture had no contribution to the titanium bonding to the substrate. Moreover, this idea was supported by the SEM image which showed no Ti/epoxy mixture layer between the polyimide and titanium coating. The most likely reason these substrates were able to achieve titanium deposition and coating buildup is that the epoxy added rigidity to the substrates. The extra rigidity of the substrate allowed for a closer standoff distance and high input temperature and pressure. A shorter standoff distance and high temperature and pressure inputs would result in higher particle temperatures and velocities at impact. With higher particle velocities, the particles would be able to deform more upon impact, therefore creating a good bond layer on the polyimide followed by further buildup of the titanium particles on the titanium deposition. The warmer particles would also experience thermal softening and would be softer when they made impact with the substrate.

In order to test this theory, thick polyimide substrates were prepared and epoxy was put on the backside of the substrates. This way the substrates had a rigidity similar to the previously tested substrates while still keeping the polyimide as the substrate material to be cold sprayed on. The

same parameters as before were used: 75 mm standoff distance, 20 mm/s traverse speed, 300°C temperature, 34.5 bar pressure, 90 degree nozzle angle, and 1 pass of the nozzle to create a single layer. Titanium coatings were successfully created on two substrates. This proved that the titanium could be cold sprayed directly on the polyimide and that the epoxy only added rigidity to the substrate. This added rigidity enabled shorter standoff distances and greater temperature and pressure inputs to be used. Images of the titanium coatings on the substrates are shown in Figure 43. These coatings looked very similar to the previous part 45. Both of these new coatings were dense and had hole defects like those seen in part 45.

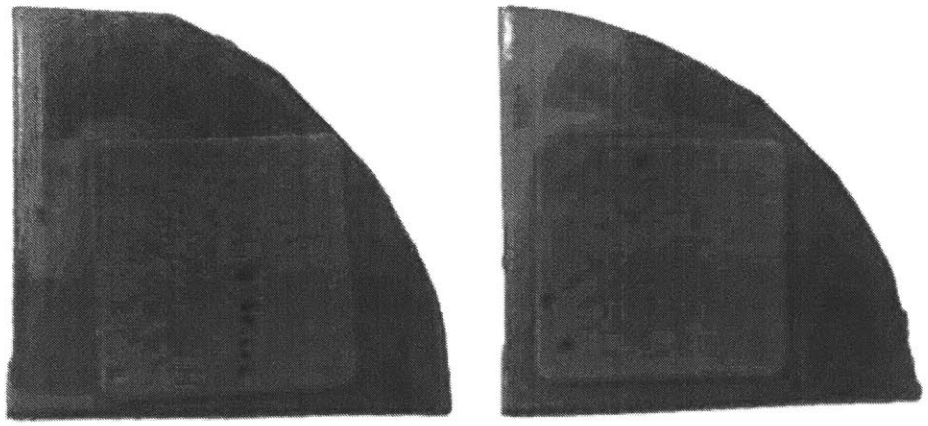

Figure 43. Titanium coatings cold sprayed directly on thick polyimide substrates. Process inputs: 300°C temperature, 34.5 bar pressure, 75 mm standoff, 20 mm/s traverse speed, and a 90° nozzle angle.

6.2 Conclusion for Titanium Coatings

Experiments were created to cold spray titanium coatings onto two different electronic materials, polyimide and silicon. No coatings could be created on the silicon, and the process only eroded the surface with all the process inputs tested. Titanium coatings could not be created on the initial thin polyimide tape substrates either. The titanium particles would break through the

polyimide material and adhere to the silicone adhesive underneath it. Although the titanium particles would bond to the adhesive, no buildup could be formed.

Additional experiments were conducted on silicon and polyimide substrates that had an additional 1 μm thick sputtered titanium layer on top. However, the high pressure of the cold spray process removed the sputtered layer. Therefore, the same results were found for these experiments.

Since titanium particles were found to break through the thin polyimide material, thicker polyimide substrates were tested as well. However, with the process inputs tested at the 150 mm standoff distance, the process only eroded the substrate.

None of the previous experiments worked. Therefore, cold spraying a softer interlayer material, copper, first followed by the titanium was tested as well. However, no copper could be deposited or built up on the substrates.

Successful titanium coatings were finally accomplished only after epoxy was added to the substrates. The epoxy added rigidity to the substrates which allowed for a shorter standoff distance with high process temperature and pressure inputs. Dense, 1/8" thick titanium coatings were cold sprayed directly on polyimide substrates. The porosity of the coating near the substrate was less than 2% and the porosity in the top 500 μm of the coating was approximately 6%. Although the majority of the coating was dense, some holes traveled all the way from the substrate to the surface of the coating.

6.3 Future Work for Titanium Coatings

Dense titanium coatings have now been successfully deposited on an electronics material, polyimide. This opens the door to many possibilities. Since spin on polyimide is used with ICs, it makes it an easy material to not only deposit on the top of ICs, but on all sides of an IC. If an IC was completely covered by polyimide, it could then be cold sprayed with titanium to fully seal the device. The polyimide would need this extra titanium layer on the outside since polyimide absorbs too much water to act as a barrier between the electronics and human tissue. Additionally, the strong titanium would act as a protective barrier to the internal electronics.

To get to the point of packaging electronics by the cold spray process, many steps still need to be taken. The titanium coatings in this research were only created after epoxy was put on the substrates to add rigidity. However, putting epoxy on ICs is not a reasonable way to prepare ICs to be cold sprayed. A more elegant way to add rigidity to the substrates needs to be developed. This would most likely be accomplished through an improved fixture device. Future research also needs to look at creating thinner coatings since the 1/8 inch thick coatings are much thicker than is desirable. A DOE would most likely need to be created to pick the correct input parameters that result in a thin and dense titanium coating. Additionally, the dense coating would need to be tested for a hermetic seal to ensure that the coating would be a physical barrier between the electronics and the surrounding fluid. Corrosion and biocompatibility properties of the material must be tested as well. Moreover, the adhesion and tensile strengths of the coating must be tested to make sure they are sufficient for the implant application.

Also, during the cold spray process substrates may heat up. Therefore an analysis may need to be conducted to measure the heat of the substrate under the polyimide layer to ensure that this temperature will not cause failure in the IC components. With specific implants it is also very important to have RF wave transmission through the implant package. Therefore RF wave losses may need to be characterized for the cold sprayed titanium coating.

7 Conclusion and Future Work

This research investigated whether cold spray can be used to package electronic implants. Cold spraying creates conformal coatings, therefore allowing even the smallest ICs to be packaged with this method. Moreover, cold spraying would be a one-step packaging process, therefore simplifying electronic implant packaging and reducing manufacturing costs. Two different biocompatible materials, UHMWPE and titanium, were cold sprayed on two different electronic material substrates, silicon and polyimide.

No successful coatings of UHMWPE were formed on the silicon or polyimide substrates. The reason for unsuccessful UHMWPE deposition and buildup is not known. However, some of the possible reasons for a lack of deposition could be due to the bow shock at the surface, the particle velocities were below the critical velocity, the particle velocities were above the erosion velocity, or the particles were not softened enough before impact. Titanium also did not deposit on the silicon substrates. Instead of depositing, the process eroded away the silicon substrate. Attempts to cold spray titanium onto sputtered layers of Ti were not successful either. Moreover, a cold sprayed interlayer of copper was attempted as well but copper deposition and buildup was not observed on the silicon or polyimide substrates at the process inputs that were used.

Although titanium did not deposit on the other substrates, dense 1/8 inch thick coatings were created on polyimide substrates after epoxy was added to the back of the substrates to give them more rigidity and strength. With added rigidity to the substrates, a shorter standoff distance of 75 mm was possible. With this standoff distance, 300°C temperature, 34.5 bar pressure, 20 mm/s traverse speed, and 1 pass of the nozzle over the substrate, a dense titanium coating was created on the polyimide substrate. This was a favorable result since polyimide is already the top passivation layer on many ICs. Moreover, polyimide can easily be deposited on all other sides of an IC and then titanium could be cold sprayed on top of the polyimide to create a hermetic seal around the electronics. The coatings were very dense, with ~2% porosity near the substrate and ~6% porosity near the surface. Except for some hole defects in the coating, the porosity did not appear to be through porosity from the surface to the substrate. Therefore, if process inputs were optimized with a DOE analysis, even denser coatings may be achieved and hole defects avoided.

With the deposition of dense titanium coatings on polyimide, the cold spray process appears to be a promising manufacturing technique to package electronic implants. With this new manufacturing process, it would be possible to create thin, conformal coatings around even the smallest electronic implants. Before this manufacturing process can become mainstream, more stages of testing need to be conducted to prove it as an acceptable alternative to traditional packaging techniques. These tests include structural tests, such as adhesion and tensile strength of the coatings, biocompatibility tests, RF transmission measurements through the coating, and hermeticity tests. With further research and development, this technology has the potential to drastically change how electronic implants are packaged.

Bibliography

[1] T. R. Shapiro, "Wilson Greatbatch, engineer who invented implantable pacemaker, dies at 92," *The Washington Post*, 28-Sep-2011.

[2] A. J. T. Teo, A. Mishra, I. Park, Y.-J. Kim, W.-T. Park, and Y.-J. Yoon, "Polymeric Biomaterials for Medical Implants and Devices," *ACS Biomater. Sci. Eng.*, vol. 2, no. 4, pp. 454–472, Apr. 2016.

[3] TJ Green Associates, LLC, "Non-Hermetic Packaging for Military and Aerospace Applications.pdf." http://www.circuitnet.com/news/uploads/2/Pacakging-for-Miltary-and-Aerospace.pdf.

[4] "ASM Medical Materials Database." http://mio.asminternational.org.libproxy.mit.edu/mmd/.

[5] T. Kramár, I. Michalec, and P. Kovacocy, "The laser beam welding of titanium grade 2 alloy," *GRANT J*, vol. 1, no. 1, pp. 77–79, 2012.

[6] International Titanium Association, "Why is titanium the metal of choice for medical applications from head to toe?" http://titaniumthemetal.org/Resources/DataSheetMedical.pdf.

[7] Medtronic Inc., "Pacemaker Media Kits." . http://www.medtronic.com/us-en/about/news/media-resources/media-kits/pacemakers.html

[8] SCHOTT AG, "Hermetic Packaging and Sealing." http://www.schott.com/d/epackaging/a67ecd2e-f020-465b-954e-932148c624cf/1.0/schott-hermetic-packaging-and-sealing-technology_eng.pdf.

[9] C. K. Bjune *et al.*, "Packaging Architecture for an Implanted System that Monitors Brain Activity and Applies Therapeutic Stimulation," *J. Microelectron. Electron. Packag.*, vol. 13, no. 2, pp. 64–70, Apr. 2016.

[10] A. Amar, A. Kouki, and H. Cao, "Power Approaches for Implantable Medical Devices," *Sensors*, vol. 15, no. 12, pp. 28889–28914, Nov. 2015.

[11] D. Stark, "Wafer-Level Hermetic Micro-Device Packages," US 2005/0275079 A1.

[12] J. Jeong, S. Hyun Bae, J.-M. Seo, H. Chung, and S. June Kim, "Long-term evaluation of a liquid crystal polymer (LCP)-based retinal prosthesis," *J. Neural Eng.*, vol. 13, no. 2, p. 25004, Apr. 2016.

[13] Seung Woo Lee, Kyou Sik Min, Joonsoo Jeong, Junghoon Kim, and Sung June Kim, "Monolithic Encapsulation of Implantable Neuroprosthetic Devices Using Liquid Crystal Polymers," *IEEE Trans. Biomed. Eng.*, vol. 58, no. 8, pp. 2255–2263, Aug. 2011.

[14] T. Stieglitz, "Manufacturing, assembling and packaging of miniaturized neural implants," *Microsyst. Technol.*, vol. 16, no. 5, pp. 723–734, May 2010.

[15] A. M. Vilardell, N. Cinca, A. Concustell, S. Dosta, I. G. Cano, and J. M. Guilemany, "Cold spray as an emerging technology for biocompatible and antibacterial coatings: state of art," *J. Mater. Sci.*, vol. 50, no. 13, pp. 4441–4462, Jul. 2015.

[16] J. Cizek, O. Kovarik, J. Siegl, K. A. Khor, and I. Dlouhy, "Influence of plasma and cold spray deposited Ti Layers on high-cycle fatigue properties of Ti6Al4V substrates," *Surf. Coat. Technol.*, vol. 217, pp. 23–33, Feb. 2013.

[17] B. AL-Mangour, R. Mongrain, E. Irissou, and S. Yue, "Improving the strength and corrosion resistance of 316L stainless steel for biomedical applications using cold spray," *Surf. Coat. Technol.*, vol. 216, pp. 297–307, Feb. 2013.

[18] K. Spencer and M.-X. Zhang, "Optimisation of stainless steel cold spray coatings using mixed particle size distributions," *Surf. Coat. Technol.*, vol. 205, no. 21–22, pp. 5135–5140, Aug. 2011.

[19] B. AL-Mangour, P. Vo, R. Mongrain, E. Irissou, and S. Yue, "Effect of Heat Treatment on the Microstructure and Mechanical Properties of Stainless Steel 316L Coatings Produced by Cold Spray for Biomedical Applications," *J. Therm. Spray Technol.*, vol. 23, no. 4, pp. 641–652, Apr. 2014.

[20] A. Sova, S. Grigoriev, A. Okunkova, and I. Smurov, "Cold spray deposition of 316L stainless steel coatings on aluminium surface with following laser post-treatment," *Surf. Coat. Technol.*, vol. 235, pp. 283–289, Nov. 2013.

[21] G. Sundararajan, P. Sudharshan Phani, A. Jyothirmayi, and R. C. Gundakaram, "The influence of heat treatment on the microstructural, mechanical and corrosion behaviour of cold sprayed SS 316L coatings," *J. Mater. Sci.*, vol. 44, no. 9, pp. 2320–2326, May 2009.
[22] M. Villa, S. Dosta, and J. M. Guilemany, "Optimization of 316L stainless steel coatings on light alloys using Cold Gas Spray," *Surf. Coat. Technol.*, vol. 235, pp. 220–225, Nov. 2013.
[23] W.-Y. Li *et al.*, "Ti and Ti-6Al-4V Coatings by Cold Spraying and Microstructure Modification by Heat Treatment," *Adv. Eng. Mater.*, vol. 9, no. 5, pp. 418–423, May 2007.
[24] J. Sun, Y. Han, and K. Cui, "Innovative fabrication of porous titanium coating on titanium by cold spraying and vacuum sintering," *Mater. Lett.*, vol. 62, no. 21–22, pp. 3623–3625, Aug. 2008.
[25] D. Qiu, M. Zhang, and L. Grøndahl, "A novel composite porous coating approach for bioactive titanium-based orthopedic implants," *J. Biomed. Mater. Res. A*, vol. 101A, no. 3, pp. 862–872, Mar. 2013.
[26] A. Hamweendo, L. Moloisane, and I. Botef, "Bio-Mechanical Compatibility Assessment of Titanium-Nickel Alloy Fabricated Using Cold Spray Process," *Mater. Sci. Forum*, vol. 828–829, pp. 351–356, Aug. 2015.
[27] W. Wong, E. Irissou, A. N. Ryabinin, J.-G. Legoux, and S. Yue, "Influence of Helium and Nitrogen Gases on the Properties of Cold Gas Dynamic Sprayed Pure Titanium Coatings," *J. Therm. Spray Technol.*, vol. 20, no. 1–2, pp. 213–226, Jan. 2011.
[28] M. Gardon, A. Latorre, M. Torrell, S. Dosta, J. Fernández, and J. M. Guilemany, "Cold gas spray titanium coatings onto a biocompatible polymer," *Mater. Lett.*, vol. 106, pp. 97–99, Sep. 2013.
[29] S. H. Zahiri, C. I. Antonio, and M. Jahedi, "Elimination of porosity in directly fabricated titanium via cold gas dynamic spraying," *J. Mater. Process. Technol.*, vol. 209, no. 2, pp. 922–929, Jan. 2009.
[30] G. Bae, Y. Xiong, S. Kumar, K. Kang, and C. Lee, "General aspects of interface bonding in kinetic sprayed coatings," *Acta Mater.*, vol. 56, no. 17, pp. 4858–4868, Oct. 2008.
[31] D. K. Christoulis, S. Guetta, V. Guipont, and M. Jeandin, "The Influence of the Substrate on the Deposition of Cold-Sprayed Titanium: An Experimental and Numerical Study," *J. Therm. Spray Technol.*, vol. 20, no. 3, pp. 523–533, Mar. 2011.
[32] X. Zhou and P. Mohanty, "Corrosion behaviour of cold sprayed titanium coatings in simulated body fluid," *Corros. Eng. Sci. Technol.*, vol. 47, no. 2, pp. 145–154, Apr. 2012.
[33] A. Choudhuri, P. S. Mohanty, and J. Karthikeyan, "Bio-ceramic composite coatings by cold spray technology," in *Thermal Spray 2009. Proc. Int. Thermal Spray Conf*, 2009.
[34] S. Kumar, V. Vidyasagar, A. Jyothirmayi, and S. V. Joshi, "Effect of Heat Treatment on Mechanical Properties and Corrosion Performance of Cold-Sprayed Tantalum Coatings," *J. Therm. Spray Technol.*, vol. 25, no. 4, pp. 745–756, Apr. 2016.
[35] M. Trexler, "Effect of Carrier-Gas Selection on Mechanical Properties of Cold-Sprayed Tantalum," *Int. J. Powder Metall.*, vol. 47, no. 5, 2011.
[36] H. Koivuluoto, J. Näkki, and P. Vuoristo, "Corrosion Properties of Cold-Sprayed Tantalum Coatings," *J. Therm. Spray Technol.*, vol. 18, no. 1, pp. 75–82, Mar. 2009.
[37] M. R. Hasniyati, H. Zuhailawati, R. Sivakumar, and B. K. Dhindaw, "Optimization of multiple responses using overlaid contour plot and steepest methods analysis on hydroxyapatite coated magnesium via cold spray deposition," *Surf. Coat. Technol.*, vol. 280, pp. 250–255, Oct. 2015.
[38] A. C. W. Noorakma, H. Zuhailawati, V. Aishvarya, and B. K. Dhindaw, "Hydroxyapatite-Coated Magnesium-Based Biodegradable Alloy: Cold Spray Deposition and Simulated Body Fluid Studies," *J. Mater. Eng. Perform.*, vol. 22, no. 10, pp. 2997–3004, Oct. 2013.
[39] K. Ravi, Y. Ichikawa, T. Deplancke, K. Ogawa, O. Lame, and J.-Y. Cavaille, "Development of Ultra-High Molecular Weight Polyethylene (UHMWPE) Coating by Cold Spray Technique," *J. Therm. Spray Technol.*, vol. 24, no. 6, pp. 1015–1025, Aug. 2015.

[40] J.-O. Kliemann, H. Gutzmann, F. Gärtner, H. Hübner, C. Borchers, and T. Klassen, "Formation of Cold-Sprayed Ceramic Titanium Dioxide Layers on Metal Surfaces," *J. Therm. Spray Technol.*, vol. 20, no. 1–2, pp. 292–298, Jan. 2011.

[41] M. Torrell, S. Dosta, J. R. Miguel, and J. M. Guilemany, "Optimisation of HVOF thermal spray coatings for their implementation as MSWI superheater protectors," *Corros. Eng. Sci. Technol.*, vol. 45, no. 1, pp. 84–93, Feb. 2010.

[42] *ASM Handbook, Volume 23: Materials for Medical Devices*. http://products.asminternational.org/hbk/index.jsp.

[43] S. S. da Rocha, G. L. Adabo, G. E. P. Henriques, and M. A. de A. Nóbilo, "Vickers hardness of cast commercially pure titanium and Ti-6Al-4V alloy submitted to heat treatments," *Braz. Dent. J.*, vol. 17, no. 2, pp. 126–129, 2006.

[44] Y.Z. Yang, J. M. Tian, Z. Q. Chen, X. J. Deng, and D. H. Zhang, "Preparation of graded porous titanium coatings on titanium implant materials by plasma spraying," *J. Biomed. Mater. Res.*, 2000.

[45] J. Pattison, S. Celotto, A. Khan, and W. O'Neill, "Standoff distance and bow shock phenomena in the Cold Spray process," *Surf. Coat. Technol.*, vol. 202, no. 8, pp. 1443–1454, Jan. 2008.

[46] T. B. Bush, Z. Khalkhali, V. Champagne, D. P. Schmidt, and J. P. Rothstein, "Optimization of Cold Spray Deposition of High-Density Polyethylene Powders," *J. Therm. Spray Technol.*, vol. 26, no. 7, pp. 1548–1564, Oct. 2017.

[47] A. Ganesan, M. Yamada, and M. Fukumoto, "Cold Spray Coating Deposition Mechanism on the Thermoplastic and Thermosetting Polymer Substrates," *J. Therm. Spray Technol.*, vol. 22, no. 8, pp. 1275–1282, Dec. 2013.

[48] A. Małachowska *et al.*, "Possibility of spraying of copper coatings on polyamide 6 with low pressure cold spray method," *Surf. Coat. Technol.*, vol. 318, pp. 82–89, May 2017.

[49] R. Lupoi and W. O'Neill, "Deposition of metallic coatings on polymer surfaces using cold spray," *Surf. Coat. Technol.*, vol. 205, no. 7, pp. 2167–2173, Dec. 2010.

[50] G. Huang, H. Wang, X. Li, and L. Xing, "Study on the Growth of Holes in Cold Spraying via Numerical Simulation and Experimental Methods," *Coatings*, vol. 7, no. 1, p. 2, Dec. 2016.